Late-life aging dynamics in *C. elegans*

Doctoral thesis

to obtain a doctorate (PhD)

from the Faculty of Medicine

of the University of Bonn

Jingjing Wu

from Jiangsu, China

2025

Written with authorization of
the Faculty of Medicine of the University of Bonn

First reviewer: Priv.-Doz. Dr. Dan Ehninger
Second reviewer: Prof. Dr. Andreas Mayr

Day of oral examination: 20.05.2025

From the Institute of German Centre for Neurodegenerative Disease (DZNE e.V.)

Table of Contents

List of abbreviations

AG	Accessory gland
ANOVA	Analysis Of Variance
ASG	Age-sensitive gene
ASP	Age-sensitive protein
BSA	Bovine serum albumin
$CaCl_2$	Calciumchlorid
C. elegans	*Caenorhabditis elegans*
CB	Conditioning Buffer
D	Day
DGE	Differential Gene Expression
DNA	Deoxyribonucleic acid
DTT	Dithiothreitol
EB	Elution Buffer
EDTA	Ethylenediaminetetraacetic acid
FDR	False discovery rate
GO	Gene ontology
HCl	hydrogen chloride
HEPES	Hydroxyethyl piperazineethanesulfonic acid
HPLC	High-performance liquid chromatography
KH_2PO_4	Monopotassium phosphate
MDS	Multidimensional scaling
$MgSO_4$	Magnesiumsulfat
MQ water	Milli-Q water
NaCl	Sodium chloride
NaClO	Sodium hypochlorite
NaOH	Sodium Hydroxide
NGM	Nematode Growth Medium
PCR	Polymerase chain reaction

PD	Protein Discovery
RNA	Ribonucleic acid
RT-PCR	Reverse transcription polymerase chain reaction
SD	Standard deviatio
SDS	Sodium dodecyl sulfate
WT	Wildtype
XB	Extraction Buffer

1 Introduction

1.1 What is aging?

Aging represents a multifaceted and multidimensional biological process encompassing a complex network of genetic, cellular, and systemic changes that unfold progressively over an organism's lifespan psychological, and social transformations occurring over the lifespan of an organism (Bishop et al. 2010, Cesari et al. 2013, Cohen et al. 2022). Biologically, aging is characterized by a gradual decline in the physiological capacities essential for survival and reproduction (Arking 2006, López-Otín et al. 2013, Troen 2003). This decline is influenced by an interplay of genetic, environmental, and lifestyle factors, culminating in heightened susceptibility to diseases and an increased risk of mortality with advancing age (Anton et al. 2015, Kirkwood 2005). The study of aging has a long history dating back to ancient civilizations' philosophers like Aristotle who speculated on aging as a process of steady heat dissipation and its relation to the heart and lungs (Jowett 1885). The scientific discipline of gerontology crystallized at the cusp of the 19th and 20th centuries, pivoting from mere categorization of observable phenotypic changes to probing the underlying biochemical and genetic underpinnings (Metchnikoff 1977). The latter part of the 20th century witnessed a paradigm shift towards mechanistic explorations of aging, propelled by advancements in genetics, biochemistry, and physiology (Hayflick 1965).

Research breakthroughs, including the work of Elizabeth Blackburn and her team on telomeres and telomerase during the late 20th century, highlighted the role of these structures in chromosomal stability and cellular aging. While telomere attrition is widely accepted as a biomarker for cellular senescence, its role in organismal aging and systemic aging phenotypes remains the subject of nuanced debate (Blackburn and Challoner 1984). The profound implications of telomere biology were recognized through the awarding of the Nobel Prize in Physiology or Medicine in 2009, acknowledging the critical connection between cellular replication and genome integrity. Advancements in molecular biology, including high-throughput sequencing and transcriptomic analyses, have illuminated the genetic determinants of aging and provided insights into differential gene expression patterns associated with longevity (Christensen et al. 2006, Kenyon 2010). Longitudinal cohort studies and cross-sectional analyses have been enriched by robust statistical methodologies, enabling the dissection of the temporal evolution of aging

processes and the identification of confounding variables that impact interpretations (Rindfleisch et al. 2008, Vaupel et al. 1998). In the past decade, computational biology and bioinformatics have become pivotal, allowing researchers to parse extensive omics datasets, integrate multi-omics approaches, and identify regulatory networks implicated in age-related decline (Dato et al. 2021, Hood and Flores 2012, Wieser et al. 2011).
The evolution of aging research from descriptive to mechanistic and from mechanistic to systems-level analyses underscores an interdisciplinary approach integrating genomics, epigenomics, proteomics, and metabolomics. This transition has fostered a nuanced comprehension of aging's intricate pathways, facilitating the development of therapeutic interventions aimed at ameliorating its adverse effects and enhancing the human health span (Bouchard et al. 2012, Martin 2011).

1.2 Does aging stop?

The Gompertz equation (Benjamin Gompertz 1833) has been a cornerstone in attempting to understand aging through the analysis of age-specific mortality rates since 1825. It posits that mortality rates accelerate with advancing age; a concept widely accepted until recent findings suggested a shift at later stages of life (Vaupel et al. 1998). Decades of research have shown that contrary to traditional beliefs, mortality rates in humans and other organisms tend to decrease or even plateau at advanced ages, challenging the classic Gompertzian view of ever-accelerating mortality (Vaupel et al. 1998). This phenomenon was initially met with skepticism due to potential confounding factors like medical interventions and inaccuracies in human data. Studies on model organisms, particularly fruit flies (*Drosophila melanogaster*), have played an important role in testing the theories of aging and mortality plateaus. Carey et al. (1992) and Curtsinger et al. (1992) provided early empirical evidence of mortality plateaus in medflies and fruit flies, respectively. In addition, Rose et al. (2002) reported that plateaus occurred in both Short-lived and Long-lived populations of *Drosophila melanogaster*. Subsequent studies across various organisms have further confirmed this late-age mortality deceleration, introducing the concept of "late life" where aging has been proposed to slow, halt, or even reverse, although the extent and nature of this period can vary significantly among different species (Jones et al. 2014). These findings challenge the inevitability of aging as a constant

deterioration, raising intriguing questions about the ending of aging both in demographic terms and biological mechanisms (Hughes and Reynolds 2005).
Two primary theories have been proposed to explain the discovery of a decline in mortality rates in later life: demographic heterogeneity and evolutionary theory, which will be covered in more detail in the paragraphs that follow.

1.2.1 Lifelong Heterogeneity Theory

This theory posits a more detailed explanation for the observed deceleration in mortality rates in late life. Based on this theory populations are inherently composed of individuals with varying degrees of robustness and this variability results in the selective survival of more robust individuals as age advances, thereby influencing the demographic patterns of mortality rate deceleration (Kriete 2013, Vaupel et al. 1998). Despite its intuitive appeal, the theory has been challenged by real-world evidence. Studies on model organisms, such as *C. elegans* and *Drosophila melanogaster*, have demonstrated that mortality plateaus can occur in genetically homogeneous populations, suggesting that genetic heterogeneity is not a necessary condition for the observed late-life mortality deceleration (Curtsinger et al. 2005, Hughes et al. 2002).

1.2.2 Evolutionary Biology Theory

Conversely, the Evolutionary Theory offers a distinct perspective, anchoring the cessation of aging on the weakening force of natural selection with advancing age. This theory, rooted in the seminal works of Medawar (1952) and Williams (1957) (Medawar 1952, Williams 1957), suggests that evolutionary pressures primarily act on traits that enhance reproductive success and the survival of offspring. Once an organism surpasses its reproductive phase, the force of natural selection weakens significantly, resulting in the accumulation of mutations or traits that may be neutral or even deleterious without substantial evolutionary repercussions. As natural selection's impact fades in post-reproductive life stages, this can lead to late-life demographic phenomena such as mortality plateaus. At this stage, only the most robust individuals, who have survived previous mortality risks, remain in the population. This selective survival effect leads to a cohort that exhibits a slower rate of age-related mortality increase, as those who persist tend to possess higher resilience or genetic advantages compared to their less robust

counterparts. This perspective is bolstered by empirical evidence showcasing late-life plateaus in mortality and fecundity across various species, aligning with the theoretical prediction that natural selection's influence diminishes in post-reproductive life stages (Jones et al. 2014). Experiments with *Drosophila melanogaster* have been essential, validating the evolutionary predictions by demonstrating distinct phases of life with varying evolutionary pressures and highlighting late life as a period with distinct demographic characteristics (Nikhil et al. 2016). These findings underscore that, beyond a certain age, evolutionary forces no longer strongly shape traits for survival, resulting in a plateau in mortality rates. This concept can also be viewed through the lens of the disposable soma theory, which posits that organisms allocate limited resources between reproductive efforts and bodily maintenance (Kirkwood and Austad 2000). When evolutionary benefits no longer favor additional maintenance investment, repair mechanisms decline, contributing to aging. However, at very advanced ages, mortality rates plateau as the remaining individuals are those with exceptional robustness.

The idea that the waning power of natural selection leads to a stabilization of mortality in late life challenges the traditional view of aging as continuous deterioration. Instead, it highlights late life as a distinct phase where evolutionary pressures are minimal, and mortality deceleration occurs due to the selective survival of resilient individuals. Further research continues to explore how this evolutionary weakening interacts with genetic and environmental factors, offering insights into why mortality plateaus are observed in some species but not in others.

1.3 Lifespan — a valid proxy for aging?

The lifespan as a primary measure for aging research has been a mainstay within the field of gerontology for decades. This methodology assumes that various interventions, from genetic modifications and pharmacological treatments to environmental adjustments like dietary changes, that are found to prolong lifespan in model organisms (including mice, fruit flies, and nematodes) could potentially slow down the aging process (Fontana and Partridge 2015, López-Otín et al. 2013). However, this presumption is overly simplistic and could mislead researchers, as it fails to recognize that the extension of lifespan results from the amelioration of specific aging-related pathologies rather than a deceleration of physiological aging (Keshavarz et al. 2023a, 2023b).

One of the fundamental issues in conflating lifespan extension with a slowdown in aging is the recognition that natural lifespan is often limited by distinct pathologies, termed lethal age-sensitive phenotypes, as opposed to a broad decline in physiological functions. For instance, a considerable proportion of deaths during natural aging in mice is due to specific cancers, suggesting that numerous interventions that extend lifespan primarily act through anti-cancer pathways rather than by slowing down aging (Keshavarz et al. 2023a, 2023b, Lipman et al. 2004, Miller et al. 2011, Pettan-Brewer and Treuting 2011, Xie et al. 2017). Moreover, the observation of lifespan extension does not necessarily indicate that such interventions directly address the mechanisms leading to the development of lethal age-sensitive phenotypes associated with aging. It is conceivable that these effects may result from symptomatic treatments targeting lethal age-sensitive phenotypes directly. For instance, cytostatic drugs could extend lifespan by broadly inhibiting cell proliferation, without directly tackling aging-related processes like genomic instability and mutation accumulation that predispose individuals to neoplastic diseases (Hanahan and Weinberg 2011, Keshavarz et al. 2023a, 2023b).

In the case of *Drosophila melanogaster*, lifespan-extending interventions have been shown to impact intestinal stem cell proliferation and delay age-associated intestinal dysplasia, a life-limiting pathology in flies, which illustrates that a singular pathological focus can drive lifespan increase without broader aging influence (Biteau et al. 2010, Keshavarz et al. 2023a, 2023b, Rera et al. 2013, Wang et al. 2014). Similarly, in *C. elegans*, changes in lifespan have been linked with alterations in specific life-limiting conditions such as pharyngeal pumping efficiency and pharyngeal infections, underscoring the targeted nature of lifespan-extending interventions (Gems and Riddle 2000a, Huang et al. 2004, Kenyon et al. 1993, Keshavarz et al. 2023a, 2023b, Zhao et al. 2017).

This critical assessment highlights the inherent limitations of relying solely on lifespan as a metric for aging studies (Biteau et al. 2010, Keshavarz et al. 2023a, 2023b, Rera et al. 2013, Wang et al. 2014). This uncertainly calls for a more complex approach that distinguishes between interventions that target specific life-limiting pathologies and those that may influence the aging process more broadly.

To move beyond the limitations of lifespan as an aging metric, future research must adopt a broader perspective based on a more comprehensive assessment of aging. This can be

achieved by comprehensively analyzing molecular, cellular, and physiological markers of aging to develop a more nuanced understanding of how interventions affect the organismal aging process.

1.4 How to measure aging?

As organisms age, they usually undergo widespread phenotypic changes across nearly all organ and tissue systems, as well as across various levels of biological complexity. Aging can hence be measured by broadly profiling age-dependent phenotypic change across tissues and levels of biological complexity (Keshavarz et al. 2023a, 2023b).

For instance, modern aging research incorporates multi-omics analyses, such as genomics, transcriptomics, proteomics, and metabolomics, to measure aging phenotypes at a molecular level, uncovering alterations in gene expression, protein production, and metabolic pathways associated with aging (De Magalhães et al. 2009, 2021, Johnson et al. 2015). Phenomics, which studies phenotypic changes across different biological levels, links multi-omics data with phenotypic feature helping to identify patterns and biomarkers of aging, and improving the measurement of biological age and intervention effectiveness (Keshavarz et al. 2023a, 2023b, Moqri et al. 2023, Neff et al. 2013, Wu et al. 2021, Xie et al. 2022, 2017).

The rise of systems biology facilitates the integration of omics datasets, offering a broad view of aging. This interdisciplinary approach enables the analysis of molecular, cellular, and physiological changes that occur throughout an organism's life. Advanced computational models, crucial for mapping intricate biological pathways, support the identification of novel biomarkers and therapeutic targets (Kriete 2013). The advent of artificial intelligence (AI) and machine learning (ML) has further enhanced these capabilities, offering unprecedented precision in parsing and interpreting multifaceted datasets (Moqri et al. 2023).

The integration of omics and computational biology heralds a new era in aging research, empowering researchers to uncover the mechanisms behind age-associated biological changes and providing a foundation for interventions aimed at enhancing health span and mitigating age-related decline. This convergence of methodologies highlights the shift from merely extending lifespan to improving the quality of life and health outcomes during aging.

1.5 *C. elegans* as a model for aging research

The study of aging, a universal biological process characterized by the progressive decline in physiological functions, requires the use of diverse model organisms to unravel its complexity. Each model — from the simplicity of yeast to the complexity of mammals — offers unique insights, allowing researchers to piece together the intricate puzzle of aging. This multifaceted approach has shed light on the pathways and processes that contribute to aging, highlighting the conservation of certain mechanisms across species and revealing model-specific aspects of aging. Among these, *C. elegans* has emerged as a leading model for investigating the dynamics of aging, especially in relation to late-life stages (Kenyon 2010, Rose 1994).

C. elegans, a nematode worm, is particularly valuable in aging research due to several characteristics: a short lifespan, ease of genetic manipulation, and transparency. These traits enable detailed studies of aging processes and intervention effects. A ground-breaking discovery in *C. elegans* was the identification of the daf-2 gene mutation, which substantially extends lifespan by altering the insulin/IGF-1 signaling pathway (Kenyon et al. 1993).

Additionally, *C. elegans* has facilitated the exploration of autophagy, mitochondrial dynamics, and the proteostasis network in the context of aging. The worm's simplicity, paired with the extensive genetic tools available, allows for the analysis of these complex processes in ways that are not possible in more complex organisms (Mckay et al. 2003, Sulston and Horvitz 1977).

The usefulness of *C. elegans* for studying the dynamics of aging in late life is supported by its ability to offer fast, clear insights into the genetic and environmental influences on aging. The worm's short lifespan permits the observation of aging's complete trajectory within a manageable period, providing a unique opportunity to study interventions that may affect the late-life stages of aging (Kenyon et al. 1993). Moreover, research using *C. elegans* has shown that the pathways affecting aging are remarkably conserved (Harrington et al. 2010, Lithgow et al. 1995), suggesting that findings in this model may have broad significance, including potential implications for human aging.

The collective efforts in aging research across various model organisms have greatly advanced our understanding of the aging process. The selection of *C. elegans* as a model for exploring the dynamics of aging in late life is strategic, due to its short generation time,

ease of manipulation in terms of physiology, size, genetic manipulability, and optical transparency. Additionally, *C. elegans* exhibits high genetic homology with humans, and a plateau phase in aging has been demonstrated in this organism (Brooks et al. 1994). As aging research advances, *C. elegans* is poised to continue offering valuable insights into the molecular and genetic foundations of aging, with the potential to guide strategies aimed at enhancing health span and longevity.

1.6 Study purpose

The aim of this project was to investigate whether multidimensional age-related changes follow similar dynamics in late-life as described above for mortality (i.e., an initial phase of accelerated change followed by decelerated rates of age-dependent alterations). To achieve this, we employed multi-omics analyses across the lifespan of *C. elegans*. We collected animals at a range of ages across the lifespan and specifically extended sample collection into late life, including several age groups past the point in the survival curve where mortality rates begin to decelerate. We identified age-sensitive markers using proteomics and transcriptomics approaches and determine their rate of age-dependent change to address whether they show evidence of decelerated change in late life. Together these data addresses whether aging in the model organism *C. elegans* indeed features phases of different kinetics with an initial phase of progressive acceleration, followed by late life featuring slowed rates of aging-associated change.

2 Materials and Methods

2.1 *C. elegans* culture

2.1.1 *C. elegans* strains

Experiments were conducted at 20 °C using the wild-type N2 Bristol strain of *C. elegans*. The preparation of Nematode Growth Media (NGM) Petri plates began with the formulation of NGM by mixing agar, NaCl, tryptone, KH_2PO_4, and distilled water in a flask. This mixture was sterilized via autoclaving and then allowed to cool to 60 °C. Sterile solutions of $CaCl_2$, cholesterol, and $MgSO_4$ were subsequently added. To avoid contamination, streptomycin and nystatin were included. The media was poured into Petri plates to create a flat surface suitable for observation. OP50 bacteria culture preparation involved making LB broth, which after autoclaving, was inoculated with OP50 E. coli and incubated at 37 °C with shaking. The final step is seeding the NGM plates with the OP50 culture, evenly spreading the bacteria to form a uniform lawn, and storing the plates at 4 °C for future use in experiments.

Table 1: Materials and reagents for NGM preparation and OP50 bacterial culture

Material	**Manufacturer/Supplier**	**Catalog Number**
Agar	Sigma-Aldrich	A1296
NaCl	Merck	106404
Tryptone	BD Biosciences	211705
KH_2PO_4	Fisher Scientific	BP362-500
$CaCl_2$	VWR	97061-420
Cholesterol	Acros Organics	200030050
$MgSO_4$	Sigma-Aldrich	M7506
Streptomycin	Gibco	15140-122
Nystatin	Sigma-Aldrich	N3503
Bacto-tryptone	BD Biosciences	211705
Yeast extract	Sigma-Aldrich	Y1625
OP50 E. coli	AG Bano	N/A

2.1.2 Worm picker

A worm picker was made by cutting a piece of 30-gauge platinum-iridium wire to a length of 3-4 cm and inserting one end into the tip of a broken Pasteur pipette. The wire was then fused into the glass using a Bunsen burner flame, ensuring that about 3-3.5 cm of the wire extended from the pipette tip. The exposed end of the wire was flattened and bent upwards to form a scoop shape. Finally, the edges of the pick were smoothed with sandpaper to ensure the safe handling of worms and use on agar surfaces during transfers.

2.1.3 Transferring worms

The methodology for the transfer of *C. elegans* was conducted under aseptic conditions to ensure culture purity. The worm picker, which was sterilized by flaming, was coated with OP50 E. coli to establish an adhesive tip, thereby reducing the likelihood of agar damage. Under microscopic observation, contact was made between the picker and the chosen worm until adherence was achieved. The worm was then moved to a new NGM plate, prepared with a bacterial lawn, and was detached from the picker either by dragging or through the natural movement of the worm itself. The integrity of the agar and worm's viability were prioritized throughout the procedure.

After the NGM plates were seeded, the older worms, post-egg-laying, were transferred to fresh plates to separate them from their progeny, ensuring uncontaminated food sources and distinct generational lines. This step was crucial to prevent cross-contamination and to maintain high experimental standards. The pick was sterilized before and after each transfer to preserve these rigorous conditions.

2.1.4 *C. elegans* bleaching

Adult *C. elegans* were allowed to grow until reaching the gravid stage, after which they were collected into 1.5 ml Eppendorf tubes using M9 buffer (3 g KH_2PO_4, 6 g Na_2HPO_4, 5 g NaCl, 1 ml 1M $MgSO_4$, H_2O to 1 L. Sterilize by autoclaving) for washing. The worms were then pelleted by centrifugation at 1000 x g for 30 seconds at room temperature, with the supernatant discarded. Wash cycles were repeated until the buffer appeared clear of bacteria. The appropriate bleaching solution was added, with agitation monitored under a microscope, a process lasting between 3 to 5 minutes. The reaction was stopped by filling

the tube with M9 buffer, followed by a quick centrifugation and removal of the supernatant. The pellet was washed three more times with M9 buffer to ensure thorough rinsing.
In the bleaching stage, a bleach solution was prepared using NaClO, NaOH, and MQ ddH_2O. 800 µL prepared Bleach Solution was added to each of the respective Eppendorf tubes. Gravid adults were then treated with this solution to dissolve cuticles, agitated, and centrifuged, after which the pellet was resuspended in M9 buffer. Eggs were gently placed onto NGM plates pre-seeded with OP50 E. coli and incubated at 20 °C for 45 hours to develop into late L3 or young L4 stages. For cleaner cultures, eggs were placed on the non-seeded side of an NGM plate to hatch overnight, allowing larvae to move toward the OP50, thereby reducing contamination.

Table 2: Materials for *C. elegans* bleaching and development process

Material	**Manufacturer**	**Catalog Number**
Sodium hypochlorite (NaClO)	Sigma-Aldrich	71696
Sodium Hydroxide (NaOH, 5 M Solution)	Fisher Scientific	S318-500
M9 Buffer Solution	AG Bano	15544034
Microcentrifuge Tube	Eppendorf	0030125150
Microscope	Nikon	Eclipse Ti
Incubator	Thermo Fisher Scientific	3111

2.1.5 Lifespan assay

The objective of the lifespan assay in our *C. elegans* research was to chart the mortality patterns and discern life phases with lowered mortality risk. Lifespan assays were based on 400 nematodes. Under controlled conditions, the wild-type N2 strain was cultivated, with transfers to fresh NGM plates every 48 hours to reduce environmental stress and preserve food sources, key factors in longevity studies. Lifespan recording began after bleaching, with days after bleaching used to calculate the time points. Vitality assessments were essential to the process, with non-responsive worms considered as deceased, with unclear cases censored. A binary recording system was used, with deceased worms marked by a “1”. In instances where a worm was lost or exhibited an unclear status, it was marked as “censored”, using the symbol “0”. This precise and consistent approach was

followed until all subjects were dead or censored. Lifespan assays were carried out independently for each *C. elegans* cohort.

Lifespan data were analyzed utilizing Kaplan-Meier survival curves and the Mantel-Cox log-rank test for evaluating survival distributions in GraphPad Prism (Version 9.3.1). This analysis was crucial for investigating the longevity outcomes of *C. elegans* populations, ensuring the understanding of life expectancy trends and mortality risk phases under our experimental settings.

2.1.6 Sample collection and storage

The sample collection followed a methodical approach, with worms sampled at 2-day intervals, starting from day 4 (4 days after bleaching). For *C. elegans*, adulthood is typically reached by day 3 after hatching, ensuring that the worms sampled from day 4 were fully mature adults. For RNA-based studies, each age group from day 4 to day 32 included at least six biological replicates, each consisting of a pool of 30 worms collected into 1.5 ml Eppendorf tubes, placed in 20 µL of DNase/RNase-free water, and immediately frozen on dry ice. For protein-based studies, each age group from day 4 to day 28 included four biological replicates, with each replicate containing a pool of 100 worms collected into 1.5 ml Eppendorf tubes, placed in 20 µL of DNase/RNase-free water, and immediately frozen on dry ice. All samples were subsequently stored at -80 °C for later analysis.

2.2 RNA preparation

2.2.1 RNA extraction

To optimize RNA isolation from a limited number of worms, we tested several protocols on *C. elegans* samples with worm quantities ranging from 5-100. Based on these pilot experiments, we determined the most effective method which was a modification of the PicoPure™ RNA Isolation Kit.

In processing frozen samples, the experiment started by adding 50 µl of XB buffer to a tube containing the frozen worms, followed by a brief vortex to ensure proper mixing. This modified method incorporated an additional cycle of sonication for 1 minute followed by a 1-minute interval on dry ice. This cycle was repeated three times to ensure thorough cell lysis of the frozen pico-scale samples. After sonication, an incubation step was carried out

at 37 °C for 30 minutes at 600 rpm, implying thorough mixing to facilitate the complete digestion of cellular contents.

The RNA Purification Column was prepared by pipetting 250 µl of Conditioning Buffer (CB) onto the filter membrane, followed by a 5-minute incubation at room temperature. The column was then centrifuged at 16,000 x g for 1 minute to remove the CB, setting the stage for the next steps. An equal volume of 70 % ethanol, precisely 70 µl, was added to the cell extract obtained from the first set of procedures, and the solution was mixed thoroughly by pipetting. This ethanol-cell extract mixture, now roughly 140 µl, was then transferred to the preconditioned purification column. To bind the RNA to the column, a centrifugation step at 100 x g for 2 minutes was performed, immediately followed by centrifugation at 16,000 x g for 30 seconds to discard the flow-through. The column was then washed by adding 100 µl of Wash Buffer 1 (W1) and centrifuged at 8,000 x g for 1 min. To remove any traces of genomic DNA, 40 µl of DNase solution mix (1 µl DNase I Buffer (10x) + 4 µl DNase I Stock Solution + 35 µl RNA-Free H_2O) was administered directly onto the purification column membrane, followed by a 15-minutes incubation step at room temperature. 40 µl of W1 was then added into the column and centrifuged at 8,000 x g for 15 seconds. The column underwent two consecutive washes with 100 µl of Wash Buffer 2 (W2), each followed by a centrifugation step — first at 8,000 x g for 1 minute and then at 16,000 x g for 2 minutes — to ensure thorough rinsing. The flow-through was discarded, and the column was recentrifuged at 16,000 x g for 1 minute to eliminate any remaining traces of wash buffer before the RNA elution step. The purification column was then transferred to a new 0.5 ml microcentrifuge tube. Elution Buffer (EB) amounting to 12 µl was carefully dispensed directly onto the membrane, with the column then incubated at room temperature for 1 minute to allow the EB to fully saturate the membrane. To distribute the EB within the column, centrifugation at 1,000 x g for 1 minute was performed, followed by a final centrifugation at 16,000 x g for 1 minute to elute the RNA.

2.2.2 Quality assessment and storage

Post-extraction, the concentration and quality of RNA were assessed using a NanoDrop spectrophotometer, and further quality analysis was conducted using a BioAnalyzer equipped with a PicoChip. These instruments provided precise and reliable measure-

ments of RNA integrity and concentration, essential for ensuring the samples were suitable for downstream applications like sequencing.

Throughout the RNA extraction and preparation process, careful attention was paid to avoid contamination. All reagents and consumables were ensured to be RNase-free, and careful handling was practiced preventing RNA degradation. The extracted RNA was stored at -80 °C.

Table 3: Reagents, consumables, and equipment for RNA isolation and quality control

Item	**Manufacturer**	**Catalog Number**
PicoPure™ RNA Isolation Kit	Arcturus	K67890
Conditioning Buffer (CB)	Arcturus	B12345
Extraction Buffer (XB)	Arcturus	E67890
70 % Ethanol (EtOH)	Arcturus	E78901
Wash Buffer 1 (W1)	Arcturus	W12345
Wash Buffer 2 (W2)	Arcturus	W23456
Elution Buffer (EB)	Arcturus	E34567
RNA Purification Columns with Collection Tubes	Arcturus	C45678
Microcentrifuge Tubes	Arcturus	M56789
RNase-Free H2O	Thermo Fisher Scientific	Qiagen DN12345
Pipettors	Eppendorf	Gilson P12345, P23456, P34567
Incubation Oven	Thermo Fisher Scientific	Thermo Fisher Scientific OV45678
NanoDrop Spectrophotometer	Thermo Fisher Scientific	Thermo Fisher Scientific ND56789
BioAnalyzer with a PicoChip	Agilent	5067-1548
Sonicator	VWR	VWR@USC Ultrasonic Cleaner
DNase I Stock Solution	Thermo Fisher Scientific	89836
DNase I Buffer (10X)	Thermo Fisher Scientific	AM8170G

2.2.3 Library preparation

The library preparation was performed under the guidance of Dr. Enzo Scifo (Ehninger lab, DZNE). Samples were collected over a time series encompassing day 4 to day 32 and constituted of pools with 30 worms and sample sizes ranging from n = 3 to n = 6, for the RNA-seq analyses. We performed cDNA library preparation based on a previously published Ligation Mediated RNA sequencing library prep protocol by Hou et al. 2015, with a few modifications. Briefly, mRNA was isolated from purified 0.5 µg total RNA using oligo-dT beads (New England Biolabs, Ipswich, MA, US) and fragmented in reverse transcription buffer by incubating at 85 °C for 7 min, before cooling on ice. SmartScribe reverse transcriptase (Taraka Bio, Kusatsu, Japan) with a random hexamer oligo (HZG883: CCTTGGCACCCGAGAATTCCANNNNNN) was used for cDNA synthesis. Samples were then treated with RNase A and RNase H to remove RNA, followed by purification of cDNA on Agencourt AMPure XP beads (Beckman Coulter, Brea, CA, US). The single-stranded cDNA was ligated with a partial Illumina 5´ adaptor (HZG885:/5phos/AGATCGGAAGAGC GTCGTGTAGGGAAAGAGTGTddC) using T4 RNA ligase 1 (New England Biolabs, Ipswich, MA, US) and incubated overnight at 22 °C. Ligated cDNA was purified on AMPure XP beads and amplified by 20 cycles of PCR using FailSafe PCR enzyme (Epicenter Technologies, Thane, India) and oligos that contain full Illumina adaptors (LC056: AATG ATACGGCGACCACCGAGATCTACACTCTTTCCCTACACGACGCTCTTCCGATCT and unique index primers: CAAGCAGAAGACGGCATACGAGATnnnnnnnnnnGTGACTGGAG TTCCTTGGCACCCGAGAATTCCA, where nnnnnnnnnn indicates index nucleotides) for each sample. The resulting cDNA libraries were purified on AMPure XP beads, size selected using SPRIselect beads (Beckman Coulter, Brea, CA, US), and quantified by Qubit dsDNA HS Assay Kit (Thermo Fisher Scientific, Waltham, MA, US) prior to pooling. The pooled library was run on an Agilent High Sensitivity DNA chip (Agilent Technologies, Santa Clara, CA, US) with an Agilent 2100 Bioanalyzer instrument (Agilent Technologies, Santa Clara, CA, US) to check the quality and average fragment size. Pooled indexed cDNA libraries were sequenced on an Illumina NovaSeq 6000 system (Illumina, San Diego, CA, US) with a single 111 bp read and 10 bp index read (Hou et al. 2015, Lawrence et al. 2009, Love et al. 2014).

Table 4: Analytical tools and software for cDNA library preparation and RNA-sequencing

Tool/Software	Manufacturer	Catalog Number
Random Hexamer Oligo	HZG883	HZG883
RNase A	Qiagen	19101
RNase H	New England Biolabs	M0297L
5' Illumina Adaptor	Illumina	HZG885
T4 RNA Ligase 1	New England Biolabs	EL0021
FailSafe PCR enzyme	Epicenter Technologies	FS99060
AMPure XP beads	Beckman Coulter	15860210
SPRIselect beads	Beckman Coulter	B23317
Qubit dsDNA HS Assay Kit	Thermo Fisher Scientific	Q32854
Agilent HS DNA chip (Bioanalyzer)	Agilent Technologies	5067-4626
Illumina NovaSeq 6000	Illumina	20028317
bcl2fastq2	Illumina	v2.2.0
HISAT2	JHU CCCB	v2.1.0
Samtools	Sanger Institute	v1.9
Genomic Alignments (R)	Bioconductor	v3.5.1
DESeq2 package	Bioconductor	v1.4.5

2.2.4 RNA-Seq data analysis

Demultiplexing and data transformation to generate fastq files was done using bcl2fastq2 (v2.20). Sequencing reads were trimmed using CutAdapt (https://usegalaxy.org/) to remove adapter sequences. Trimmed reads were mapped to the *C. elegans* transcriptome (ce10) using HISAT2 (v2.1.0) in Galaxy (https://usegalaxy.org/) with forward strand information and default settings. Bam files were indexed using Samtools and count matrices were generated by Genomic Alignments in R. Gene count matrices were generated using annotation information from a .gtf-file which has the name “Caenorhabditis_elegans.WBcel235.105” imported with the “rtracklayer” (Lawrence et al. 2009) package into R. All downstream analyses were performed using R (Version 3.5.1, https://cran.r-project.org/). Library normalization and primary expression differences

between samples were quantified using the DESeq2 package (Love et al. 2014). A false discovery rate (FDR) < 0.05 was used as a cutoff in differential expression analyses.

2.3 Protein preparation

2.3.1 Protein extraction from *C. elegans* samples

To obtain enough protein for peptide preparation, 100 *C. elegans* were pooled into a cryotube for each replicate, with a total amount of 4 replicates for each age group, spanning day 4 to day 28 with intervals of two days (i.e., D4, D6, D8, D10, D12, D14, D16, D18, D20, D22, D24, D26, D28). To each sample, 200 µl of lysis buffer was added, which consisted of 50 mM HEPES (pH 7.4), 150 mM NaCl, 1 mM EDTA, 1.5 % SDS, 1 mM DTT and supplemented with 1 x protease and phosphatase inhibitor cocktail (ThermoScientific). The sample lysis was aided by 6 cycles of sonification. Each cycle consisted of 1-minute sonification by 35 Hz in a water bath intermitted by 2 minutes of incubation on ice. The samples were then heated in the Thermocycler at 99 °C for 5 minutes to ensure protein denaturation, followed by centrifugation for 20 minutes at 20,000 x g to separate the cytosolic fraction. The supernatant was transferred to a new tube for every sample. The remaining pellet was suspended with 40 µl of 8 M Urea, followed by one cycle of sonification and 20 minutes of centrifugation by 20,000 x g. The supernatant was collected and combined with the previously collected supernatant in the newly prepared tubes. The protein samples were kept in a refrigerator pending further use.

2.3.2 Sodium Dodecyl Sulfate – Polyacrylamide Gel Electrophoresis (SDS-Page)

Electrophoresis is a major technique for separating proteins and nucleic acids according to their charge. This technique involves transporting the charged molecules through an immobilized medium, such as polyacrylamide gel, using an electric field. Polyacrylamide gels are the most used medium for protein separation due to their porous matrix with small pore size. In contrast, Agarose is mainly used for separating nucleic acids and large protein complexes. The Polyacrylamide gel also offers several advantages, including good chemical, temperature, and pH stability. Since there are different forms of PAGE, the SDS-PAGE is mostly used in laboratories for separating proteins based on their mass. Sodium Dodecyl Sulfate (SDS) is a detergent, that denatures proteins, cleaves the disulfide bonds in the presence of a reducing agent, and unfolds the proteins into linear chains. SDS then

binds to the protein backbone and makes them negatively charged proportional to the chain length. All negatively charged proteins are then traveling through the polyacrylamide matrix to the positively charged electrode. Proteins with lower mass travel faster than those with higher mass due to the small pore size of the polyacrylamide matrix. This results in proteins traveling different distances over a period, according to their size.

Table 5: Preparation of Polyacrylamide Gels

Reagents	**Separating gel (20 ml)**	**Stacking gel (7.5 ml)**	**Manufacturer**	**Catalog Number**
ddH_2O	6.4 ml	4.463 ml	-	-
1.5 M Tris-HCl (pH 8.8)	5.2 ml	-	Thermo Fisher Scientific	15568025
0.5 M Tris-HCl (pH 6.8)	-	1.875 ml	Thermo Fisher Scientific	21985023
10 % SDS	200 µl	75 µl	Carl Roth	2326.2-500g
30 % Acrylamide solution	8 ml	1.005 ml	Thermo Fisher Scientific	J62100.AP
10 % Ammonium persulfate	200 µl	75 µl		201530010
Tetramethylethylendiamine	20 µl	7.5 µl	Thermo Fisher Scientific	808742

Two glass plate chambers were placed on the designated rack and the separating gel was filled into the glass plate chamber, using a 1000 µl pipette. Isopropanol was added to the separating gel to remove any remaining air bubbles. After 15 minutes, the isopropanol was removed, and the glass chamber was filled with stacking gel using a 1000 µl pipette. A15–lane comb was inserted to create wells for loading the sample. After waiting an additional 15 minutes and ensuring the gel was ready, the glass chambers were placed into the electrophoresis container and the running buffer was added. Each gel contained 15 samples in total, 3 reference samples BSA, and 12 samples from previous protein extractions. The reference samples and each protein sample were labelled and prepared according to table 10 and filled into the designated well. The SDS-PAGE was started with a voltage of 75 V for 10 minutes and continued with 130 V for 100 minutes. After the

process was finished the gels were released from the glass chamber and transferred to a container for silver staining.

Table 6: Reagents and the respective volumes for SDS-PAGE

Reagent	**BSA (0.4)**	**BSA (0.8)**	**BSA (1.6)**	**Protein sample**	**Manufacturer**	**Catalog Number**
Protein lysate/BSA	2 µl	4 µl	8 µl	5 µl	Merck	A9418-100g
Loading buffer	3 µl	3 µl	3 µl	3 µl	Thermo Fisher Scientific	AM8546G
HPLC water	7 µl	5 µl	1 µl	4 µl	Thermo Fisher Scientific	51140

2.3.3 Silver staining for protein quantification

To obtain enough peptides in peptide preparation, protein quantification must be performed, to calculate the volume of solution used in peptide preparation (see section below). Protein quantification was performed, using the SilverQuest staining kit from Invitrogen, ThermoScientific, Germany. The gels were collected after the electrophoresis and transferred into a container used for silver staining. The fixation solution for the first step of silver staining was prepared with 20 ml ethanol, 5 ml acetic acid, and 25 ml MQ water. The solution was transferred to the container and the gel was incubated for 30 minutes with shaking at room temperature. After each step, the container was emptied from the previously added solution. 30 % Ethanol solution for the ethanol wash step (15 ml ethanol, 35 ml MQ water) was added to the container, followed by incubation for 10 minutes as above. For the sensitization step, sensitizer solution was prepared from 15 ml ethanol, 5ml sensitizer, and 30 ml MQ water and added to the container followed by another incubation period of 10 minutes as above. The ethanol wash step was repeated with 30 % ethanol solution and the water wash step was performed with 50 ml of MQ water and an incubation time of 10 minutes. Next, the staining solution, which consists of 0.5 ml stainer and 49.5 ml MQ water, was added to the container, followed by an incubation period of 15 minutes. 50 ml of MQ water was added and the container was shaken carefully for 10-30 seconds. The developing step was performed by adding 50 ml of developing solution, which consists of 5 ml of Developer, 1 drop of developer enhancer,

and 49.5 ml of MQ water. The gels were incubated as above for 4-10 minutes until the protein bands were visible. 2 ml of stopper solution was added before the protein bands got saturated. The gel was imaged at the ChemiDoc MP Imaging System (BioRad Laboratories) and analyzed in the Bio-Rad-Image-Lab Software to quantify the protein sample. The protein concentration was determined based on the BSA standard curve.

2.3.4 Generation of tryptic peptides

Approximately, 20 µg of total protein extracts were reduced and alkylated prior to processing by a previously described modified protocol for Filter-aided-Sample-preparation (FASP) (Scifo et al. 2015) to generate tryptic peptides for subsequent label-free quantitative mass spectrometry analysis. Samples were digested overnight with Trypsin (1:20; in 50 mM ammonium bicarbonate) directly on the filters, at 37 °C and precipitated using an equal volume of 2 M KCl for depletion of residual detergents. Tryptic peptides were then cleaned, desalted on C18 stage tips, and re-suspended in 20 µl 1 % FA for LC-MS/MS analysis. MS runs were performed with 4 biological replicates.

2.3.5 Liquid chromatography and tandem Mass Spectrometry analysis

Tryptic peptides were analyzed on a Dionex Ultimate 3000 RSLC nano system coupled to an Orbitrap Exploris 480 MS. Peptides were injected at starting conditions of 95 % eluent A (0.1 % FA in water) and 5 % eluent B (0.1 % FA in 80 % ACN), with a flow rate of 300 nL/min. They were loaded onto a trap column cartridge (Acclaim PepMap C18, 100 A, 5 mm x 300 µm i.d., #160454, Thermo Scientific) and separated by reversed-phase chromatography on an Acclaim PepMap C18, 100 A, 75 µm x 25 cm (both columns from Thermo Scientific) using a 75 min linear increasing gradient from 5 % to 31 % of eluent B followed by a 20 min linear increase to 50 % eluent B. The mass spectrometer was operated in data-dependent and positive ion mode with MS1 spectra recorded at a resolution of 120 K, mass scan range of 375 − 1550, automatic gain control (AGC) target value of 300 % (3×10^6) ions, maxIT of 25 ms, the charge state of 2-7, dynamic exclusion of 60 sec with exclusion after 1 time and a mass tolerance of 10 ppm. Precursor ions for MS/MS were selected using a top-speed method with a cycle time of 2 sec. A decision tree was used to acquire MS2 spectra with a minimum precursor signal intensity threshold of 3×10^5 for scan priority one and an intensity range of 1×10^4-3×10^5 for scan priority

two. Data-dependent MS2 scan settings were as follows: isolation window of 2 m/z, normalized collision energy (NCE) of 30 % (High-energy Collision Dissociation (HCD)), 7.5 K and 15 K resolution, AGC target value of 100 % (1×10^5), maxIT set to 20 and 50 ms, for scan priority one and two, respectively. Full MS data were acquired in the profile mode with fragment spectra recorded in the centroid mode.

2.3.6 Proteome database searching

Raw data files were processed with Proteome Discoverer™ software (v3.0.1.27, Thermo Scientific) using SEQUEST® HT search engine against the Swiss-Prot® *C. elegans* database (v2022-12-14). Peptides were identified by specifying trypsin as the protease, with up to 2 missed cleavage sites allowed and restricting peptide length between 7 and 30 amino acids. Precursor mass tolerance was set to 10 ppm, and fragment mass tolerance to 0.02 Da MS2. Static modifications were set as carbamidomethylated cysteine, while dynamic modifications included methionine and N-terminal loss of methionine, for all searches. Peptide and protein FDR were set to 1 % by the peptide and protein validator nodes in the Consensus workflow. Default settings of individual nodes were used if not otherwise specified. In the Spectrum Selector node, the Lowest Charge State = 2 and Highest Charge State = 6 were used. The INFERYS rescoring node was set to automatic mode and the resulting peptide hits were filtered for a maximum 1 % FDR using the Percolator algorithm in the Processing workflow. A second-stage search was activated to identify semi-tryptic peptides. Both unique and razor peptides were selected for protein quantification. Proteins identified by site, reverse or potential contaminants were filtered out prior to analysis.

2.4 Analyses of transcriptome and proteome data

2.4.1 Identification of age-sensitive genes (ASGs)

Analyses were conducted under the guidance of Dr. Maryam Keshavarz (Ehninger lab, DZNE). The identification of ASGs was performed using a rigorous statistical method applied to normalized read counts. Initially, the Wald test, part of the generalized linear model framework, was employed on the gene expression dataset to identify genes whose expression levels significantly changed with age. Age was treated as a continuous variable in the model to capture its incremental effect on gene expression. A linear model was fitted

for each gene with age as a predictor, and the 'glm' function in R was used to estimate the coefficients and their standard errors. The 'wald.test' function from the 'aod' package was subsequently invoked to calculate the Wald statistics and corresponding p-values, which determined the significance of the age coefficient for each gene.

To control for multiple comparisons, the p-values obtained from the Wald test were adjusted using the Benjamini-Hochberg procedure to control the false discovery rate (FDR). Genes were considered age-sensitive (ASGs) if they exhibited an adjusted p-value below a predefined threshold (FDR < 0.05) and had a significant age coefficient, indicating a meaningful change in expression with age.

2.4.2 Identification of the age-sensitive proteins (ASPs)

In this study, protein abundance data were extracted using the Protein Discoverer (PD) software, leveraging its time-series analysis capabilities to capture quantitative protein expression data across a spectrum of age groups, from young to old subjects. We performed analyses within PD to extract protein abundance data and conducted comparisons of young and old samples outside of PD after the initial extraction of data. This approach allowed us to analyze the dynamic changes in protein expression associated with aging. To address the inherent issue of missing values typical in label-free proteomics data, we employed a multivariate imputation approach (Kong et al. 2022) using the Iterative Imputer from the Python library scikit-learn, which is known for its robustness in handling missing data through an iterative process based on chained equations. This method is particularly effective as it accounts for the interrelationships among multiple variables, thus enhancing the accuracy of the missing data estimations.

To identify proteins that show significant changes in abundance with age, we conducted a one-way ANOVA (Mohallem et al. 2024), an approach well-suited for our dataset which includes multiple age groups. This analysis allowed us to discern statistically significant differences across these groups. Following the ANOVA, we applied a Bonferroni correction to adjust for multiple comparisons, a necessary step given the large number of proteins analyzed and the heightened risk of type I errors.

Proteins were considered age-sensitive (ASPs) if they exhibited an adjusted p-value below a predefined threshold (FDR < 0.05) after Bonferroni correction and demonstrated a consistent trend in abundance changes between young and old samples, indicating a

meaningful change in protein levels with age.

2.4.3 Gene ontology analysis

For the elucidation of the functional implications of transcriptome changes during aging in *C. elegans*, a rigorous Gene Ontology (GO) analysis was employed. This analysis was critical in annotating differentially expressed genes and proteins, thereby providing insights into the biological processes, molecular functions, and cellular components most changed during aging. The analysis harnessed WormBase (https://wormbase.org/), using the enrichment analysis tool to categorize gene products. The differentially expressed genes and proteins were segregated into the GO categories: “biological processes”, “molecular function”, and “cellular component”. GO analyses were carried out separately for up and downregulated ASGs. The outcome of the GO analysis was a curated set of ontological terms that provided a high-level summary of the functional attributes characterizing the transcriptomic changes in *C. elegans*.

2.4.4 Trajectory clustering in ASGs and ASPs

Transcriptomic data consisting of 3686 ASGs and proteomic data comprising 658 ASPs were analyzed. The input for this analysis was normalized read counts for genes and protein abundance measures for proteins, ensuring consistency and accuracy in downstream processes. Initially, the normalized data were processed to calculate the mean expression levels across different samples for each gene and protein, respectively. The data were then standardized using z-score normalization to facilitate comparability across genes and proteins. For clustering, the data were organized into an “ExpressionSet” object. Using the “Mfuzz” package in R, the genes and proteins were segregated into three distinct clusters based on their expression profiles. This decision was made after evaluating cluster definitions ranging from two to eight clusters, ultimately identifying three distinct trajectory clusters that effectively represented the flow of expression changes over time. The optimal fuzzifier value was determined via the “Mestimate” function within the “Mfuzz” toolkit.

The clustering results were visualized using the “Mfuzz. plot2” function, which facilitated the examination of gene and protein expression patterns across the predefined clusters.

For the transcriptomic data, gene identifiers (IDs) for each cluster were extracted and input

into the WormBase enrichment analysis tool to identify enriched GO terms. The top ten most significant GO terms for each cluster were recorded, highlighting the biological processes predominantly associated with the genes in each cluster.

For the proteomic data, the membership list for each cluster was first converted into corresponding gene IDs using the UniProt Retrieve/ID mapping platform. Like the transcriptomic data, these gene IDs were then analyzed using the WormBase enrichment tool to ascertain the top ten significant GO terms, which provided insights into the primary biological functions influenced by the proteins in each cluster.

2.4.5 Multidimensional scaling (MDS)

The identified ASGs and ASPs, respectively, were subjected to multidimensional scaling (MDS) analysis using the Python library “sklearn.manifold”. MDS is a dimension-reduction tool that provides a means to visualize the level of similarity of individual cases of a dataset. By applying MDS to the expression data of the identified ASGs and ASPs, a two-dimensional plot was generated, which facilitated the observation of patterns in gene and protein expression changes related to the aging process. The MDS plot clarifies the relationship between samples based on their transcriptomic and proteomic profiles.

2.4.6 Transcriptome and proteome-based vector distance calculation

To address age-dependent transcriptomic/proteomic changes developed across age groups, vector distances were calculated, comparing gene (protein) expression vectors for each sample with the average of the corresponding young adult D4 vectors. Specifically, the cosine distance between gene/protein expression vectors for each sample and the average expression vector of the young adult group (D4) were calculated using the Python function “scipy.spatial.distance.pdist”. These distances were plotted to visualize the divergence of gene or protein expression profiles from the young reference as the organism ages (showing, for each age group, the mean +/- SD of the distances to the average of the young adult D4 group).

2.4.7 Visualization of overall gene and protein expression changes

Visualizations of gene/protein expression changes across all ASGs/ASPs were generated as described below. First, min-max scaling was applied to the normalized read counts for transcriptomics and the normalized protein abundance data for proteomics using “MinMaxScaler” from Python library “sklearn.preprocessing”. The min-max scaling process adjusted the expression values of each gene and protein across all samples, setting the minimum expression value to zero and the maximum to one. Consequently, all intermediate values were scaled proportionately within this range. This normalization ensured that all genes and proteins, regardless of their baseline expression levels, could be compared on a uniform scale ranging from zero to one. To balance the direction of changes in the expression with aging, all the genes or proteins that decreased with age were multiplied by minus one. This inversion harmonized the direction of gene and protein expression changes, making all age-related shifts positive and thus comparable across the dataset. By flipping the sign of declining genes and proteins, the analysis avoided the neutralizing effect that would occur if increasing and decreasing trends were combined. These data were then plotted across all age groups included in the study.

2.4.8 Individual gene and protein-based progression analysis

The progressive age-related gene expression analysis involved a sequence of pairwise statistical comparisons between all age groups and a designated young reference group, in this case, D4. The objective was to determine the point in the organism's life where ASGs showed their last significant change relative to previous time points. Pairwise comparisons began with the young reference group (D4) and continued with each subsequent age group to detect the first instance of a statistically significant difference in gene/protein expression values (for transcriptomic data, normalized read counts were used; for proteomic data, protein abundance data was used). After identifying the first age at which a significant change from the young reference was observed, subsequent age groups were compared not against the baseline but against this initial point of change. The analysis proceeded with each age group, comparing it to the prior group where a significant change was noted. This process was iterated until the last available age group, D32 for transcriptomics and D28 for proteomics, was analyzed. For an age-related change to be progressive in the pro-aging direction it did not only have to be significant relative to

the previous time point, but it also had to point in the pro-aging direction. This requirement ensured that only consistent age-related progressions were accounted for. The age at which the last significant progression occurred relative to an earlier age group was then plotted, revealing the distribution of these last significant changes across different time points.

2.5 Identifying stable reference genes

2.5.1 Determination of criteria for reference gene selection

To thoroughly assess the stability of known reference gene expression during the aging process and identify the most stable genes that can be used as reference genes in aging qPCR experiments, a thorough approach was employed. This included robust statistical and quantitative analyses such as the calculation of the adjusted p-value (padj), which serves as a critical filter to reduce false-positive results. The base mean expression levels provided a quantitative reference for gene expression across all samples and conditions, establishing an average around which variability could be measured. Additionally, the lowest standard deviation percentage (%STDEV) across the genes was analyzed to identify those with the most consistent expression levels, an indispensable characteristic of reliable reference genes. Hence, to accurately assess the stability of gene expression during aging, extensive metrics — adjusted p-value (padj), base mean expression levels, and the lowest %STDEV — were evaluated for all the genes under study. These measures are essential for the prioritization of genes, ensuring the selection of those with the highest stability and adequate expression for reliable normalization in gene expression studies.

Applying these metrics, the analysis targeted the top 1000 genes with the most non-significant padj values to maximize the likelihood of identifying genes exhibiting stable expression throughout aging. This was followed by a refinement process, where any gene with a base mean expression level below 200 was excluded, thus narrowing the pool to include only those genes with sufficient expression levels. The subsequent phase involved a detailed examination of the standard deviation percentage of expression levels across various samples and conditions. The top 200 genes that demonstrated the lowest %STDEV were earmarked for additional scrutiny. The expression patterns of the top 50 genes from this subset were then visualized using Rstudio (Version 4.3.3) and GraphPad Prism (Version 9.3.1) to pinpoint the most stable genes. Using one-way ANOVA

as well as a careful visual assessment, 16 genes were selected for further validation by qPCR, under the guidance of Dr. Maryam Keshavarz (Ehninger lab, DZNE).

2.5.2 Primer design

The DNA sequences of the respective genes were extracted using the UCSC Genome Browser, which provides access to genomic sequences and annotations for a variety of species including *C. elegans*. Precise target regions were selected based on gene annotations, exon-intron boundaries, and conserved domains to prevent polymorphisms that could impair primer binding.

Primer-BLAST was then used, combining primer design with BLAST searches to establish optimal primer characteristics, including melting temperature (Tm), length, and GC content, while mitigating potential self-complementarity.

Simulated PCR was performed to verify the specificity of the primer designs, ensuring the exclusive amplification of the intended targets. The OligoAnalyzer tool from Integrated DNA Technologies further assisted in identifying potential secondary structures and dimer formations, which could compromise RT-qPCR performance.

Following *in silico* validation, empirical testing of the primers in RT-qPCR reactions was undertaken. This phase included adjustments of primer concentration, annealing temperature, and magnesium chloride concentration, which are essential for maximizing amplification efficiency and specificity.

2.5.3 cDNA Synthesis

A total of 500 ng RNA was used to perform cDNA synthesis, using the High-capacity cDNA RT kit from Thermo Fischer Scientific. 14.2 ng of RNA was added to the 5.8 µl PCR master mix solution (Table 7) in a labelled PCR microtube. The sample was mixed with a 20-µl pipette, briefly centrifuged, and placed into the RT-Thermocycler (program: 10 min 25 °C, 120 min 37 °C, 5 min 85 °C) for cDNA synthesis. After the program was finished, the cDNA was stored at -20 °C until further use.

Table 7: Reagents and volumes for PCR master mix solution

Reagent	Volume (µl)	Manufacturer	Catalog Number
10x RT buffer	2	Thermo Fisher	AM1006
25x dNTPs	0.8	Thermo Fisher	R0191
10x primers	2	IDT	-
Reverse Transcriptase	1	Invitrogen	18080044

2.5.4 Real-time quantitative PCR (RT-qPCR)

Real-time quantitative polymerase chain reaction (qPCR) is a method of choice for gene expression analysis in molecular biology laboratories due to its sensitivity, specificity, and simplicity. The qPCR method combines reverse transcription PCR (RT-PCR) with quantitative PCR and uses a fluorescent dye. In our lab, we used the RT-qPCR QuantStudio Flex 6 and 7 with SYBR Green Master Mix for gene expression analysis. SYBR Green is the most commonly used intercalating dye, which binds to the newly synthesized double-stranded DNA during the extension phase and emits a green fluorescent signal. The intensity of this signal is measured after each cycle and correlates to the amount of double-stranded DNA present in the sample. The qPCR starts with the initiation step, where no fluorescent intensity is detected. During the denaturation step, the sample is heated to 95 °C and the cDNA is denatured into single-stranded DNA. Next, in the annealing step, the temperature is lowered to 60 °C, allowing the primers, which are short DNA sequences that are complementary to the target sequence, to bind to the single-stranded DNA. In the extension phase (72 °C), the enzyme DNA polymerase binds to the primers and adds nucleotides to the DNA, extending the target sequence. During this process, the fluorescent dye SYBR Green binds to the double-stranded DNA and emits a fluorescent signal, which is detected by the machine. The intensity of the fluorescent signal correlates with the amount of generated dsDNA.

For running qPCR, we used the MicroAmp Optical 384-well plate and a prepared master mix solution, for each well according to Table 8. First, 5.8 µl of master mix solution was added to each well, followed by 4.2 µl of cDNA (2 ng/µl). The PCR plate was sealed with an adhesive cover and centrifuged for 1 minute to eliminate any air bubbles. Next, the plate was transferred to the QuantStudio Flex 6 and 7 qPCR machine, and the qPCR reaction was initiated. The amplification curve, which shows the increase in fluorescence

over time, was generated and interpreted as follows: at the beginning of the reaction, there is no fluorescence emitted, which serves as the baseline. As the reaction progressed, a lesser number of cycles were needed, because of the high number of templates, to reach the point where the fluorescent signal is statistically defined as CT value. However, the limited number of templates will eventually slow down the reaction, and the amplification curve will reach a plateau phase. Once the process is complete, the amplification plot is normalized to a fluorescent signal of 0.2 using a 50x low ROX, which helps eliminate pipetting errors or variations in RNA or cDNA quality. The results were then exported to Excel for further analysis.

Table 8: Master mix solution reagents for Real-Time PCR (qPCR)

Reagent	**Volume (µl)**	**Manufacturer**	**Catalog Number**
PCR MasterMix	5	Bio-Rad	1725121
Forward primer solution	0.3	IDT	-
Reverse primer solution	0.3	IDT	-
Low ROX 50x	0.2	Thermo Fisher	A41138

Table 9: Primer sequences

Gene	Known/New Reference gene	F (Forward sequence) 5' to 3'	R (Reverse sequence) 5' to 3'
pmp-3	known	TGCCTTGAAACTGATCGTCC	CTCTTCCTGCTCATCTCGTTC
ZK1307.8	new	TCCACAACTGACACCTTCCG	AGTTCCGGGCTCATCACTTC
aars-2	new	TGTGGTCTTGGACTCGAACG	CGAACGCCACTTCCTTTGTG
gtf-2F1	new	TTCCTGCCAGCGATTACTCA	ACGTTTCTGCTGCTCTGTCA
praf-3	new	AAGTTTTAAGATGCGCACGG	CAAGGCAAAGGCAACCACAA
unc-16	new	AACAAAATGGGCATGGCTGC	TCGTCTTGCCAGTCTTCGTT
orc-2	new	TGGAACAACTGGGCTTCGAG	CCATTTCCAGCACGTCTTCC
nasp-1	new	CGTCGTCGAGAAAAATCGCC	CGTCCTTGGTTTTGCCGAAG
ZK858.6	new	ATTTTTCGAGAGACCGCCCA	AGCCACTCCAGGCACATAAA
ddx-19	new	CCAGCTTTTGTTCCACGACC	CTTCTGTTGCCGGTTTCGTG
rbm-22	new	AAAATCTGTGAGCGCCCATTC	GTCTGGCACACATTCTTCACT
agef-1	new	CCGCGCAGAAGGAAAAAGAA	ATCAATCCGCGTACCACTTG
npp-2	new	TCCTCACCTGATGCACCTCT	AGTCGGAACTGCTGTGAGAC
rnp-6	new	TATCTTCAACCGGCATCCGT	CTCGGCGAATTAGAGAACAGGT
ran-5	new	CGCAATGGGACCAGAGATCA	CCAATTTCAGCAGGTCGCTC
ZK792.5	new	ATGGATAACTGGGCGGATGC	CAACCTTTGGCCTTGCTGAC

3 Results

3.1 Lifespan analysis and sample collection in *C. elegans*

The first objective of our research was to investigate mortality patterns during aging in *C. elegans*. Our study involved lifespan analysis of four cohorts, designated as WT-1, WT-2, WT-3, and WT-4, each comprising 400 specimens, to examine the consistency of survival rates among genetically identical groups. Censoring occurred predominantly at early ages, with 32 individuals censored in WT-1, 14 in WT-2, 31 in WT-3, and 47 in WT-4. Survival curves generated through the Kaplan-Meier method for each cohort allowed us to analyze the survival over the nematodes' lifespan. In the context of our experiments, the maximal lifespan was 34 days. A Log-rank (Mantel-Cox) test ($P = 0.9699$) revealed no significant difference in lifespans across the cohorts (Figure 1 A). Median survival times for WT-1, WT-3, and WT-4 converged on D24, while WT-2 exhibited a median survival of 26 days, indicating that the observed mortality patterns were overall fairly consistent. Interestingly and as expected (Brooks et al. 1994, Vaupel et al. 1994), the survival curves suggested a deceleration of mortality rates with advancing age, reflected in the tendency of the survival curves to show an inflection point at around D28.

For our study it was vital to monitor the gene expression changes into very advanced age given that we wanted to be able to capture a possible eventual stabilization of age-related changes in late life. To achieve this goal, we started sample collection from a large population around 3000 to compensate for attrition and included a broad range of time points, covering also very advanced ages. In Figure 1 B, we detailed a collection schedule across 15 time points from D4 to D32, each with six biological replicates. The schedule was adjusted to the observed survival data, making sure that advanced ages are represented in the collected samples.

A

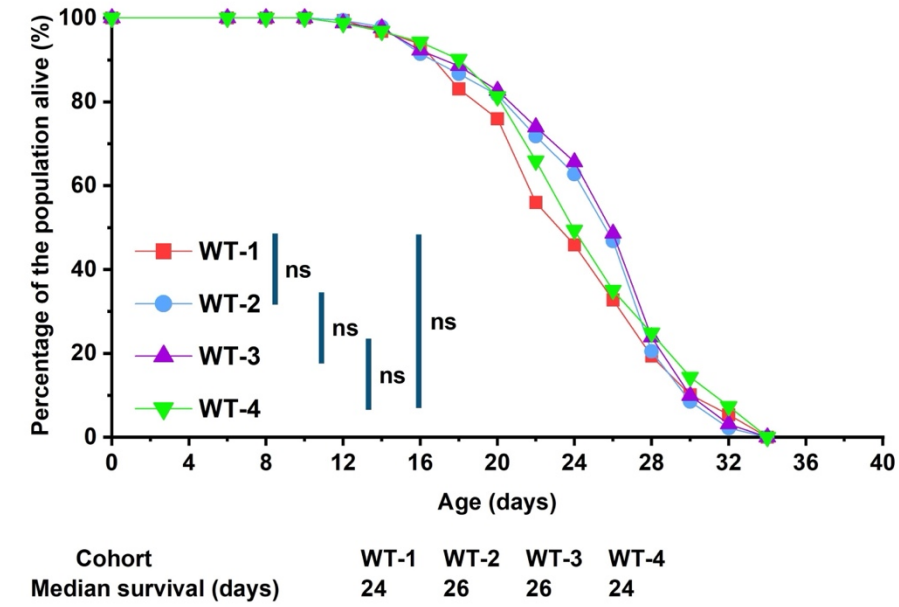

B

Time points	Replicates
D4	6
D6	6
D8	6
D10	6
D12	6
D14	6
D16	6
D18	6
D20	6
D22	6
D24	6
D26	6
D28	6
D30	6
D32	6

Figure 1: Lifespan and sampling strategy in *C. elegans*. (A) Survival curves for four cohorts (WT-1 to WT-4) of *C. elegans*, each starting with 400 individuals with Kaplan-Meier survival analysis. The lifespan data was analyzed using the Log-rank (Mantel-Cox) test (ns, p = 0.9699). (B) The collection schedule with 15 designated time points, each with 6 biological replicates (each biological replicate was comprised of a pool of 30 worms).

3.2 Comparative analysis of RNA isolation protocols across different *C. elegans* sample sizes in pooled samples

This part of our study aimed to optimize RNA isolation protocols to recover high-quality RNA from a limited number of worms.

To achieve this goal, we evaluated ten RNA isolation techniques across sample sizes varying from 5 to 100 worms (n = 5 to n = 100), the results of which are summarized in Figure 2 (A-J). This systematic approach enabled us to determine the efficiency and purity of RNA extraction protocols under conditions that mimic the typical sample limitations in aging studies.

The use of the Trizol extraction method (Figure 2 A) resulted in low RNA yields for the smallest cohorts, such as 1.1 ng/µl for ten worms (n = 10), which increased proportionally with the number of worms. However, purity assessments indicated contamination, with A260/A280 and A260/A230 ratios falling below optimal thresholds across all sample sizes. When combined with a Cleanup Kit (Figure 2 B), Trizol's effectiveness improved significantly, showing a substantial rise in RNA concentration, achieving up to 317.9 ng/µl

for 50 worms (n = 50). Nonetheless, the elevated A260/A280 ratios suggested persistent contamination by other nucleic acids, a pattern consistent across the tested range.

Employing the RNA mini Kit (Figure 2 C) alone or with Trizol (Figure 2 D) led to improvements in RNA yields, but did not resolve the presence of contaminants. For instance, when a pool of 100 worms was processed with the RNA mini Kit, we observed a high A260/A280 ratio of 2.38, yet the A260/A230 remained at a low 0.03, underscoring unresolved contamination.

Notably, the protocol using Trizol with proteinase K (Figure 2 E) for samples as small as five worms (n = 5) produced an exceptional RNA concentration of 3944.1 ng/µl, however A260/A230 ratio was still above the desired range.

The Plus Micro Kit protocols, both standalone (Figure 2 F) and with Trizol (Figure 2 G), showed fluctuating RNA yields and inconsistent purity ratios, such as an A260/A230 ratio of 0.59 for 50 worms (n = 50), indicating a need for method refinement to ensure reliability.

The PicoPure™ Kit (Figure 2 H) and its adaptation with Trizol (Figure 2 I) demonstrated variable efficiency, with some sample sizes showing significant purity levels but others, like the 100-worm group (n = 100) with an A260/A280 ratio of 2.59, indicating possible overestimation of RNA purity or contamination.

The optimization of the PicoPure™ Kit (Figure 2 J) produced promising outcomes. The optimization steps included an additional cycle of sonication with dry ice intervals and the application of DNase solution onto the purification column membrane. An optimized sample of 15 worms (n = 15) presented a substantial RNA concentration of 59.3 ng/µl and a near-optimal A260/A230 ratio of 2.16, reflecting the kit's improved efficiency at larger sample sizes (please see the method section for more details).

Our results shows that the RNA isolation efficacy from *C. elegans* is highly dependent on the chosen protocol and sample size. The Trizol method, although effective for RNA recovery, requires supplemental purification steps to enhance RNA purity. The combination of Trizol with proteinase K has proven as a superior protocol for obtaining high-quality RNA, especially from microscale samples. While the Plus Micro Kit and PicoPure™ Kit protocols show potential, their variable results highlight the need for ongoing refinement to achieve consistent RNA purity. This is particularly crucial for downstream applications such as qPCR and RNA sequencing, which necessitate RNA of the highest

integrity. Finally, the optimization of the PicoPure™ Kit method (Figure 2 J) was chosen for our project, 30 worms were collected for each replicate to ensure good RNA quality.

A — Trizol only

n	Nucliec Acid	Unit	A260 (Abs)	A280 (Abs)	A260/A280	A260/A230
10.00	1.1	ng/µl	0.03	0.02	1.12	0.12
20.00	3.7	ng/µl	0.09	0.06	1.47	0.11
30.00	4.2	ng/µl	0.11	0.07	1.61	0.44
50.00	4.3	ng/µl	0.11	0.05	1.99	0.17

B — Trizol with Clean-up Kit

n	Nucliec Acid	Unit	A260 (Abs)	A280 (Abs)	A260/A280	A260/A230
10.00	52.5	ng/µl	1.31	0.70	1.88	-0.75
20.00	59.7	ng/µl	1.49	0.49	3.06	-0.18
30.00	251.0	ng/µl	6.28	2.72	2.31	-0.75
50.00	317.9	ng/µl	7.95	3.71	2.15	-0.96

C — RNA mini Kit

n	Nucliec Acid	Unit	A260 (Abs)	A280 (Abs)	A260/A280	A260/A230
5.00	6.1	ng/µl	0.15	0.06	2.66	0.01
10.00	6.1	ng/µl	0.15	0.08	1.99	0.02
20.00	6.2	ng/µl	0.16	0.05	2.89	0.01
50.00	19.9	ng/µl	0.50	0.21	2.38	0.03
100.00	18.7	ng/µl	0.47	0.31	1.52	0.11

D — RNA mini Kit with trizol

n	Nucliec Acid	Unit	A260 (Abs)	A280 (Abs)	A260/A280	A260/A230
5.00	13.6	ng/µl	0.34	0.26	1.31	0.08
10.00	35.3	ng/µl	0.88	0.74	1.19	0.08
20.00	27.8	ng/µl	0.69	0.49	1.43	0.07
50.00	26.9	ng/µl	0.67	0.57	1.18	0.08
100.00	43.3	ng/µl	1.08	0.83	1.31	0.09

E — Trizol with proteinase K Kit

n	Nucliec Acid	Unit	A260 (Abs)	A280 (Abs)	A260/A280	A260/A230
5.00	3944.1	ng/µl	98.60	46.85	2.10	5.19
10.00	4342.1	ng/µl	108.55	49.85	2.18	6.47
20.00	3690.8	ng/µl	92.27	44.52	2.07	5.47

F — Plus micro only

n	Nucliec Acid	Unit	A260 (Abs)	A280 (Abs)	A260/A280	A260/A230
5	17.3	ng/µl	0.433	0.288	1.51	0.53
10	7.9	ng/µl	0.197	0.126	1.57	0.34
20	4.1	ng/µl	0.102	0.061	1.67	0.12
50	59.3	ng/µl	1.481	0.981	1.51	0.59
100	5.0	ng/µl	0.125	0.074	1.70	0.09

G — Plus micro with trizol

n	Nucliec Acid	Unit	A260 (Abs)	A280 (Abs)	A260/A280	A260/A230
5	92.1	ng/µl	2.302	1.591	1.45	0.43
10	74.3	ng/µl	1.858	1.254	1.48	0.46
20	113.7	ng/µl	2.842	1.952	1.46	0.42
50	82.9	ng/µl	2.072	1.385	1.50	0.37
100	99.8	ng/µl	2.495	1.570	1.59	0.60

H — PicoPure™ Kit with original protocol

n	Nucliec Acid	Unit	A260 (Abs)	A280 (Abs)	A260/A280	A260/A230
5	17.9	ng/µl	0.449	0.283	1.58	0.06
10	7.6	ng/µl	0.190	0.078	2.42	0.01
20	5.2	ng/µl	0.130	0.050	2.59	0.01
50	4.5	ng/µl	0.113	0.044	2.58	0.01
100	5.6	ng/µl	0.139	0.054	2.59	0.01

I — PicoPure™ Kit with trizol

n	Nucliec Acid	Unit	A260 (Abs)	A280 (Abs)	A260/A280	A260/A230
5	16.7	ng/µl	0.417	0.290	1.44	0.18
10	26.1	ng/µl	0.653	0.441	1.48	0.75
20	35.4	ng/µl	0.885	0.566	1.56	0.71
50	52.4	ng/µl	1.309	0.879	1.49	0.63
100	54.7	ng/µl	1.367	0.890	1.54	0.37

J — PicoPure™ Kit with optimization method

n	Nucliec Acid	Unit	A260 (Abs)	A280 (Abs)	A260/A280	A260/A230
10	39.5	ng/µl	64.600	1.616	0.759	2.13
15	59.3	ng/µl	1.854	0.872	2.13	2.16
20	66.8	ng/µl	2.986	1.386	2.15	1.91
25	92.1	ng/µl	1.516	0.719	2.11	1.84

Figure 2: Results under different RNA isolation protocols with different sample sizes in *C. elegans*. The comparison of different RNA isolation protocols (A-J), measuring each method's efficiency in isolating nucleic acids from a sample size of 5 to 100 worms. The data presentation focuses on absorbance at 260 nm to determine nucleic acid yields and ratios of A260/A280 and A260/A230 to evaluate purity. Red numbers denote problematic results, such as low purity ratios or values that suggest contamination. Green numbers indicate values within the desired range for RNA purity or concentration, highlighting optimal results. Black numbers represent baseline or intermediate outcomes, neither optimal nor critically deficient. (A) Trizol extraction alone resulted in the lowest yields, with declining purity suggested by negative purity ratios in larger sample volumes. (B) Combining Trizol with a Cleanup Kit significantly improved yield and purity, albeit with a slight reduction in purity at higher sample volumes. Utilizing RNA mini kits (C) with or without Trizol (D), yielded consistent results, while integrating proteinase K with Trizol (E) significantly boosted nucleic acid levels, though with a risk of other substance contamination, as indicated by elevated A260/230 values. (F) The Plus Micro Kit and its Trizol-combined version (G) provided moderate nucleic acid quantities with satisfactory

purity levels. (H) The original PicoPure™ RNA Isolation Kit and its Trizol-modified counterpart (I) showed limited success with small worm counts. (J) Optimized PicoPure™ RNA Isolation Kit methods displayed enhanced performance, with higher yields and better purity correlating with increased sample sizes.

3.3 Quality assessment of bulk RNA-seq data for aging studies in *C. elegans*

Aging manifests as a gradual accumulation of subtle transcriptomic alterations over time. Detecting of these modifications demands not just extensive but also highly accurate sequencing data. With this in mind, we performed a thorough quality assessment of our bulk RNA-seq transcriptomic data. The purpose of the analysis was to establish a rigorous quality control framework with multiple checkpoints for evaluating the transcriptomic data. By conducting this assessment, we aimed to prevent the conflation of technical noise with biological signals, which could lead to incorrect interpretations and conclusions.

Figure 3 shows data from one sample. With over 10 million sequences ranging from 18-111 bases and a calculated G+C content of 37 %, we ensured a comprehensive dataset for analysis. Although these metrics alone do not prove a broad representation of the genome, they provide a strong indication of sequencing depth and quality, laying a robust foundation for further analyses in aging research (Figure 3 A).

The uniformity of sequence quality across all tiles, as evidenced by the consistent dark blue coloration in the "Per tile sequence quality" chart, suggests to a level of consistency that is critical for identifying subtle transcriptomic variations associated with the aging phenotype. The absence of lighter shades suggested a lack of potentially problematic lower-quality sequences, which could introduce bias into the analysis (Figure 3 B). Other samples showed a similarly strong, uniform pattern with minimal lighter shades, reinforcing the reliability of the sequencing data across all samples.

The "Per base sequence quality" chart showed a high-quality onset with an expected slight decline toward the rear ends (Figure 3 C), which is consistent with the reduced availability of sequencing reagents. The stability in base quality aligns with the uniformity observed in Figure 3 B, ensuring that the high standards at the onset were maintained throughout the sequencing process. Similar trends were observed in other samples, confirming consistent high-quality sequencing throughout the dataset.

The minimal adapter content emphasized the efficiency of our library preparation (Figure 3 D). The integrity of our sequencing run, previously demonstrated in Figure 3 A

and B, was further confirmed, delineating a dataset not compromised by technical artifacts. Other samples displayed similarly low levels of adapter content, supporting the overall robustness and quality of the dataset.

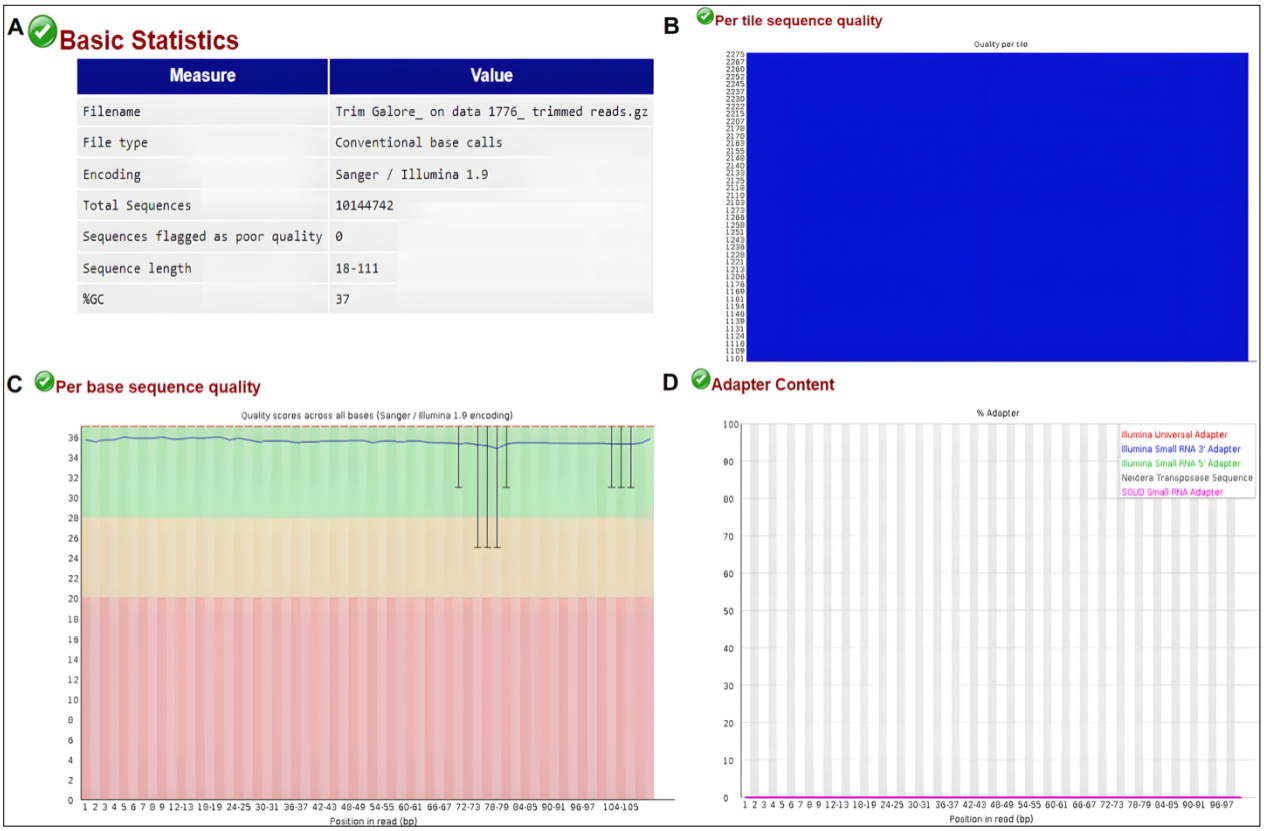

Figure 3: Quality assessment of bulk RNA-seq transcriptomic data in a sample. (A) Over 10 million sequences were processed, with a length range of 18-111 bases, and a G+C content of 37 %. (B) The "Per tile sequence quality" chart, indicates that the sequencing run had consistently high-quality scores across all tiles on the flow cell, as evidenced by the uniform dark blue coloration. There were no apparent deviations in the form of lighter shades, which would have suggested lower quality scores, reflecting a successful sequencing process with uniformly high data quality. (C) Quality scores start high (green zone) and show a typical decline toward the end of the reads. The chart's median and percentile indicators highlight the variation in quality at each base position. (D) The analysis shows the negligible presence of adapter sequences across the read lengths, suggesting effective pre-processing trimming or minimal adapter integration during sequencing.

3.4 Analyses of age-dependent transcriptomic changes in *C. elegans* populations

3.4.1 Identification of ASGs in *C. elegans*

To identify ASGs, we employed a methodological approach that combined the Wald test within a generalized linear model framework and the DESeq2 package to perform differential gene expression analysis. Each gene was modeled using age as a continuous predictor through the glm function in R, allowing for the estimation of coefficients and their standard errors. The significance of the age coefficient for each gene was then determined by calculating the Wald statistics and corresponding p-values using the “wald.test” function in R. The DESeq2 package was utilized to enhance the analysis, providing robust normalization and differential expression analysis capabilities. This dual approach ensured detection and quantification of gene expression changes. The final list of 3686 ASGs was derived from this combined analysis, incorporating the strengths of both the Wald test-based approach and DESeq2 to capture significant age-related changes in gene expression, setting the stage for all downstream analyses.

3.4.2 Gene ontologies associated with ASGs in *C. elegans*

To elucidate the functional consequences of gene expression changes during aging in *C. elegans*, we performed gene ontology (GO) analyses, focusing on ASGs identified above and comparing them against the entire genome of *C. elegans*, which includes all genes regardless of differential expression status. The enrichment analysis identified over-represented GO terms among differentially expressed genes, aligning our findings with established biological processes known to be associated with aging (Kim 2007, Vidović and Ewald 2022).

An Illustration of a functionally grouped network of GO terms linked to the 3686 ASGs is depicted in Figure 4 A. The gene network shows the interconnectivity of the biological processes associated with these ASGs. Nodes represent specific GO terms, sized proportionally to the significance of their enrichment, and connected by edges reflecting the kappa statistic, denoting shared genes between terms.

The network identifies several pathways linked in aging. Most notably, it confirms previously identified pathways linked to aging, such as the mitotic cell cycle, cell-cell adhesion, and sensory perception stimulus detection (Riera and Dillin 2016, Voutetakis et al. 2015), supporting the validity of our findings. Enrichment in pathways

such as epithelial cell differentiation and cilium organization emphasizes the importance of cellular integrity and signaling mechanisms. Similarly, pathways related to sensory perception, such as those involved in smell detection, highlight changes in the sensory system with aging (Doty et al. 1984, Linford et al. 2011, Riera and Dillin 2016).

Critical pathways related to cell cycle and DNA metabolic processes were highlighted, indicating potential alterations in DNA maintenance and metabolic regulation during aging. Moreover, our analysis corroborates pathways identified in earlier studies (Meng et al. 2020), such as mitotic nuclear division and RNA processing, which may contribute to cellular responses during aging by facilitating regulation of RNA synthesis and processing.

GO analyses were also carried out for up- and down-regulated ASGs separately (Figure 4 B). Among the upregulated genes, there was significant enrichment in terms such as cell projection (GO:0042995); cell projection organization (GO:0030030); cilium organization (GO:0044782); non-motile cilium assembly (GO:1905515); DNA-binding transcription factor activity (GO:0003700); transcription regulatory region nucleic acid binding (GO:0001067); double-stranded DNA binding (GO:0003690); sequence-specific DNA binding (GO:0043565); taxis (GO:0042330); non-motile cilium (GO:0097730).

Conversely, the downregulated genes showed significant enrichment in the following GO terms: membrane microdomain (GO:0098857), A band (GO:0031672), cellular component assembly involved in morphogenesis (GO:0010927), sarcomere organization (GO:0045214), structural constituent of cuticle (GO:0042302), muscle system process (GO:0003012), collagen trimer (GO:0005581), supramolecular polymer (GO:0099081), organic acid metabolic process (GO:0006082), and myofibril (GO:0030016).

These observations, supported by a strict false discovery rate (FDR < 0.05) to ensure statistical reliability, indicate that our results capture a broad spectrum of biological processes, molecular functions, and cellular components affected by aging (Evans et al. 2023). This analysis not only confirms known age-related pathways but also reveals new areas of potential interest for further study into aging mechanisms, demonstrating the robustness and reliability of our results (Li et al. 2022).

A

Network of GO terms

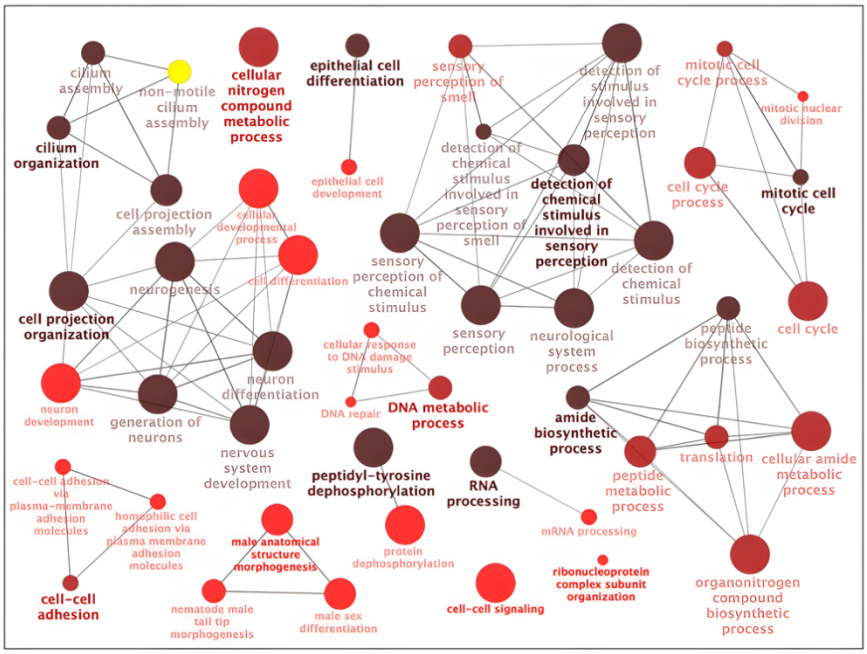

B

Up and down regulated genes GO analysis (Top 10)

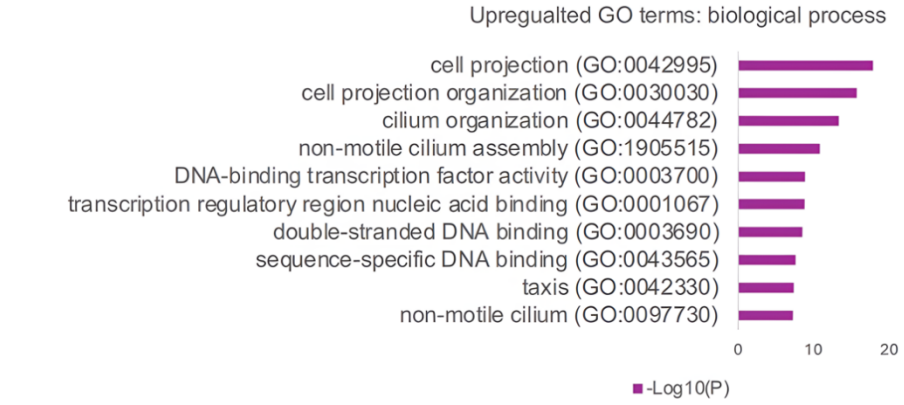

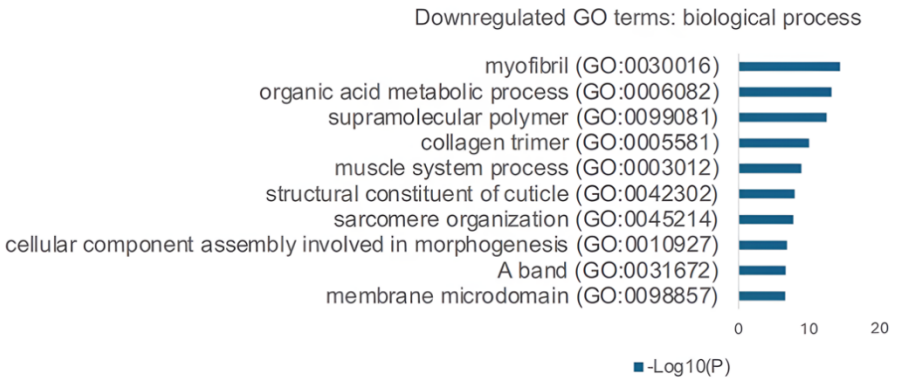

Figure 4: Gene ontology analysis of ASGs in *C. elegans*. (A) Functionally grouped network of GO terms associated with 3686 identified ASGs. Nodes represent GO terms linked by their kappa score, indicating shared genes between terms, with edge thickness denoting the strength of association. Node size correlates with the term's enrichment significance, with larger nodes representing more significant terms. The colors of the nodes differentiate between biological processes, molecular functions, and cellular components: red shades represent biological processes, yellow shades indicate cellular components, and darker tones correspond to molecular functions. Thicker edges indicate stronger associations between GO terms. (B) Top 10 enriched GO terms for upregulated and downregulated genes, indicating predominant biological themes influenced by differential gene expression. Enrichment fold change is quantified on the x-axis. Statistical relevance is established at FDR < 0.05, ensuring confidence in term associations.

3.4.3 Analysis of global trends in age-dependent transcriptomic changes

In the next step of our analysis, we wanted to assess global trends in age-dependent transcriptomic changes. Towards this end, we first applied min-max scaling to the normalized read count data of all ASGs, utilizing the "sklearn.preprocessing.MinMaxScaler" in Python. This preprocessing step adjusted the dataset, normalizing the range of expression values within each ASG such that the lowest recorded expression level was set to zero, and the highest to one, allowing for an equitable comparison across ASGs with varying baseline expressions. Further refining our analysis, we addressed the directionality of gene expression changes over the nematode's lifespan. For genes whose expression decreases with age, we reversed these values by multiplying them by minus one. This transformation ensured that all age-related changes were represented as positive values, thus simplifying the interpretation of trends across the dataset and preventing the confounding effect of combined increasing and decreasing trends.

Figure 5 illustrates the result of these analytical efforts. We observed a steady linear increase in transformed ASG values from D4 to D22, suggesting initially progressive departure from the young adult state. Beyond this age, a notable stabilization occurred in the expression patterns, suggesting no further age-related progression in age groups older than 22 days.

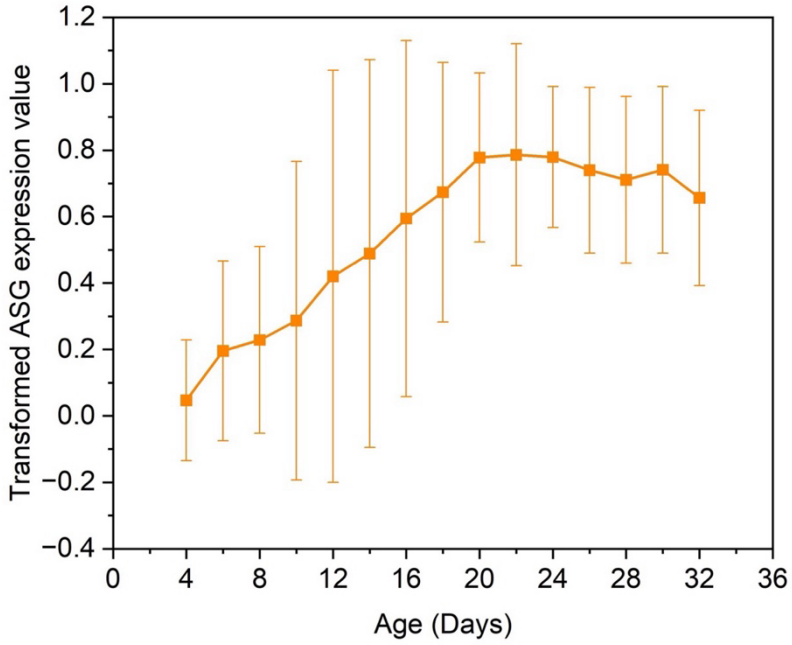

Figure 5: The graph depicts overall transcriptomic trends in *C. elegans* across various life stages. Transformed ASG expression levels steadily increased until reaching a point around D22, beyond which they stabilized, suggesting no further progression of transcriptomic changes in later life. Data shown represent means +/- SD.

3.4.4 ASG expression trajectories in *C. elegans*

A trajectory analysis was conducted on the 3686 ASGs that were identified in the previous section to identify groups of genes that follow similar temporal progressions during the aging process. The genes were ultimately classified into three distinct clusters, each representing unique expression patterns across the organism's lifespan. This decision followed an evaluation of cluster definitions ranging from two to eight clusters, with three clusters found to most effectively capture the expression changes over time.

The results of the trajectory analysis, encompassing all time points from D4 to D32, are shown in Figure 6 A. Cluster 1, consisting of 491 genes, exhibited a downward trend in expression levels, suggesting a possible downregulation of essential biological processes as the organism aged. This aligns with known age-related declines in metabolic and structural functions, consistent with findings in previous research on aging-related gene expression changes. Cluster 2, the largest cluster with 2,049 genes, displayed an increase in expression peaking at D24 before stabilizing, which may reflect a regulatory mechanism that activates key genes during mid-life to maintain cellular function and homeostasis. This

pattern is supported by previous studies indicating that mid-life stages involve adaptive responses that uphold vital processes. Conversely, Cluster 3, containing 1,146 genes, showed an increase in expression up to D18, followed by a decline at D22 and then a plateau, potentially indicating age-dependent shifts in gene regulation.

To gain further insight into the functional annotations of ASGs within these clusters, Gene Ontology (GO) enrichment analysis was performed using the WormBase enrichment tool (Figure 6 B). Cluster 1 genes were significantly enriched for GO terms related to organic acid metabolic processes (GO:0006082) and muscle system processes (GO:0003012), reflecting a documented decline in metabolic efficiency and muscular function during aging (Kirkwood 2005, López-Otín et al. 2013). Cluster 2 showed significant enrichment in GO terms such as gated channel activity (GO:0022836) and synaptic signaling (GO:0099536), consistent with findings that synaptic function plays a critical role in maintaining neurological health and adapting to the cellular changes that occur during aging (Citri and Malenka 2008).

The terms enriched in Cluster 3 included cell projection organization (GO:0030030) and neuron development (GO:0007399**).** While neuron development primarily occurs in early life (D4 and earlier), the continued regulation of related genes may be linked to maintaining neural function and plasticity throughout the lifespan, an aspect that remains essential for longevity and adaptation during aging (Kaletsky and Murphy 2010). The suggestion of links to neurodegenerative processes, as seen in higher organisms, is less applicable here, as *C. elegans* does not exhibit classic neurodegeneration during its aging process.

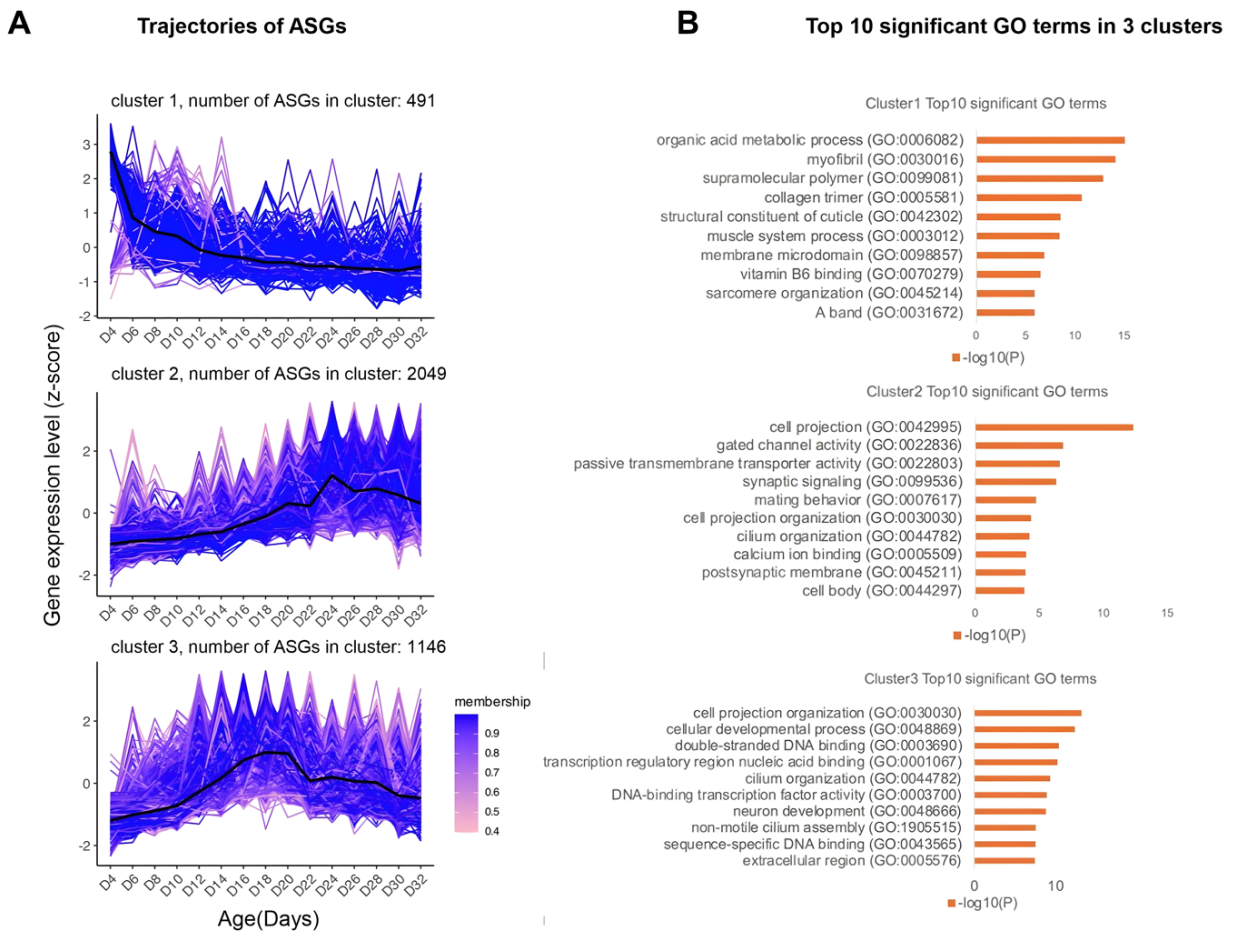

Figure 6: Gene expression trajectory clusters and GO enrichment analysis in *C. elegans*. (A) This panel illustrates the z-scored expression trajectories of ASGs across three clusters from D4 to D32. Line color codes for cluster membership strength. The black line shows the median expression trajectory within a given cluster. (B) The bar graphs represent the top 10 most significant Gene Ontology (GO) terms associated with each gene cluster, based on their -log10(p-value), signifying the enrichment significance.

3.4.5 Visualization of ASG vectors based on multidimensional scaling (MDS)

In our quest to comprehend the transcriptomic trajectory of *C. elegans* across its lifespan, we applied multidimensional scaling (MDS) to visually represent the complex gene expression data pertaining to ASGs. The MDS-generated plot (Figure 7) indicated that samples from the earlier adult stages of life, specifically from D4 to D10, clustered relatively closely together, suggesting relative stability of gene expression profiles in these earlier adult stages of life in *C. elegans*. The graphical representation further revealed a clear shift, with advancing age, of data points in phenotypic space. Importantly, this shift appeared to stop at some point (around D22), with no further progression away from the

younger age groups, suggesting a possible stabilization of changes in gene expression as the organism approaches the later stages of its lifespan.

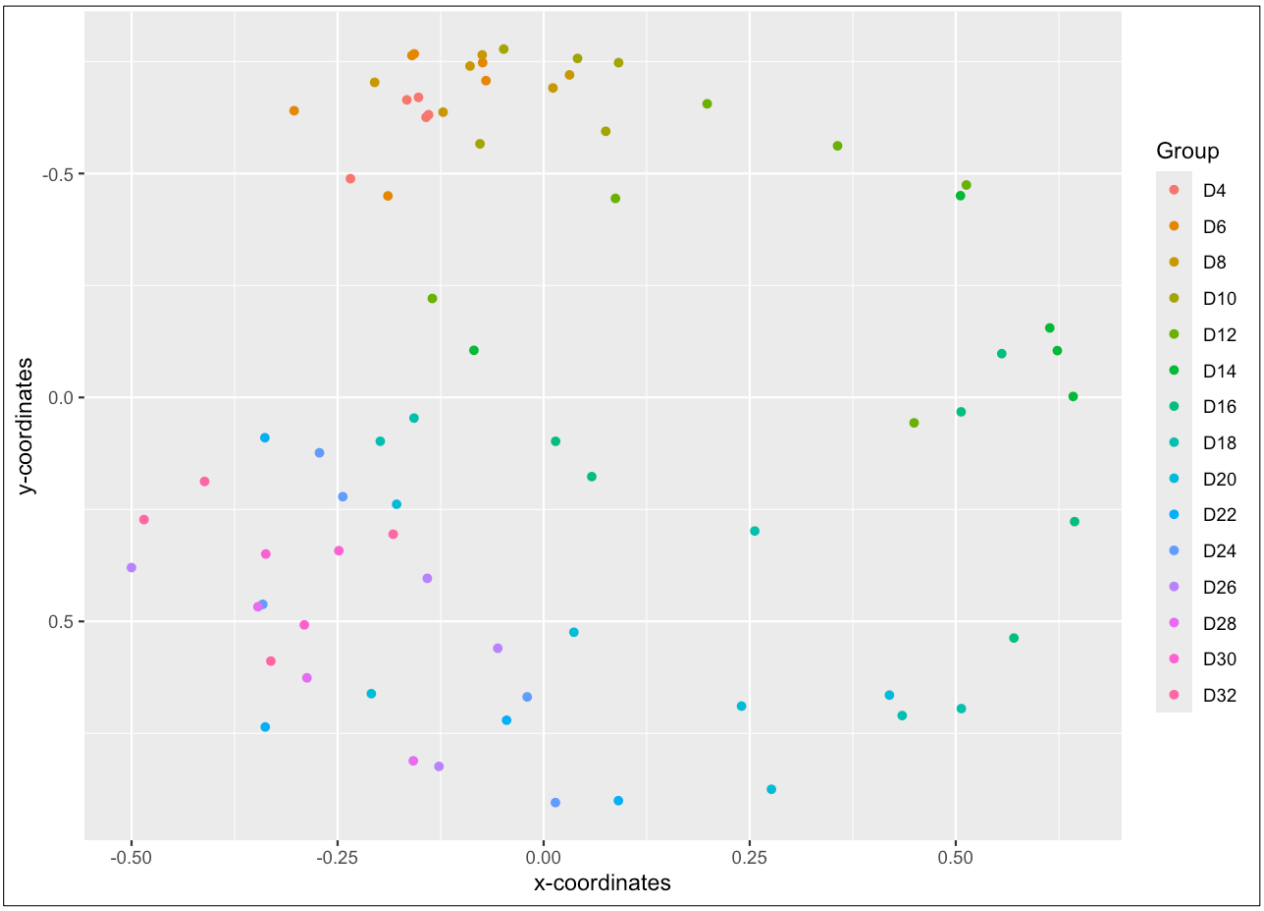

Figure 7: Multidimensional scaling (MDS) plot of transcriptomic vectors based on ASGs. MDS plot visualizes gene expression changes in *C. elegans* over its lifespan. Each data point corresponds to a sample. D4-D10 samples are in relative proximity to each other. With advancing age, the shift of data points away from D4 samples reflects age-dependent transcriptomic changes relative to the young adult baseline. Post-day 22, data points appear to lack a further progression away from the young adult samples, suggesting stabilized gene expression in late life.

3.4.6 Transcriptome-based vector distance calculation

To elucidate the dynamics of gene expression across the lifespan of *C. elegans* in high-dimensional space, we embarked on an analysis rooted in the comparative quantification of transcriptomic deviations. In this analysis the average of ASG vectors of the young adult (D4) group (geometrically corresponding to the center of the D4 vectors) was used as reference, and served as a benchmark against which we measured the cosine distances of gene expression profiles from various age stages (from D6 to D32; focusing on ASGs

only), using the pdist function from the scipy.spatial.distance library which computes pairwise distances between observations in n-dimensional space. The rationale for this approach was to visually and quantitatively capture the transcriptomic drift as *C. elegans* aged. In this analysis, younger samples, those in close chronological proximity to the D4 reference, exhibit gene expression profiles largely like this early adult stage. In the schematic shown in Figure 8 A, this is indicated by the relative proximity of data points corresponding to young samples to the D4 center. With advancing age, in contrast, we expected a larger sample distance to the D4 center (Figure 8 A).

Figure 8 B shows the trajectory of transcriptome-based vector distances in high-dimensional space from the D4 center throughout the nematodes' lifespan. Specifically, this panel shows means +/- standard deviations for each age group of cosine distances of individual sample's ASG vectors relative to the average of the young adult (D4) ASG vector. We noted an increase in distance across age groups, taking place between D4 and D22, after which the distances plateaued, hinting at an emergent phase of transcriptomic stability in later life stages.

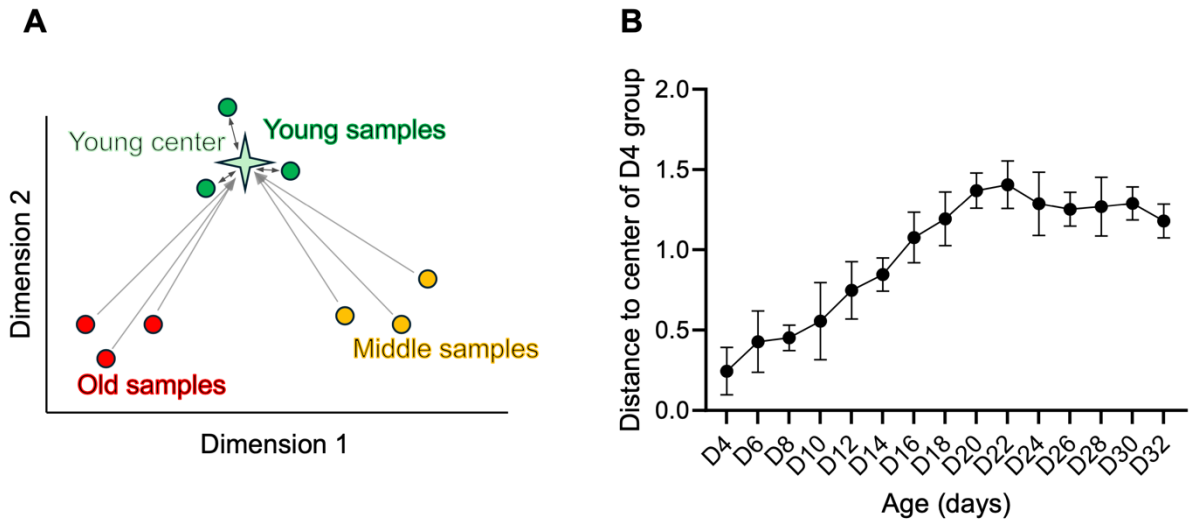

Figure 8: Transcriptome-based vector distance analysis. (A) Schematic representation of gene expression states in *C. elegans*. The center (marked by the star) represents the averaged ASP gene expression state in young adult animals (i.e., at D4). Green points depict young samples clustered tightly around this D4 center, reflecting their similarity in gene expression to the average D4 state. Yellow points represent mid-aged samples, and red points represent old samples, plotted further away from the D4 center, illustrating the progressive divergence in gene expression with age. (B) The plot shows the evolution of

transcriptome-based vector distances from the D4 young reference across the worms' lifespan. Each point represents, for each age group, the average cosine distance across all samples in that age group to the D4 center. Error bars denote standard deviations of the corresponding distance distributions. A clear progressive increase in distances to the young D4 center is observed between D8 and D22, after which this development plateaus, suggesting a stop in progression of age-related transcriptomic change.

3.4.7 Analysis of age-dependent change in individual ASGs

Next, we wanted to study age-dependent expression changes in specific genes to better define aging trajectories within individual ASGs. Towards this end, we performed pairwise comparisons of normalized read count data for individual ASGs across age groups, starting with a comparison against the young adult (D4) reference group and asking at which age a significant difference to the young adult baseline is first detected. Following the identification of an age at which a significant deviation from the young reference was noticed, all subsequent (i.e., older) age groups were compared against this initial point of change instead of the D4 baseline, asking if any of the subsequent age groups showed a significant progression in the pro-aging direction beyond this initial point of change. This process was repeated until the last age group (D32) was examined. For a change to be considered significantly deviating from the baseline/a subsequent age group, it had to not only be statistically significant in the respective pairwise comparison but also had to point in the respective pro-aging direction (see Material and Methods for details). This requirement ensured that only consistent age-related progressions were accounted for. The age at which the last significant progression occurred relative to an earlier age group was then plotted, revealing the distribution of these last significant changes across different time points (Figure 9 A). If aging was an ever-progressing phenomenon, we would expect a considerable proportion of ASGs to feature last changes at the last time point (D32). In contrast, if it was not ever-progressing it would be expected to see last changes mainly at time points distinct from the oldest age group (D32).

Figure 9 B illustrates the distribution of ages at last significant changes in ASG expression. We observed a peak of last significant changes in expression across ASGs at D20, indicating that ASGs featuring no further change in the pro-aging direction past D20 were common.

In the next step, we divided the ASGs into two categories based on their direction of change. The first set of ASGs with “increased” expression and the second set of genes

with “decreased” expression. We then performed the same analysis as before, this time separately for each increasing or decreasing group. ASGs with aging-associated increases in expression showed a peak in distribution at D20 (Figure 9 C), while ASGs with age-related decreases in expression had a distribution peak at D18 (Figure 9 D). This implies that ASGs commonly do not follow an ever-progressing pattern of change during aging, irrespective of their direction of changes in their expression.

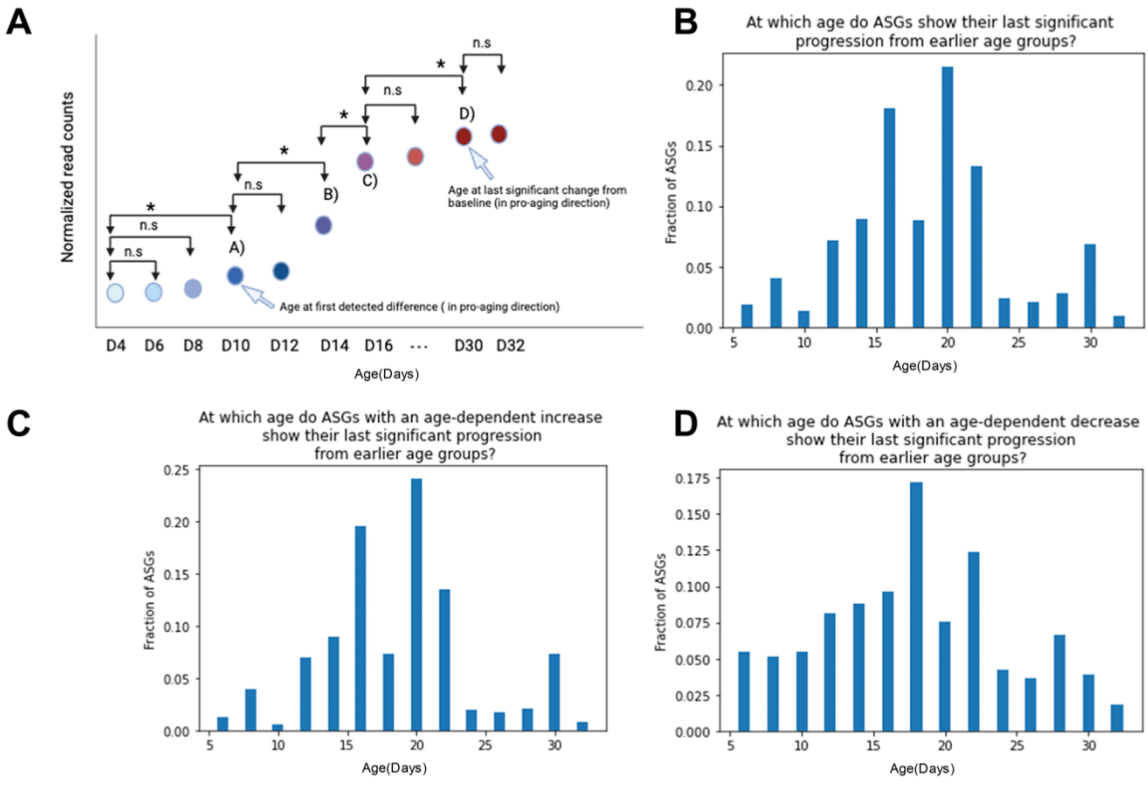

Figure 9: Individual gene-based progression analysis in *C. elegans*. (A) Systematic comparisons were conducted across age groups, starting with the baseline D4 group, to identify when age-sensitive genes (ASGs) first and last exhibited significant deviations. (B-D) The histograms depict the distribution of the last significant changes in expression among all ASGs (B), ASGs associated with age-dependent increases in expression (C) and ASGs associated with age-dependent decreases in expression (D). Overall, there were few ASGs that featured last changes relative to previous time points at D32, suggesting that most ASGs did not follow patterns consistent with ever-progressing change.

3.5 Analyses of age-dependent proteomic changes in *C. elegans* populations

3.5.1 Protein expression profiling in *C. elegans*

To identify ASPs in *C. elegans*, we analyzed the expression of proteins across various life stages. Utilizing Protein Discovery (PD) software, we extracted protein abundance data through a time-series analysis, capturing quantitative changes across a broad age spectrum. In label-free proteomics, missing values are a common challenge due to several factors, including the stochastic nature of mass spectrometry detection, variations in sample preparation, and the presence of low-abundance proteins that fall below the detection threshold. These missing values can introduce biases and reduce the statistical power of downstream analyses if not appropriately handled. It is crucial to impute these missing values to ensure the completeness and accuracy of the dataset, allowing for more reliable identification of age-related changes in protein expression. Given the inherent issue of missing values in label-free proteomics (Jin et al. 2021, Kong et al. 2022), we employed a multivariate imputation approach using “sklearn’s IterativeImputer” in Python. This is a strategy for imputing missing values by modeling each feature with missing values as a function of other features in a round-robin fashion. This imputation approach not only addressed the missing data effectively but also preserved the relationships among multiple variables, enhancing the overall data integrity and reliability of our subsequent analyses (Kong et al. 2022).

To pinpoint significant alterations in protein abundance that correlate with aging, we performed a one-way ANOVA on the imputed dataset. Recognizing the potential for type I errors due to the large number of proteins analyzed, we applied the Bonferroni correction to adjust for multiple comparisons, ensuring that our findings were statistically robust. This rigorous approach led to the identification of 658 ASPs that exhibited significant changes in abundance with age.

3.5.2 ASP expression trajectories in *C. elegans*

In our proteomic analysis of *C. elegans*, we conducted a detailed classification of 658 ASPs, categorizing them into three distinct clusters according to their expression profiles from D4 to D28. This decision also followed an evaluation of cluster definitions ranging from two to eight clusters, with three clusters effectively capturing the expression changes over time.

Figure 10 A depicts the z-scored expression trajectories of ASPs across the studied time frame. Cluster 1 contained 141 proteins and showed a trend of a progressive increase until D20 and then a decline until D24 following by a plateau phase. The largest cluster, Cluster 2, included 339 proteins which showed a progressive decrease until D22 followed by a plateau phase. Cluster 3, which consists of 178 proteins, exhibited an initial phase of relatively stable expression levels from D6 up to approximately D12. This phase was followed by a gradual increase between D14 and 18, culminating in a pronounced peak at D20. After reaching this peak, the expression levels began to decline steadily and eventually stabilized in the later stages of the observed period.

Figure 10 B complements these findings with a functional enrichment analysis of the protein clusters. The bar graphs illustrate the top 10 most significant Gene Ontology (GO) terms associated with each cluster, selected based on their statistical significance as indicated by -log10(p-values). For instance, Cluster 1 proteins are significantly associated with GO terms such as chromatin organization (GO:0006325), a key process in the regulation of gene expression that is intimately connected with aging and longevity (Kim et al. 2012, Tissenbaum and Guarente 2001). Proteins in Cluster 2 show enrichment in functions such as the cytosolic large ribosomal subunit (GO:0022625), integral to protein synthesis, which often becomes dysregulated with age (Rath 2020, Turi et al. 2019). Notably, Cluster 3 proteins are related to GO terms involving detoxification (GO:0098754) and the cellular response to toxic substances (GO:0097237), which are critical for cellular homeostasis and commonly implicated in the aging process (Ullah et al. 2024, Živančević et al. 2021).

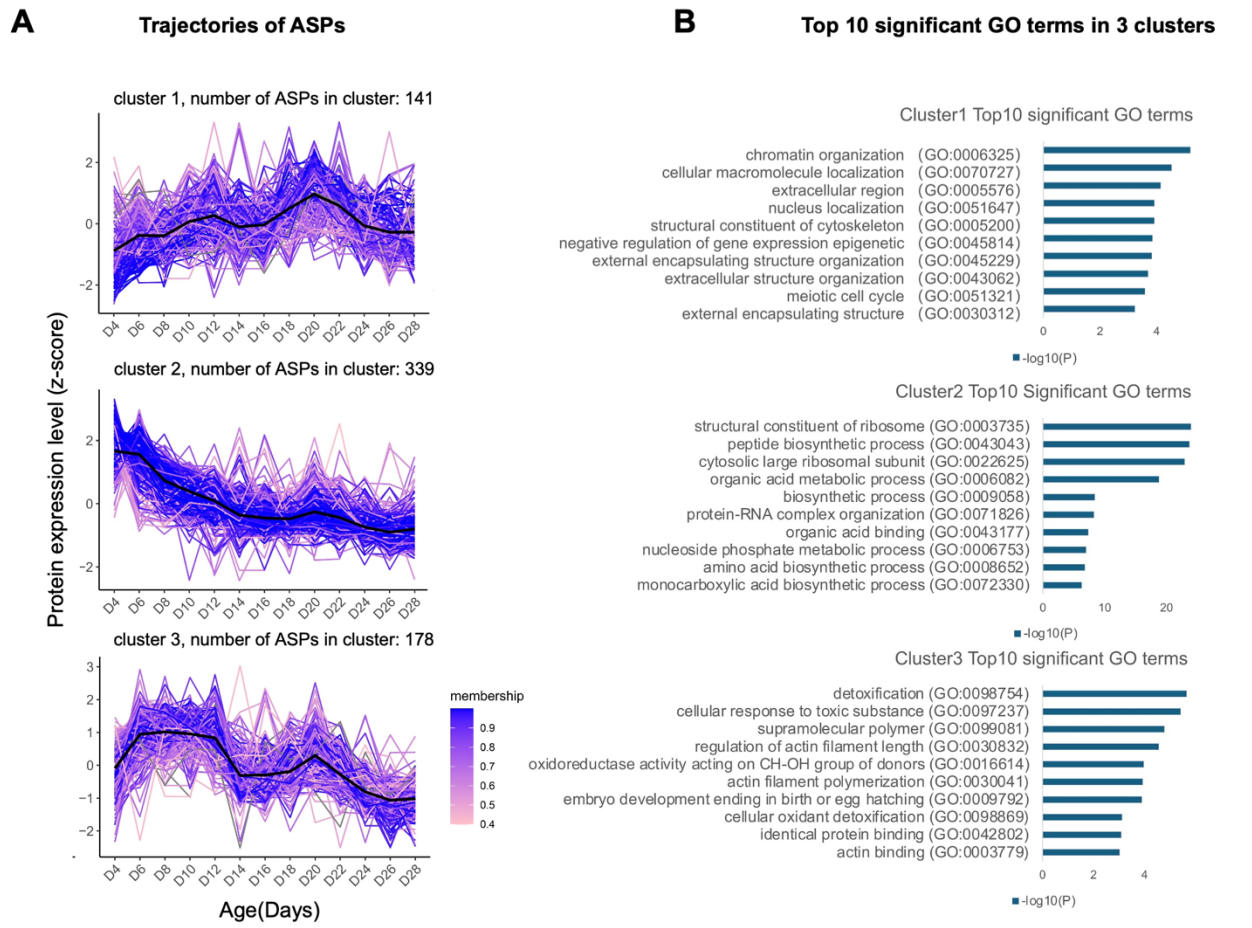

Figure 10: Protein expression trajectory clusters and GO enrichment analysis in *C. elegans*. (A) This panel presents the z-scored expression profiles of ASPs categorized into three clusters over D4-D28. Each pink, purple and blue line represents the trajectory of an individual protein's expression, while the black line highlights the median trend within each cluster. (B) The bar graphs display the top 10 most significant Gene Ontology (GO) terms for each protein cluster, as determined by their -log10(p-value), a measure of enrichment significance.

3.5.3 Analysis of global trends in age-dependent proteomic changes

We wanted to assess global trends in age-dependent proteomic changes. Towards this end, we first applied min-max scaling to the protein abundance data of all ASPs, utilizing the “sklearn.preprocessing.MinMaxScaler” in Python. This process involved adjusting the protein expression levels so that the minimum observed value, within a given ASP, was anchored at zero, and the maximum at one. This normalization allowed for a more straightforward comparison across proteins with diverse expression levels.

Further refining our analysis, we addressed the directionality of protein expression changes over the nematode's lifespan. For proteins whose expression decreases with age, we reversed these values by multiplying them by minus one. This transformation ensured that all age-related changes were represented as positive values, thus simplifying the interpretation of trends across the dataset and preventing the confounding effect of combined increasing and decreasing trends.

Figure 11 presents the results of these analyses. The graph shows an age-dependent increase in transformed protein levels with a possible stabilization in the most advanced age groups, although this is less clear than in our transcriptome-based analyses.

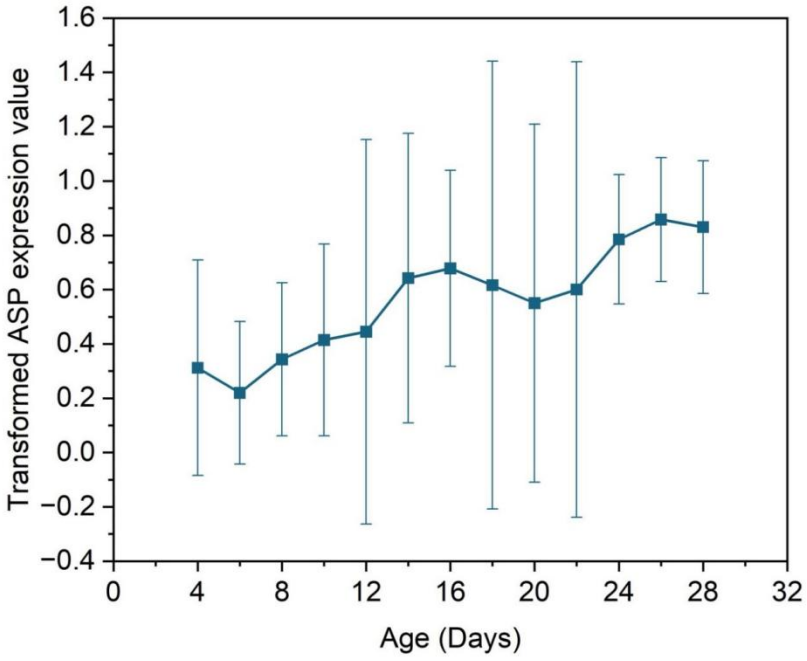

Figure 11: The graph depicts overall proteomic trends in *C. elegans* across various life stages. Transformed ASP expression levels increase with advancing age, with a possible stabilization in the most advanced age groups. Data shown represent means +/- SD.

3.5.4 Visualization of ASP vectors based on multidimensional scaling (MDS)

To further delineate the proteomic landscape of *C. elegans* across its lifespan, we employed multidimensional scaling (MDS) to aid in the interpretation of the complex patterns of protein expression changes associated with aging. The resulting MDS plot (Figure 12) delineates the proteomic trajectory from D4 to D28, providing a visual representation of protein expression dynamics in response to aging.

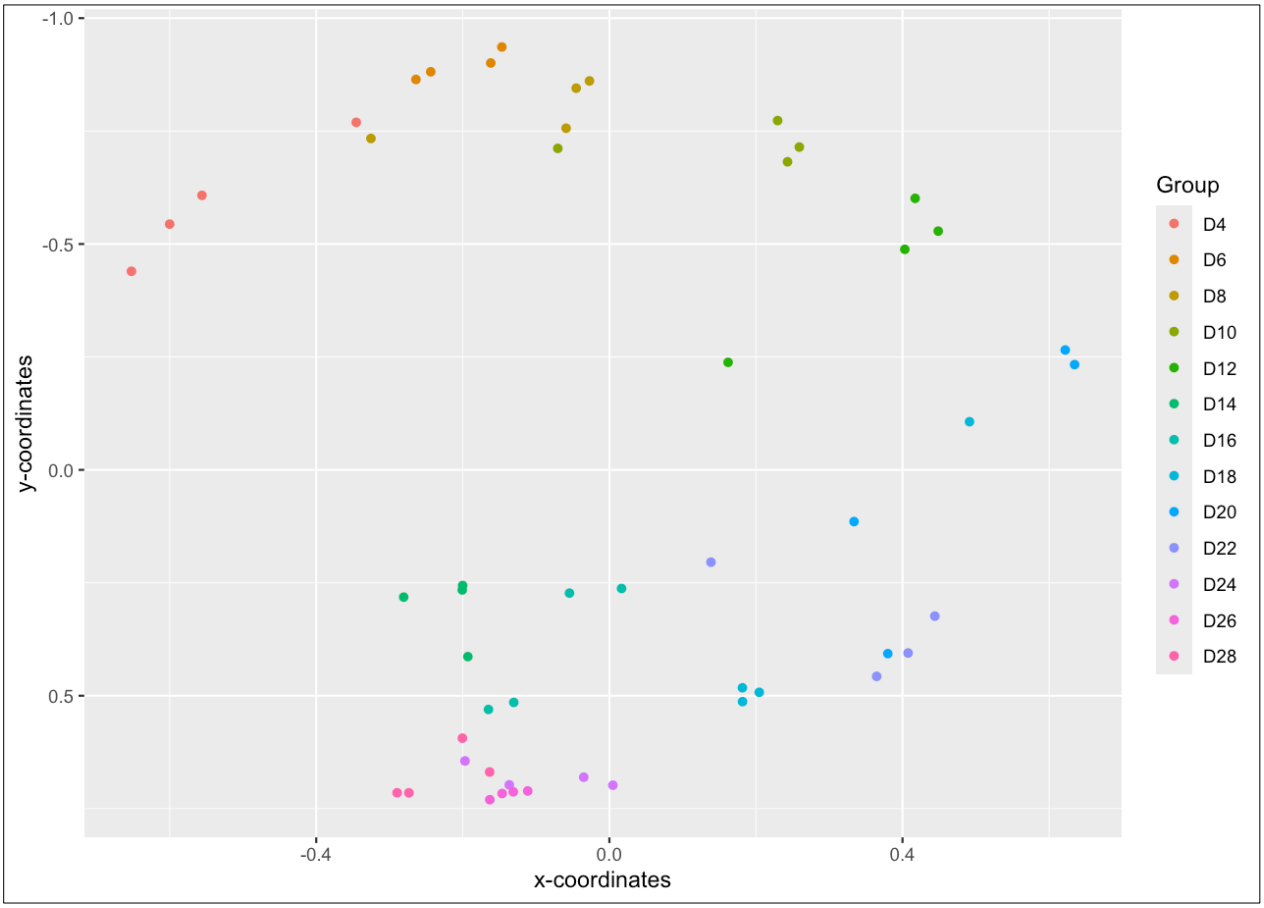

Figure 12: Multidimensional scaling (MDS) plot of proteomic vectors based on ASPs. MDS plot visualizes protein expression changes in *C. elegans* over its lifespan. Each data point corresponds to a sample. D4-D10 samples are in relative proximity to each other, at least with respect to their y-coordinates. With advancing age, the shift of data points away from D4 samples (mainly along the y-coordinates) reflects age-dependent proteomic changes relative to the young adult baseline. Post-day 24, data points appear to lack a further progression away from the young adult samples, suggesting stabilized protein expression in late life.

In the younger adult age groups, spanning D4 to D10, the data points are distributed with moderate dispersion rather than forming a tightly clustered group. This distribution

indicates some variability in the proteomic profiles during the early developmental stages of the nematode, suggesting a level of heterogeneity in protein expression patterns that still maintains a degree of similarity characteristic of this phase

As the organism matured beyond D10, the plot revealed a progressive shift of data points along the y-coordinates.

Post-day 24, a notable convergence in the distribution of data points was observed, consistent with a relative stabilization of proteomic profiles and a lack of further change away from the young adult reference group (D4).

3.5.5 Proteome-based vector distance calculation

To investigate the dynamic changes in protein expression throughout the lifespan of *C. elegans*, we conducted a proteome-based vector distance calculation in high-dimensional space, using the average of D4 vectors as a reference point. The analysis employed protein expression data (protein abundance vectors including data from all ASPs), charting the cosine distances of protein expression profiles from all samples of various stages of life (D6-D24) relative to the average D4 center.

Figure 13 A illustrates the proximity of younger samples shown in cyan to the average D4 center, indicating a high similarity in their protein expression profiles to the young adult state. Yellow points represent mid-aged samples and red points represent older samples, plotted further away from the average D4 center, signifying a divergence in protein expression as the nematode ages.

Figure 13 B shows the results of proteome-based vector distance analysis in high-dimensional space, showing cosine distance to the D4 center point for samples from all age groups. We noted a pronounced linear increase in distance with advancing age, based on changes mainly from D4-D14, after which the distances plateaued, hinting at an emergent phase of proteomic stability in later life stages.

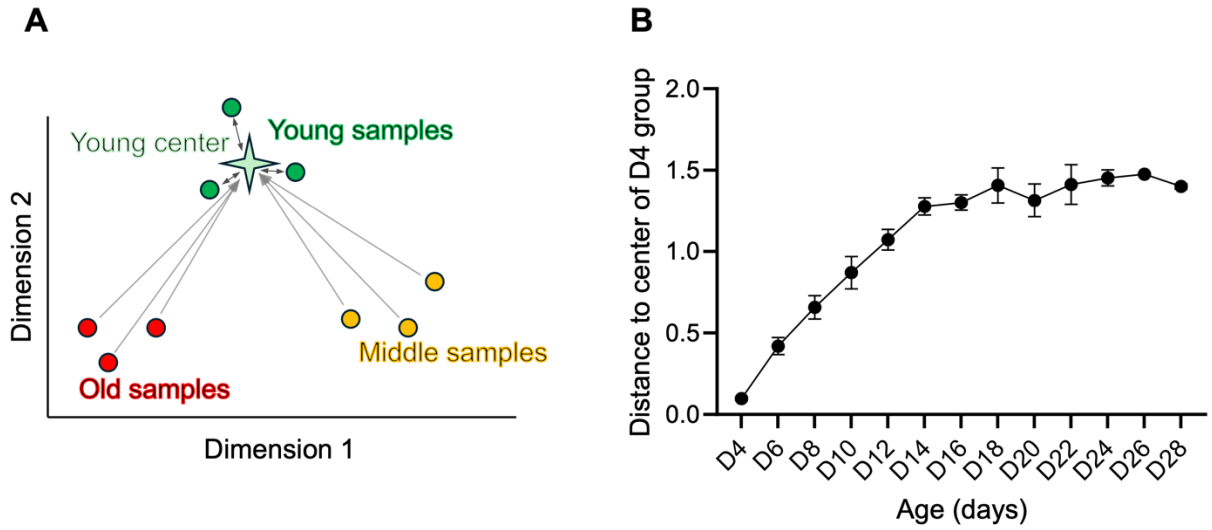

Figure 13: Proteome-based vector distance analysis. (A) The center (marked by the star) represents the averaged ASP expression state in young adult animals (i.e., at D4). Green points depict young samples clustered tightly around this D4 center, reflecting their similarity in protein expression to the average D4 state. Yellow points represent mid-aged samples, and red points represent old samples, plotted further away from the D4 center, illustrating the progressive divergence in protein expression with age. (B) The plot shows the evolution of proteome-based vector distances away from the D4 young reference across the worms' lifespan. Each point represents, for each age group, the average cosine distance across all samples in that age group to the D4 center. Error bars denote standard deviations of the corresponding distance distributions. A clear progressive increase in distances to the young D4 center is observed between D4 and D14, after which this development plateaus, suggesting a stop in progression of age-related proteomic change.

3.5.6 Analysis of age-dependent change in individual ASPs

Next, we wanted to study age-dependent expression changes in specific proteins to better define aging trajectories within individual ASPs. Towards this end, we performed pairwise comparisons of protein abundance data for individual ASPs across age groups, starting with a comparison against the young adult (D4) reference group and asking at which age a significant difference to the young adult baseline is first detected.

Following the identification of an age at which a significant deviation from the young reference was noticed, all subsequent (i.e., older) age groups were compared against this initial point of change instead of the D4 baseline, asking if any of the subsequent age groups showed a significant progression in the pro-aging direction beyond this initial point of change. This process was repeated until the last age group (D28) was examined. For a change to be considered significantly deviating from the baseline/a subsequent age

group, it had to not only be statistically significant in the respective pairwise comparison but also had to point in the respective pro-aging direction (see Material and Methods for details). This requirement ensured that only consistent age-related progressions were accounted for. The age at which the last significant progression occurred relative to an earlier age group was then plotted, revealing the distribution of these last significant changes across different time points (Figure 14 A). If aging was an ever-progressing phenomenon, we would expect a considerable proportion of ASPs to feature last changes at the last time point (i.e., at D28). In contrast, if it was not ever-progressing it would be expected to see last changes mainly at time points distinct from the oldest age group (D28).

Figure 14 B illustrates the distribution of ages at last significant changes in ASP expression. We observed a peak of last significant changes in expression across ASPs at D26, indicating that ASPs featuring no further change in the pro-aging direction past D26 were common.

In the next step, we divided the ASPs into two categories based on their direction of change. The first set of ASPs with “increased” expression and the second set of genes with “decreased” expression. We then performed the same analysis as before, this time separately for each increasing or decreasing group. ASPs with aging-associated increases in expression showed a peak in distribution at D12 (Figure 14 C), while ASPs with age-related decreases in expression had a distribution peak at D26 (Figure 14 D). This implies that ASPs commonly do not follow an ever-progressing pattern of change during aging, irrespective of their direction of changes in their expression.

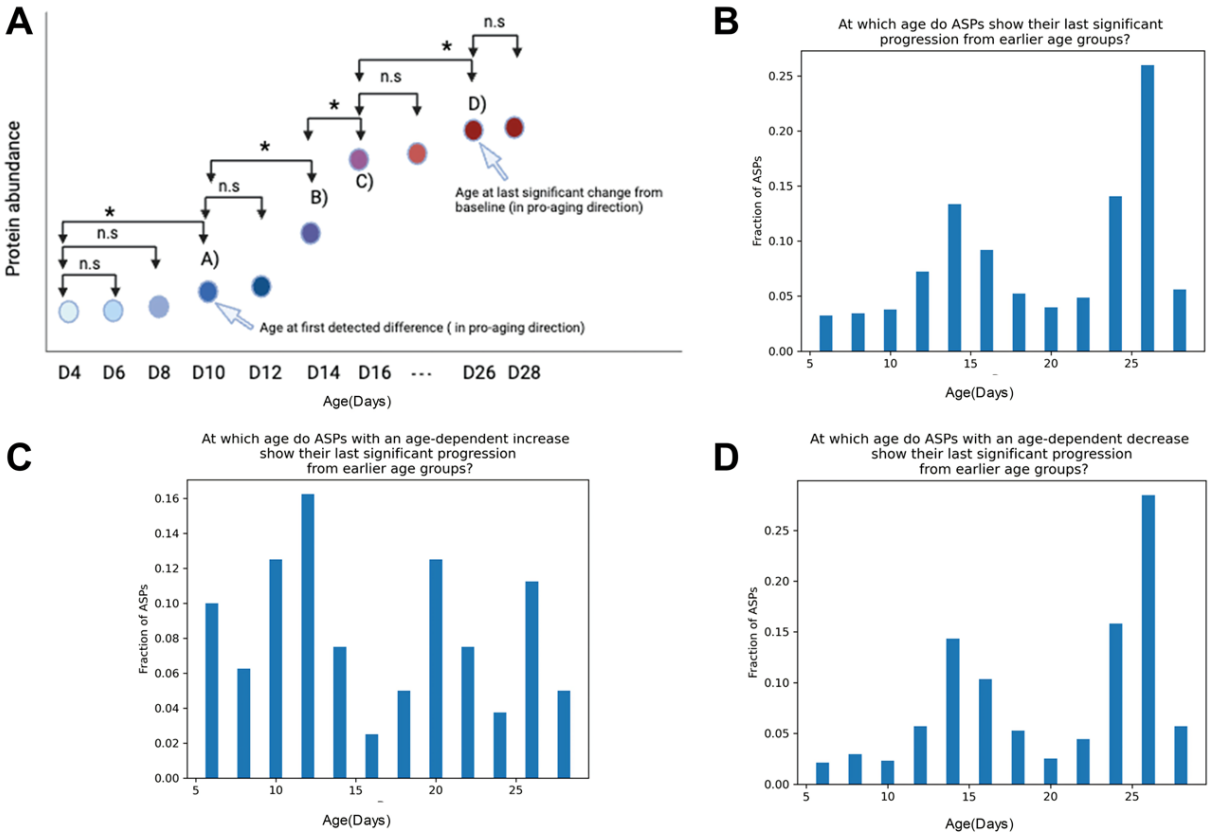

Figure 14: Individual protein-based progression analysis in *C. elegans*. (A) Systematic comparisons were conducted across age groups, starting with the baseline D4 group, to identify when ASPs first and last exhibited significant deviations. (B-D) The histogram depicts the distribution of the last significant changes in expression among all ASPs (B), ASPs associated with age-dependent increases in expression (C) and ASPs associated with age-dependent decreases in expression (D). Overall, there were relatively few ASPs that featured last changes relative to previous time points at D28, suggesting that most ASPs did not follow patterns consistent with ever-progressing change.

3.6 Stable reference genes across temporal, genetic, and environmental conditions in *C. elegans*

3.6.1 Evaluation of stable reference genes during aging in *C. elegans*

The field of functional genomics has always relied heavily on genome-wide expression analysis. However, a reliable tool is needed to validate the data produced by high-throughput RNA sequencing (RNA-seq). Due to its high sensitivity, quick turnaround time, and specificity, quantitative real-time PCR (qPCR) has been widely used to validate gene expression data (Tao et al. 2020). However, RNA integrity and quality, cDNA synthesis

efficiency, and PCR efficiency inevitably affect the reliability of qPCR results. Reference genes are frequently used as internal controls to minimize the risk of misinterpreting expression data and to accurately quantify gene expression under various spatial and temporal conditions. Therefore, it is essential to investigate the stability of expression patterns of known reference genes in *C. elegans* during aging. By performing comprehensive RNA-seq analysis across 15 time points (D4-D32), we captured the expression landscape throughout the aging process (Figures 4-9). This provided a valuable resource for exploring the stability of commonly used qPCR reference genes in aging studies (Hoogewijs et al. 2008) using *C. elegans* as a model.

Table 10 presents the expression pattern of nine well-known *C. elegans* "reference genes", act-1, act-2, act-3, act-4, act-5, ama-1, eif3.c, cdc42, and pmp-3, during aging. This analysis revealed no significant change in expression levels for only two of these genes, act-3 ($p = 0.2858$), and pmp-3 ($p = 0.5559$), suggesting their potential as stable reference genes through aging. However, act-3 showed high variability across samples, questioning its suitability to be used as a reference gene in aging studies. For the other genes, notable changes were detected for act-2 (** $p \leq 0.0001$), act-4 (**** $p \leq 0.0001$), act-5 (* $p \leq 0.05$), ama-1 (* $p \leq 0.05$), eif3.c (*** $p \leq 0.001$), and CDC-42 (*** $p \leq 0.001$). However, act-1 ($p = 0.0544$), act-4 ($p = 0.7804$), and ama-1 ($p = 0.8157$) showed no significant change between late and early stages under DESeq2 analysis. In contrast, act-2, act-5, eif3.c, and CDC-42 displayed significant changes, indicating their sensitivity to age-related factors and raising concerns about their suitability for qPCR normalization in aging studies.

Table 10: One-way ANOVA analysis based on normalized read count data at all 15 time points (D4-D32) in *C. elegans*, focusing on previously with 9 established “references genes”.

Ensembl Gene ID	Gene	p-value
WBGene00000063	act-1	0.0544
WBGene00000064	act-2	**** p ≤ 0.0001
WBGene00000065	act-3	0.2858
WBGene00000066	act-4	**** p ≤ 0.0001
WBGene00000067	act-5	* p ≤ 0.05
WBGene00000123	ama-1	0.81565453
WBGene00001226	eif-3.C	*** p ≤ 0.001
WBGene00000390	cdc-42	*** p ≤ 0.001
WBGene00004060	pmp-3	0.5559

Considering these findings, we assessed genes to identify those with expression levels unaffected by aging—a necessary feature for reference genes. Our approach was in-depth, beginning with the selection of the top 1000 genes that showed the most consistently non-significant changes during aging, based on adjusted p-values (padj) calculated in the previous DESeq2 analysis. We then narrowed our focus by excluding any gene with a base mean expression level below 200, ensuring we targeted genes with sufficient expression to be reliably measured. Next, we refined our gene pool by selecting the top 200 genes with the lowest expression variability, as indicated by the lowest standard deviation percentage (%STDEV). To identify reference genes with stable expression across the aging continuum of *C. elegans*, we visualized the expression patterns of the top 50 candidate genes using GraphPad Prism. This detailed analysis aimed to identify genes with consistent expression levels across various developmental stages, providing a reliable baseline for qPCR experiments.

From the resulting curated list, we identified 16 genes that convincingly showed stability in expression across multiple time points, both statistically and visually (Table 11).

Table 11: DESeq2-derived statistical data of the identified 16 reference genes comparing differential gene expression (DGE) between late VS early stages.

Ensembl Gene ID	Gene	p-value
WBGene00017070	praf-3	0.99816625
WBGene00006755	unc-16	0.99694753
WBGene00015296	gtf-2F1	0.99242127
WBGene00014249	ZK1307.8	0.99231215
WBGene00007500	nasp-1	0.98804567
WBGene00000197	aars-2	0.98769716
WBGene00012386	agef-1	0.985993
WBGene00014119	ZK858.6	0.98407882
WBGene00011722	rbm-22	0.98016112
WBGene00003882	orc-2	0.969631
WBGene00011580	ddx-19	0.96330832
WBGene00004306	ran-5	0.88001722
WBGene00004389	rnp-6	0.74825771
WBGene00004060	pmp-3	0.6730486
WBGene00014078	ZK792.5	0.55480149
WBGene00003788	npp-2	0.52677768

To validate our findings, we conducted a qPCR experiment on seven genes—comprising the established reference gene pmp-3 and six newly identified candidates: orc-2, praf-3, aars-2, unc-16, gtf-2F1, and ZK1307. These genes were examined across seven distinct time points (D6, D8, D12, D14, D18, D20, D24), representing a range from early to late adulthood. Validation was based on the same samples used for RNA-seq, but only these time points had enough samples to be included. One-way ANOVA-based analyses suggested relative consistency in gene expression, with no significant changes detected for any of these genes across the selected time points. The p-values were as follows: pmp-3 ($p = 0.4585$), orc-2 ($p = 0.4696$), praf-3 ($p = 0.1133$), aars-2 ($p = 0.2074$), unc-16 ($p = 0.1145$), gtf-2F1 ($p = 0.3345$), and ZK1307.8 ($p = 0.7656$) (Figure 15).

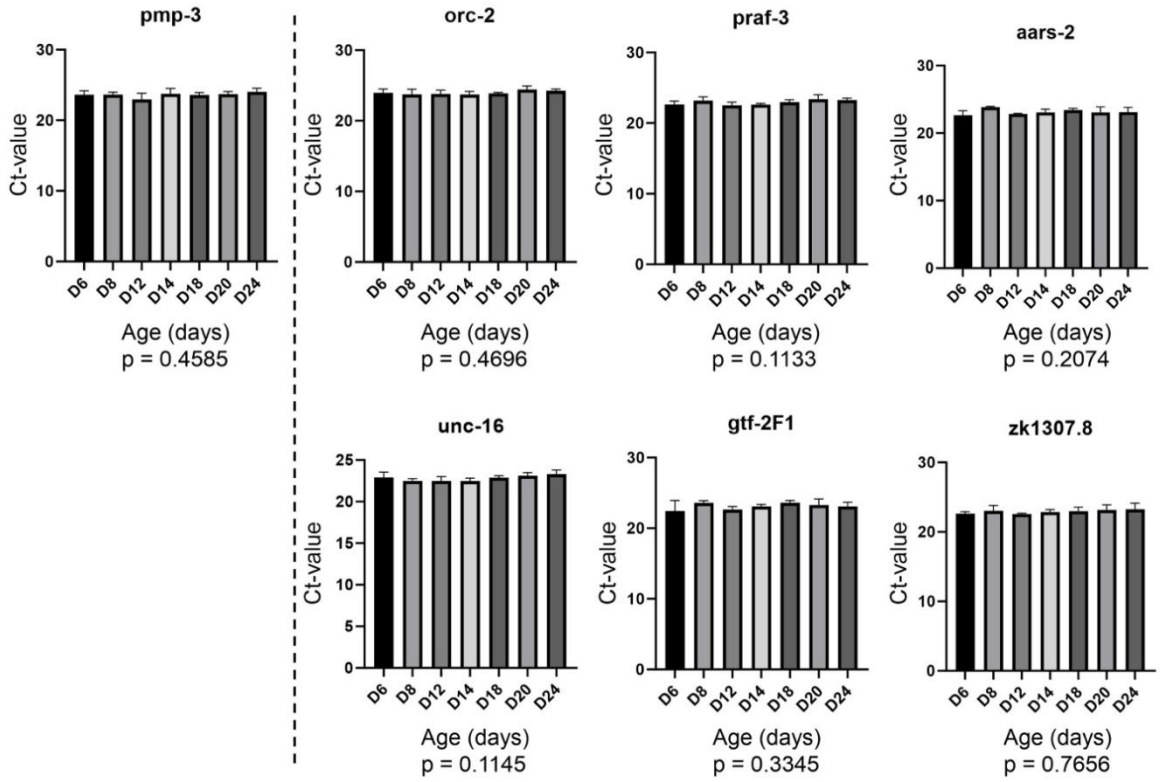

Figure 15: Stability of the expression of seven identified reference genes across aging in *C. elegans*. The established reference gene pmp-3 and six newly identified genes (orc-2, praf-3, aars-2, unc-16, gtf-2F1, and ZK1307.8) were evaluated by qPCR at seven different time points (D6, D8, D12, D14, D18, D20, D24). Statistical analysis was performed using one-way ANOVA, which revealed no significant changes in expression across time points for any of the genes (pmp-3, p = 0.4585; orc-2, p = 0.4696; praf-3, p = 0.1133; aars-2, p = 0.2074; unc-16, p = 0.1145; gtf-2F1, p = 0.3345; ZK1307.8, p = 0.7656).

3.6.2 Stability of the identified 7 reference genes in known *C. elegans* longevity mutant strains

In our exploration of gene expression stability, we expanded our analysis to include three known long-lived mutants of *C. elegans*. We evaluated the expression levels of the seven gene candidates in age-1, daf-2, and isp-1 at D8, as shown in Table 12. The expression of pmp-3, aars-2, and gtf-2F1 was significantly altered in the isp-1 line at D8 (Table 12), whereas no significant changes were observed in the age-1 and daf-2 strains (Table 12). These non-significant findings further confirm the stability of the examined reference genes candidates, indicating that, apart from the specific instances noted, most of the genes maintained a consistent expression pattern despite the genetic mutations (commonly used in longevity experiments).

Table 12: Stability of the identified 7 reference genes in comparisons WT vs. mutant strains at D8.

pmp-3	
Group	p-value
WT VS age-1	0.20861812
WT VS daf-2	0.791285319
WT VS isp-1	0.006677304

orc-2		**praf-3**	
Group	p-value	Group	p-value
WT VS age-1	0.500973782	WT VS age-1	0.476241065
WT VS daf-2	0.156445629	WT VS daf-2	0.188069415
WT VS isp-1	0.017186856	WT VS isp-1	0.986237837
aars-2		**unc-16**	
Group	p-value	Group	p-value
WT VS age-1	0.021533134	WT VS age-1	0.123880977
WT VS daf-2	0.03506704	WT VS daf-2	0.181099987
WT VS isp-1	0.008003836	WT VS isp-1	0.799878011
gtf-2F1		**zk1307.8**	
Group	p-value	Group	p-value
WT VS age-1	0.397614367	WT VS age-1	0.782924165
WT VS daf-2	0.851068688	WT VS daf-2	0.250355378
WT VS isp-1	0.002989317	WT VS isp-1	0.57913745

3.6.3 Stability of the identified 7 reference genes at different temperatures

To explore the impact of environmental fluctuations on gene expression, our study evaluated the stability of the seven identified reference genes in *C. elegans* across three temperature conditions. Wild-type *C. elegans* were incubated at 15 °C, 20 °C, and 25 °C, representing a range from below to above the typical maintenance temperature (Table 13). Samples were collected at D8 (eight days post-hatch), to assess potential changes in gene expression due to temperature variation.

For each gene, expression levels were quantified and compared across the temperatures at D8. Statistical analysis, using a two-way ANOVA with the assumption of equal variances, showed no statistically significant differences in gene expression across the tested temperatures at these time points (Table 13).

This uniform lack of significant expression change suggests that the tested genes maintain homeostatic regulation even when exposed to temperatures below and above the standard cultivation condition of 20 °C. Their stable expression profiles across different temperatures and developmental stages attest to their robustness and potential utility as reliable reference genes in experiments involving thermal stress or varying environmental conditions. Consequently, this assessment across a range of temperatures reinforces the suitability of these seven genes as reference controls for gene expression studies in *C. elegans*, ensuring that the chosen reference genes provide consistent and reliable data for normalization, regardless of minor variations in incubation temperatures.

Table 13: Stability of the identified 7 reference genes in 15 °C, 20 °C, 25 °C at D8

Gene	**15 °C v.s. 20 °C**	**25 °C v.s. 20 °C**	**15 °C v.s. 25 °C**
pmp-3	p = 0.8729	p = 0.7281	p = 0.7195
orc-2	p = 0.9538	p = 0.4857	p = 0.5877
praf-3	p = 0.7558	p = 0.7537	p = 0.8988
aars-2	p = 0.7258	p = 0.9963	p = 0.7229
unc-16	p = 0.7365	p = 0.6032	p = 0.5134
gtf-2F1	p = 0.8917	p = 0.7289	p = 0.9754
ZK1307.8	p = 0.7797	p = 0.7577	p = 0.9295

4 Discussion

4.1 Exploring dynamics of aging

4.1.1 Stabilization of aging processes

In our study, we prioritized transcriptomic and proteomic analyses to investigate aging trajectories, moving beyond the traditional focus on mortality and survival metrics. By leveraging these approaches, we aimed to capture a wider range of aging-related changes, encompassing a wide range of organismal alterations that occur over time. This shift allowed us to examine whether age-dependent phenotypes, such as transcriptomic and proteomic changes, exhibit stabilization trends analogous to the mortality plateaus reported in previous studies (Carey et al. 1992, Curtsinger et al. 1992, Rose et al. 2002). Traditional lifespan assays, while valuable for understanding survival patterns, have significant limitations (Keshavarz et al. 2023a, 2023b). These methods often reflect only specific causes of death that dominate late-life stages, potentially obscuring the broader dynamics of aging. Mortality rates, though informative for demographic trends, are not comprehensive proxies for the complex biological processes taking place during aging. By employing omics data, we sought to uncover more granular insights into biological changes characterizing the aging process. This approach provides a broader perspective, enabling a deeper understanding of the mechanisms contributing to age-related stabilization of molecular and physiological processes. Our findings emphasize the importance of expanding the methodological focus in aging research to capture the full complexity of late-life biological changes.

Evolutionary theories provide a possible explanation for mortality plateaus. According to the Medawar-Williams theory, natural selection weakens with age as reproductive capacity diminishes. Post-reproductive individuals experience reduced evolutionary pressures, leading to the accumulation of mutations or traits that do not directly affect reproductive success (Medawar 1952, Williams 1957). This weakening of selection may contribute to stabilizing mortality rates in late life (Demetrius 2001). The findings from our *C. elegans* study support this theory, as mortality deceleration occurred even in a genetically homogeneous setting where demographic heterogeneity is negligible. This indicates that the plateau may reflect intrinsic biological processes rather than population-level selection effects.

One key factor contributing to late-life mortality plateaus in *C. elegans* may be the stabilization of biological processes observed at advanced ages. Our results showed that transcriptomic and proteomic changes tend to stabilize after D22, aligning with the trend of decelerating mortality rates in later life stages, which become more pronounced around D28. This stabilization could indicate that physiological systems, including those critical for survival, reach a relatively static state in old age. Such findings align with earlier studies on other species, including Drosophila melanogaster, which also exhibit mortality deceleration in late life despite genetic homogeneity (Curtsinger et al. 1992).

4.1.2 Cross-sectional profiling of aging in *C. elegans*

In our study, we employed a cross-sectional design to analyze the transcriptomic and proteomic profiles of *C. elegans* across its lifespan, focusing on molecular changes from early adulthood to late life. Transcriptomic data were collected from D4 to D32, while proteomic data spanned D4 to D28. This design involved sampling from different individuals at each time point, as transcriptomics and proteomics require sacrificing the animals for data collection. The larval stages were excluded to focus specifically on adult aging processes, minimizing the confounding effects of developmental gene expression. Due to high mortality rates, collection into very old ages requires very large sample sizes. To ensure robust datasets, we analyzed six biological replicates across 15 time points for transcriptomics and four biological replicates across 13 time points for proteomics.

Cross-sectional designs, such as ours, provide critical insights into population-level changes associated with aging. While longitudinal designs—which involve repeated measurements from the same individual—eliminate bias caused by population heterogeneity and provide direct insights into individual aging trajectories, they are incompatible with destructive techniques like transcriptomics and proteomics. Our approach balances the need for high-resolution molecular data with the practical constraints of studying *C. elegans*, a short-lived and small organism. Nonetheless, longitudinal-compatible techniques, such as live imaging, could complement cross-sectional analyses by enabling dynamic assessments of aging processes in the same individuals over time.

Our findings align with previous research on age-related transcriptomic changes in *C. elegans*. For example, a study by (Ewald et al. 2015) identified specific genes whose

expression levels change with age, highlighting a role for extracellular matrix remodeling in insulin/IGF-1-dependent lifespan regulation. Similarly, our data reveal alterations in genes associated with stress responses and metabolic processes, consistent with observations by (Lund et al. 2002), who reported age-dependent gene expression shifts linked to these functions. These parallels suggest that certain molecular pathways are consistently involved in the aging process of *C. elegans*, reinforcing the validity of our results.

To advance aging research further, integrating live imaging techniques with omics data collection holds significant promise. Fluorescence imaging allows for real-time monitoring of molecular and metabolic changes, making it invaluable for studying dynamic processes in aging. For example, fluorescent markers can be used to track oxidative stress, mitochondrial function, and protein aggregation, which are the key features of aging in *C. elegans* (De Boer et al. 2021, Jung et al. 2023, Wang et al. 2013). By providing high spatial and temporal resolution, fluorescence imaging complements transcriptomic and proteomic analyses, enabling researchers to correlate molecular changes with observable phenotypic alterations. Such integration offers a holistic view of the aging process and can help uncover the intricate biological mechanisms underlying age-related changes.

4.1.3 Reliability and reproducibility in molecular aging studies

Our study utilized high-quality RNA and protein to enable transcriptomic and proteomic analyses. The RNA extraction protocol was carefully optimized to recover intact RNA with minimal contamination, even from small sample sizes. By employing the enhanced PicoPure™ Kit (Figure 2), supplemented with additional sonication cycles and DNase treatments, the RNA purity reached an A260/A230 ratio of approximately 2.16, making it suitable for downstream transcriptomic analyses (Castro et al. 2017). Similarly, the protein extraction process was refined through multiple sonication cycles and stringent filtration steps, yielding high-quality protein samples. Quality assurance methods, such as SDS-PAGE and silver staining, confirmed the integrity of these samples (Gallagher 2012, Laemmli 1970). These improvements were crucial for ensuring the reliability of label-free proteomic quantification, as the accuracy of mass spectrometry heavily depends on input sample quality (Bantscheff et al. 2007, Domon and Aebersold 2010).

The datasets generated through these optimized protocols enabled precise identification of transcriptomic and proteomic aging trajectories. The analysis revealed distinct expression clusters based on transcriptomic data from 15 time points and proteomic data from 13 time points. High-resolution data provided insights into subtle mid-life peaks and late-life stabilization patterns, highlighting the importance of sample quality in uncovering nuanced molecular changes during aging.

Compared to previous studies, our approach offered several advantages. First, the optimized extraction protocols significantly improved the recovery of high-quality material from small sample sizes, addressing a common challenge in molecular aging research. Small sample sizes present a significant challenge in molecular aging research, often leading to issues such as overfitting and reduced reproducibility. For example, (Bell et al. 2019) discuss the complexities in epigenetic clock studies, noting that limited sample sizes can hinder the accurate quantification of biological aging rates. Similarly, (Brinkley et al. 2022) emphasize the necessity for robust measures and longitudinal studies in aging research, highlighting that inadequate sample sizes can compromise the validity of findings. These examples underscore the importance of optimizing protocols to maximize data quality and reliability when working with small sample sizes in molecular aging studies. Second, the inclusion of more time points facilitated higher-resolution analyses, allowing for the detection of patterns in age-dependent phenotypic change that remain obscured in studies with fewer time points (Dhondt et al. 2017, Shavlakadze et al. 2019). Additionally, stringent quality control measures and replicates enhanced the reliability and reproducibility of our findings, particularly in label-free mass spectrometry analyses, where sample quality is paramount (Bittremieux et al. 2017).

4.1.4 Environmental and epigenetic modulation of aging

In this study, we maintained stringent culture conditions to minimize variability in the aging trajectories of *C. elegans*, focusing on the expression of ASGs and ASPs. By controlling environmental factors such as diet, temperature, and microbial exposure, we aimed to better isolate the intrinsic molecular mechanisms underlying aging. However, in natural populations, environmental factors interact with epigenetic mechanisms—such as DNA methylation and histone modifications—to shape aging phenotypes (Molina-Serrano et al. 2019). Additionally, (Feil and Fraga 2012) discuss how environmental influences can lead

to epigenetic changes that affect gene expression and contribute to aging processes. They highlight that factors like diet, pollutants, and stress can induce epigenetic modifications, thereby influencing aging trajectories. These interactions highlight the complex relationship between environmental inputs and the molecular regulation of aging.

Although we compared temperature effects in the study of stable reference genes and confirmed that gene expression stability was maintained under different temperature conditions, this comparison has not yet been extended to the "plateau" project examining expression stability in later life stages. Future studies could integrate temperature and plateau-specific expression dynamics to comprehensively investigate how temperature influences the regulation of age-related gene expression.

Our findings underscore the need to extend aging research into more ecologically relevant contexts. While controlled conditions facilitate the identification of ASGs and ASPs, future research should explore how diverse environmental factors modulate their expression. For instance, long-term experiments exposing *C. elegans* to varying diets or temperature conditions could illuminate the dynamic relationships between environmental factors and aging-related molecular pathways. Previous studies have shown that dietary restriction and temperature changes significantly influence lifespan and stress resistance in *C. elegans*. For example, (Tissenbaum and Guarente 2001) found that dietary restriction extends lifespan through a pathway requiring the FOXO transcription factor DAF-16 and the NAD+-dependent deacetylase SIR-2.1. Additionally, (Ogg et al. 1997) reported that reduced insulin/IGF-1 signaling, which can be influenced by dietary intake, enhances thermotolerance and extends lifespan via DAF-16 activation. These studies provide specific evidence of how dietary restriction and temperature changes modulate aging and stress resistance in *C. elegans*.

To complement environmental studies, epigenetic profiling tools such as chromatin immunoprecipitation sequencing (ChIP-seq) and whole-genome bisulfite sequencing have proven invaluable in revealing how environmental variables reshape the epigenetic landscape during aging. These tools provide critical insights into the regulation of ASGs and ASPs. ChIP-seq has been used to identify histone modifications associated with specific ASG/ASP clusters (De Lima Camillo et al. 2023, Rye et al. 2011), while bisulfite sequencing maps DNA methylation changes driven by environmental conditions.

Studies in *C. elegans* have shown that environmental factors like diet and temperature significantly impact epigenetic modifications, influencing aging phenotypes. (Li et al. 2021) used ChIP-seq to investigate changes in the repressive histone mark H3K9me3 in aged somatic tissues, revealing region-specific gains and losses linked to aging. (Jänes et al. 2018) examined chromatin accessibility dynamics throughout *C. elegans* development and aging, offering valuable insights into the temporal evolution of chromatin states.
These findings highlight the importance of epigenetic profiling tools in uncovering the complex interactions between environmental factors and molecular regulation of aging. While these studies have advanced our understanding of aging, they also reveal gaps and directions for future research. How specific environmental factors drive targeted epigenetic modifications remains unclear. Long-term experiments in ecologically relevant settings, such as manipulating diet, temperature, or other environmental variables, could provide further insights. Such studies could clarify how environmental factors and epigenetic changes interact to influence aging, improving our understanding of the aging process.

4.1.5 Aging-related changes explored through transcriptomics and proteomics

To explore general trends and patterns within the sets of ASGs and ASPs, we performed clustering analyses of gene/protein expression trajectories. Our analyses revealed three clusters of ASGs and ASPs, each with unique trajectories over time.
Transcriptomic Cluster - Cluster 1: Exhibited a progressive decline in expression and was enriched in processes such as organic acid metabolism (GO:0006082) and muscle system processes (GO:0003012). These changes align with reductions in metabolic efficiency and muscular function observed during aging (Kirkwood 2005, López-Otín et al. 2013). Cluster 2: Peaked in expression at mid-life (D24) before stabilizing. Genes in this cluster were associated with synaptic signaling (GO:0099536) and gated channel activity (GO:0022836), which may play roles in maintaining neural function and adapting to cellular stress (Citri and Malenka 2008). Cluster 3: Displayed increased expression until D18, followed by a decline and plateau. This cluster was enriched in cell projection organization (GO:0030030) and neuron development (GO:0007399), processes potentially linked to neural plasticity and longevity (Kaletsky and Murphy 2010).

Proteomic Clusters - Cluster 1: Proteins in this cluster increased until D20, then declined and stabilized. These were enriched in chromatin organization (GO:0006325), a process critical for genomic stability and gene regulation (Kim et al. 2012, Tissenbaum and Guarente 2001). Cluster 2: Showed a progressive decline in expression until D22, associated with the cytosolic large ribosomal subunit (GO:0022625). This highlights the role of protein synthesis and its disruption in aging (Manhas and Rath 2020, Turi et al. 2019). Cluster 3: Peaked at D20 and was enriched in detoxification (GO:0098754) and cellular responses to toxic substances (GO:0097237). These processes are vital for mitigating oxidative stress and maintaining cellular homeostasis (Ullah et al. 2024, Živančević et al. 2021).

The interplay between transcriptional and proteomic changes during aging underscores the importance of chromatin remodeling, synaptic signaling, and stress response pathways in regulating lifespan. Transcriptomic data highlight shifts in gene expression, while proteomic analyses reveal functional consequences, including post-transcriptional and post-translational regulatory mechanisms. However, alignment between ASGs and ASPs is often limited due to factors like mRNA stability, translation efficiency, and protein turnover (Liu et al. 2016, Vogel and Marcotte 2012).

For instance, proteins involved in cell cycle regulation and metabolic pathways exhibit delayed or diminished changes compared to their transcriptomic counterparts (Wei et al. 2015). Late-life stabilization phases (D22) in proteomic data were enriched in chromatin remodeling, sensory perception, and mitochondrial function, suggesting these pathways are critical for maintaining homeostasis in late life.

Some findings align with age-related changes observed in higher organisms, while others highlight species-specific dynamics. For example, synaptic signaling in ASG Cluster 2 peaked in mid-life (D20-D24) and stabilized, suggesting compensatory mechanisms to maintain neural function despite synaptic decline (Chen et al. 2013, Toth et al. 2012). In mammals, synaptic signaling typically decreases with age, leading to reduced plasticity and cognitive impairments (Morrison and Baxter 2012).

Similarly, ASP Cluster 3's upregulation of detoxification pathways highlights the importance of mitigating oxidative stress during aging. These findings align with observations in higher organisms, where stress responses are vital for longevity (Tan et al. 2018). However, the persistent upregulation of stress-related pathways in *C. elegans*

suggests greater resilience compared to mammals, possibly due to the absence of neurodegenerative diseases like Alzheimer's or Parkinson's (Calabrese et al. 2008).

Conversely, consistent downregulation of ASGs and ASPs linked to muscle system processes, sarcomere organization, and metabolic pathways was observed throughout the lifespan of *C. elegans*. For example, genes related to collagen production and mitochondrial function declined significantly after D18, mirroring patterns seen in mammals where similar declines correlate with sarcopenia and reduced metabolic activity (Demontis et al. 2013, Houtkooper et al. 2011). Late-life stabilization of these pathways in *C. elegans* raises questions about whether this is a conserved feature across species.

The temporal synchronization of ASGs and ASPs provides valuable insights into aging dynamics. Early and mid-life peaks in stress-response genes and proteins suggest active compensatory mechanisms, while late-life stabilization indicates a shift to maintenance. This pattern aligns with findings in higher organisms, where antioxidant enzymes and heat shock proteins peak in mid-life but decline with advanced age (Chandra et al. 2022, Hall et al. 2001).

Genes and proteins linked to synaptic signaling, sensory perception, and detoxification pathways in *C. elegans* show persistent upregulation into late life, reflecting robust adaptive mechanisms. This resilience may be due to simpler organismal structures and the absence of neurodegenerative decline. In contrast, mammals often exhibit diminished compensatory responses with age, leading to cognitive impairments (Hertzog et al. 2008, Wong et al. 2021).

To enhance the accuracy and consistency of multi-omics studies, advanced tools such as magnetic bead-based purification systems could improve RNA and protein extraction from small samples. Investigating aging-related traits inherited across generations in *C. elegans* offers a promising research direction. Additionally, integrating computational models with multi-omics data—including transcriptomics, proteomics, and epigenetics—may identify key regulatory networks and potential therapeutic targets, such as epigenetic regulators and NRF2 activators, to delay aging and extend healthy lifespan (Lewis et al. 2010, López-Otín et al. 2013).

4.1.6 Validation of stable reference genes during aging studies in *C. elegans*

Accurate normalization in gene expression studies, especially during aging, requires stable reference genes due to physiological and molecular changes that introduce variability. Our study expanded on current methodologies by examining *C. elegans* across multiple age stages, genetic backgrounds, and environmental conditions to identify reliable reference genes for aging-related analyses.

Previous studies often focused on specific developmental stages or conditions, such as juvenile stages (e.g., L3 larvae) or stress-induced dauer states. (Hoogewijs et al. 2008) analyzed gene expression across several developmental and stress-responsive conditions, including wild-type adults, dauers, and L3 larvae. However, their work did not address mid or late life transitions—critical periods for observing significant shifts in gene expression. Our study extends this by specifically analyzing gene expression during early, mid and late stages, providing a broader perspective on gene stability across different age stages in *C. elegans.* Although we lacked samples from other time points (due to a lack of material left from these time points), we were still able to cover much of the adult *C. elegans* life cycle (D6, D8, D12, D14, D18, D20, and D24), capturing young, mid-life, and old-age stages. A limitation of the current study is that the stable reference genes identified here are validated only for the age range specified above but their utility as stable markers outside this age range has not yet been confirmed.

Using results from differential expression analyses and normalized read counts, we identified stable reference genes based on an evaluation of *padj* values and %STDEV. Seven robust candidates—*pmp-3, orc-2, praf-3, aars-2, unc-16, gtf-2F1,* and *ZK1307.8*—demonstrated consistent expression across the lifespan and diverse experimental conditions.

Our study included genetically diverse backgrounds by analyzing wild-type strains alongside mutants with well-characterized aging traits (*age-1, daf-2,* and *isp-1*). These mutants target key longevity pathways, such as insulin/IGF-1 signaling and mitochondrial function, which significantly impact lifespan and stress responses. For example, *daf-2* and *age-1* mutations extend lifespan and enhance stress resistance via activation of DAF-16, the FOXO transcription factor homolog (Van Heemst 2010). Conversely, *isp-1* mutants, which affect mitochondrial function, alter oxidative phosphorylation and energy regulation (Akbari et al. 2019, Barbieri et al. 2003).

Our analysis revealed that while *unc-16* displayed stable expression in *daf-2* and *age-1* mutants, *pmp-3* showed variability in *isp-1* mutants. This highlights the genetic background's influence on reference gene performance. A significant aspect of our study was evaluating reference gene stability under varying environmental conditions, including temperature changes (15°C, 20°C, and 25°C). Our findings confirmed that genes like pmp-3, orc-2, and unc-16 maintained stable expression across these temperature shifts, making them robust for normalization beyond standard laboratory settings. Our study extends the work of (Hoogewijs et al. 2008) by not only validating the stability of reference genes in *C. elegans* under controlled conditions but also incorporating environmental fluctuations such as varying temperatures (15°C, 20°C, and 25°C). This allows us to assess the robustness of these genes under more ecologically relevant conditions, which was not explored in previous studies

It is very important to check if reference genes stay stable under different environmental conditions because even small changes can greatly affect gene expression. Future studies could build on this work by looking at how oxidative stress or changes in nutrients affect reference genes, making them more useful in a variety of experimental settings.

Our results provide a reliable way to choose stable reference genes, helping to ensure accurate qPCR analyses in aging studies using different *C. elegans* strains. The consistent stability of these reference genes under various conditions shows they are suitable for experiments with genetic and environmental differences. Future research should also test if the same stable gene sets seen in *C. elegans* apply to other organisms. This could help us better understand how molecular systems remain stable and improve the accuracy of gene expression studies in a wider range of biological systems.

By covering more age stages, genetic backgrounds, and environmental conditions, our study improves the accuracy of gene expression normalization and helps reveal shared processes that influence aging and stress responses.

4.2 Distinct phases and dynamics of aging in *C. elegans*

4.2.1 Plateau phase in transcriptomic and proteomic changes

The observed stabilization of transcriptomic and proteomic changes in *C. elegans* post-D22 suggests a distinct late-life phase characterized by a plateau in aging-related biological decline. This stabilization indicates that molecular and physiological changes

during aging may not be continuously progressing but may reach a threshold beyond which further changes are minimal.

Our data show that ASGs exhibit distinct expression trajectories that stabilize post-day 22. Trajectory analysis identified three major clusters, with Cluster 1 genes showing consistent downregulation, Cluster 2 genes peaking around D20-22 before stabilizing, and Cluster 3 genes stabilizing after an initial decline (Figure 6). These findings indicate that while early and mid-life stages are characterized by significant transcriptomic shifts, late-life marks a phase of more limited transcriptomic change, consistent with the notion of a biological plateau. Similar trends were observed in multidimensional scaling (MDS) plots and transcriptome-based vector distance analyses, where the divergence of transcriptomic profiles from a young adult reference (D4) plateaued post-day 22 (Figures 7 and 8).

This stabilization aligns with demographic studies showing mortality deceleration in late life, where age-related change in mortality rates slows as organisms reach advanced ages (Vaupel et al. 1998). However, the stabilization observed in *C. elegans* may differ from patterns in higher organisms due to its lack of complex aging phenotypes such as chronic diseases and neurodegeneration (Tarkhov et al. 2019). Further comparative studies across species could determine whether transcriptomic stabilization reflects a conserved characteristic of aging or a feature unique to simpler organisms.

Proteomic analysis also revealed distinct stabilization patterns, with ASPs clustering into three groups. Cluster 1 proteins, primarily involved in chromatin organization, showed early increases followed by stabilization post-day 24. Cluster 2, comprising proteins linked to ribosomal function and metabolic processes, showed consistent downregulation with a plateau post-day 22. Cluster 3, including proteins associated with detoxification, peaked in mid-life and stabilized in late life (Figure 10). These results support the notion that proteomic changes mirror transcriptomic trends, with stabilization occurring concurrently across different gene/protein sets.

The stabilization of proteomic changes further supports the hypothesis that late-life plateaus in expression levels represent a phase of physiological homeostasis rather than continued decline. Upon reviewing the available literature, there is limited evidence of such plateaus in higher organisms. For example, a study on *Drosophila melanogaster* observed that mortality rates decelerate and eventually plateau in late life, suggesting a

stabilization of physiological decline (Mueller et al. 2011). However, the degree of stabilization may vary due to species-specific factors, such as metabolic rates and life history strategies.

4.2.2 Late-life phase as a biological threshold

The concurrent stabilization of transcriptomic and proteomic changes suggests that late life may represent a biological threshold beyond which the organism's capacity or need for adaptive responses significantly declines. This phase reflects a state of functional maintenance, where overall expression patterns plateau. Our data show that genes and proteins related to synaptic signaling and detoxification maintain stable expression during late life. Prior to this stabilization, their expression levels showed an initial increase during mid-life stages, with synaptic signaling genes peaking around D18-D20 and detoxification-related proteins peaking at D20 before plateauing, potentially contributing to the preservation of neural and cellular homeostasis as overall expression changes stabilize.

In late life, a potentially diminished capacity for adaptive responses may stem from the organism reallocating resources to maintain fundamental functions. While transcriptomic and proteomic changes plateau, certain processes, such as detoxification and neural signaling, remain actively maintained. The stabilization of gene and protein expression across most processes in late life reflects a broader shift toward prioritizing critical functions. This is achieved through more widespread, rather than selective, molecular activities aimed at supporting survival, such as clearing accumulated cellular damage or maintaining neural system integrity (Santra et al. 2019).

Similar late-life stabilization phases have been hypothesized in higher organisms, but the presence of additional complicating factors, such as chronic inflammation and age-related diseases, makes it more challenging to isolate and study these patterns as clearly as in simpler model systems (Franceschi et al. 2018). In contrast, *C. elegans* provides a simplified model system, as its aging process lacks chronic diseases and neuro-degeneration, allowing intrinsic dynamics of late-life stabilization to be studied more clearly. Comparative analyses across species, such as between mammals and short-lived model organisms, can help elucidate the evolutionary significance and potential conservation of this stabilization phase (Ricklefs 1998).

Mechanisms such as genome stability, proteostasis, and mitochondrial function are central to the process of late-life stabilization, as they help preserve cellular integrity in the face of accumulated damage (López-Otín et al. 2013). For example, pathways involved in neural signaling and detoxification remain active in late life, likely serving as vital responses to mitigate the effects of age-related cellular damage (Tan et al. 2018). Similarly, conserved mechanisms such as DNA repair and protein folding may be essential for maintaining molecular stability during late life, as they help prevent the accumulation of mutations and misfolded proteins that would otherwise disrupt cellular function. Together, these processes contribute to the stabilization of the organism's molecular landscape, supporting survival by maintaining critical cellular functions despite aging-related decline. Comparative studies across species with varying lifespans and aging phenotypes are necessary to assess how general late-life stabilization patterns are.

4.2.3 Critical life stages and mid-life activation of regulatory mechanisms

The mid-life peak in expression of Cluster 2 ASGs and ASPs around D20-24 in *C. elegans* highlights a critical period during which genes linked to synaptic signaling, detoxification, and stress responses show increased expression. While these observations suggest that such changes may be part of adaptive mechanisms, further experiments manipulating these pathways are needed to directly assess their functional impact. Investigating whether similar patterns occur across species or are specific to *C. elegans* could offer insights into the potential universality of aging mechanism.

Trajectory analysis of *C. elegans* revealed a pronounced peak in Cluster 2 ASGs and ASPs around D24, followed by stabilization (Figures 6 A and 10 A). GO enrichment analyses identified associations with key biological processes, such as synaptic signaling (GO:0099536), detoxification (GO:0098754), and stress-response pathways (Figure 10 B). The findings underscore a temporally coordinated response, potentially marking a critical adaptive phase to mitigate mid-life stressors and maintain homeostasis. This mid-life activation may represent a turning point in the aging trajectory, offering insights into the timing of therapeutic interventions.

Proteins in Cluster 3, associated with detoxification and stress responses, also peaked in mid-life, indicating coordinated activation across transcriptomic and proteomic levels. This response is likely an adaptive mechanism to mitigate molecular damage, consistent with

the onset of age-related functional decline (Liang et al. 2014, López-Otín et al. 2013). The stabilization observed after the peak may indicate that compensatory mechanisms have reached a functional limit, or it may reflect a plateau in the accumulation of molecular damage that no longer requires adaptive responses. Without direct experiments, it is difficult to determine whether this is due to exhaustion of compensatory capacity or a shift in the need for additional adaptations, potentially setting the stage for late-life stabilization of molecular changes.

The mid-life activation of regulatory pathways in *C. elegans* aligns with similar phenomena observed in higher organisms. For example, in mammals, mid-life is marked by heightened activity in stress-response pathways, including heat shock proteins and antioxidant enzymes, which protect against protein aggregation and oxidative damage (Taylor and Dillin 2011). Some studies suggest that synaptic signaling pathways may be upregulated in aging rodents, possibly contributing to cognitive function during mid-life. However, more direct evidence is needed to fully support this claim, as the relationship between synaptic signaling and cognitive decline in aging rodents remains an area of ongoing research (Mattson and Arumugam 2018). These parallels suggest that mid-life activation of homeostatic mechanisms is a conserved feature across species, although the specific pathways and their timing may differ.

However, significant differences exist between *C. elegans* and higher organisms. Unlike mammals, *C. elegans* does not develop complex age-related diseases such as neurodegenerative disorders, including Alzheimer's and Parkinson's, which significantly influence mid-life and late-life molecular trajectories (Zhang et al. 2020). The absence of these pathologies may allow for a clearer observation of compensatory regulatory mechanisms during mid-life in *C. elegans*. Furthermore, the organism's shorter lifespan and simpler neural architecture provide a streamlined model for studying aging processes without the confounding effects of chronic diseases and prolonged stressor exposures that are common in mammals (Jeayeng et al. 2024). These differences underscore the advantages of *C. elegans* as a model system for isolating fundamental aging mechanisms while also highlighting the limitations in directly extrapolating findings to higher organisms, where the aging process is more intertwined with environmental and disease-related complexities (Ruprecht et al. 2024).

The mid-life regulatory peak observed in *C. elegans* offers a pivotal opportunity to investigate interventions that can enhance both lifespan and health span. Targeting pathways linked to synaptic signaling and detoxification during mid-life through genetic or pharmacological modulation could provide insights into potential strategies to mitigate age-associated decline. However, it is important to clarify whether these pathways are compensatory responses to age-related stress or key drivers of aging processes. If they are compensatory, countering them would not be expected to lead to beneficial outcomes, making further investigation crucial before therapeutic interventions are proposed. These pathways, underpinned by mechanisms like the integrated stress response (ISR) and transcriptional regulators such as ATF4, are evolutionarily conserved, emphasizing their translational relevance for broader aging research. The capacity of these interventions to modulate stress resilience and maintain proteostasis during mid-life supports their importance for translational applications in humans, as seen in studies of ISR modulation that enhance cognitive function in aged mammals (Derisbourg et al. 2021).

Further comparative research is necessary to delineate the extent of conservation of these mid-life regulatory patterns across taxa. Investigating species with diverse lifespans and aging phenotypes could clarify whether mid-life peaks in regulatory activity reflect universal aging mechanisms or adaptations unique to certain life history strategies. These efforts are critical to contextualize the findings from *C. elegans* within the broader framework of geroscience and develop targeted interventions for improving health span across species.

4.2.4 Evolutionary conservation of aging mechanisms

The late-life stabilization of transcriptomic and proteomic changes observed in *C. elegans* provides insights into aging mechanisms, although further studies across a broader range of species are required to determine whether this phenomenon is conserved across evolutionary distances. This stabilization, particularly evident in the trajectory analyses of ASGs and ASPs (Figures 6 and 10), highlights that aging does not represent a continuous decline but instead involves distinct phases. Late-life stabilization has been proposed as an adaptive evolutionary strategy, preserving some level of organismal functions necessary for survival during post-reproductive stages when evolutionary pressure is reduced. This aligns with the concept of "mutation accumulation" and "antagonistic

pleiotropy" theories, which suggest a declining selection pressure in later life stages, allowing mechanisms that maintain basic functionality to persist. Furthermore, this stabilization phase might reflect a conserved biological response across species, as similar patterns of plateauing have been reported in mammals (at least with respect to age-related change in mortality rate) (Johnson et al. 2019).

The findings in *C. elegans* emphasize the importance of studying aging mechanisms across diverse species. While the enrichment of pathways like chromatin organization and cellular signaling highlights shared aspects of aging biology, their interaction with species-specific traits requires further exploration. Future studies should explore the molecular processes involved in aging by integrating omics data from species with different lifespans and aging phenotypes. Longitudinal studies may be challenging, particularly for species from which repeated tissue sampling is difficult, but such approaches would offer valuable insights into the dynamics of aging. Techniques like live imaging and single-cell sequencing could provide high-resolution data on how specific pathways, such as those regulating stress responses or protein homeostasis, evolve across species.

4.3 Conclusion

By employing an extensive series of time points and integrating multi-omics analyses, we identified 3686 ASGs and 658 ASPs in *C. elegans*. One key finding is that transcriptomic and proteomic aging in *C. elegans* follows clear patterns. Early and mid-life stages show rapid changes. Later in life, these changes slow down and eventually level off. This late-life stabilization matches the observed mortality plateaus. It suggests that aging does not entail continuous decline but instead includes a phase where biological systems tend to stabilize. By identifying this plateau phase in both transcriptomic and proteomic profiles, the study highlights critical periods of organismal change vs. stabilization during aging. These periods could be important for developing ways to support health during aging. The results offer new opportunities to study how to slow down aging and improve health in later life.

This study also validated the stability of reference genes under different conditions, including changes in age, genotype and environmental factors. Stable reference genes, such as pmp-3, will support robust gene expression studies in *C. elegans* comparing age groups, various genotypes and environmental factors, respectively.

Overall, this project improves our understanding of aging and shows the value of studying *C. elegans* as a model organism. The findings may help researchers identify new ways to improve health span and extend functional life. Future studies should focus on the late-life plateau phase to find strategies for delaying aging and keeping people healthy for longer.

5 Abstract

Aging is a complex biological process marked by a progressive decline in physiological function, leading to increased vulnerability for diseases and mortality. While early and mid-life aging dynamics are well-characterized, less is known about the physiological changes that occur in late life. This thesis investigates the dynamics of aging in the model organism *C. elegans*, focusing on whether late life presents a deceleration in age-related changes, akin to the mortality plateau observed in many species. Our aim was to characterize proteomic and transcriptomic changes in *C. elegans* across the lifespan, including late life, thus contributing to a deeper understanding of the aging process.

Our methods included RNA-seq and mass spectrometry to profile age-sensitive genes (ASGs) and age-sensitive proteins (ASPs). Lifespan assays were used to identify critical periods in the aging trajectory, allowing for targeted sample collection in early, middle, and late life phases.

Our transcriptomic and proteomic analyses identified 3686 ASGs and 658 ASPs, respectively, that were used to study the kinetics of age-dependent phenotypic change across the lifespan in *C. elegans*. These analyses revealed two distinct phases: an initial period of age-related change, followed by a plateau phase in late life as demonstrated by a stabilization of changes in ASGs and ASPs expression. This late-life phase is also associated with a plateau in mortality rates, suggesting a biological transition where some age-sensitive pathways stabilize or even reverse.

Additionally, we used these datasets to identify genes that feature stability across a range of conditions and that may therefore be useful as reference genes in *C. elegans*. Our work identified 7 stable reference genes (pmp-3, orc-2, praf-3, aars-2, unc-16, gtf-2F1, and ZK1307.8) that maintain consistent gene expression across various conditions, including multiple age groups (days 6, 8, 12, 14, 18, 20, 24), different mutant strains (WT, age-1, daf-2, isp-1), and a range of temperatures (15°C, 20°C and 25°C), whereas previous studies typically focused on a limited set of time points.

To our knowledge, these findings represent the first study to systematically demonstrate, beyond mere lifespan data, that age-dependent changes follow a dynamic that entails a plateau phase in late life, indicating that aging-associated changes stop progressing and stabilize at advanced ages. Future studies need to address the generality of this finding

by incorporating longitudinal analysis approaches and extending the assessments to additional biological systems.

6 List of Figures

7 List of Tables

8 References

Akbari M, Kirkwood TBL, Bohr VA. Mitochondria in the signaling pathways that control longevity and health span. Ageing Res Rev 2019; 54: 100940

Anton SD, Woods AJ, Ashizawa T, Barb D, Buford TW, Carter CS, Clark DJ, Cohen RA, Corbett DB, Cruz-Almeida Y, Dotson V, Ebner N, Efron PA, Fillingim RB, Foster TC, Gundermann DM, Joseph A-M, Karabetian C, Leeuwenburgh C, Manini TM, Marsiske M, Mankowski RT, Mutchie HL, Perri MG, Ranka S, Rashidi P, Sandesara B, Scarpace PJ, Sibille KT, Solberg LM, Someya S, Uphold C, Wohlgemuth S, Wu SS, Pahor M. Successful aging: Advancing the science of physical independence in older adults. Ageing Res Rev 2015; 24: 304–327

Arking R. Biology of aging: observations and principles. Oxford University Press 1998

Bantscheff M, Schirle M, Sweetman G, Rick J, Kuster B. Quantitative mass spectrometry in proteomics: a critical review. Anal Bioanal Chem 2007; 389: 1017–1031

Barbieri M, Bonafè M, Franceschi C, Paolisso G. Insulin/IGF-I-signaling pathway: an evolutionarily conserved mechanism of longevity from yeast to humans. Am J Physiol-Endocrinol Metab 2003; 285: E1064–E1071

Bell CG, Lowe R, Adams PD, Baccarelli AA, Beck S, Bell JT, Christensen BC, Gladyshev VN, Heijmans BT, Horvath S, Ideker T, Issa J-PJ, Kelsey KT, Marioni RE, Reik W, Relton CL, Schalkwyk LC, Teschendorff AE, Wagner W, Zhang K, Rakyan VK. DNA methylation aging clocks: challenges and recommendations. Genome Biol 2019; 20: 249

Bishop NA, Lu T, Yankner BA. Neural mechanisms of ageing and cognitive decline. Nature 2010; 464: 529–535

Biteau B, Karpac J, Supoyo S, DeGennaro M, Lehmann R, Jasper H. Lifespan Extension by Preserving Proliferative Homeostasis in Drosophila. SK Kim (ed.). PLoS Genet 2010; 6: e1001159

Bittremieux W, Valkenborg D, Martens L, Laukens K. Computational quality control tools for mass spectrometry proteomics. PROTEOMICS 2017; 17: 1600159

Blackburn EH, Challoner PB. Identification of a telomeric DNA sequence in Trypanosoma brucei. Cell 1984; 36: 447–457

Bouchard C, Blair SN, Haskell WL. Physical activity and health. Human Kinetics 2012

Brinkley TE, Justice JN, Basu S, Bauer SR, Loh KP, Mukli P, Ng TKS, Turney IC, Ferrucci L, Cummings SR, Kritchevsky SB. Research priorities for measuring biologic age: summary and future directions from the Research Centers Collaborative Network Workshop. GeroScience 2022; 44: 2573–2583

Brooks A, Lithgow GJ, Johnson TE. Mortality Rates in a Genetically Heterogeneous Population of *Caenorhabditis elegans*. Science 1994; 263: 668–671

Calabrese V, Cornelius C, Mancuso C, Pennisi G, Calafato S, Bellia F, Bates TE, Giuffrida Stella AM, Schapira T, Dinkova Kostova AT, Rizzarelli E. Cellular Stress Response: A Novel Target for Chemoprevention and Nutritional Neuroprotection in Aging, Neurodegenerative Disorders and Longevity. Neurochem Res 2008; 33: 2444–2471

Carey JR, Liedo P, Orozco D, Vaupel JW. Slowing of mortality rates at older ages in large medfly cohorts. Science 1992; 258: 457–461

Castro JC, Rodríguez HN, Maddox JD, Jiu B, Petterman JB, Marapara JL, Cobos M. A Simple and efficient method for high-quality total RNA isolation from Oleaginous microalgae. Plant Cell Biotechnol Mol Biol 2017; 18: 15–21

Cesari M, Vellas B, Gambassi G. The stress of aging. Exp Gerontol 2013; 48: 451–456

Chandra PK, Cikic S, Rutkai I, Guidry JJ, Katakam PVG, Mostany R, Busija DW. Effects of aging on protein expression in mice brain microvessels: ROS scavengers, mRNA/protein stability, glycolytic enzymes, mitochondrial complexes, and basement membrane components. GeroScience 2022; 44: 371–388

Chen C-H, Chen Y-C, Jiang H-C, Chen C-K, Pan C-L. Neuronal aging: learning from C. elegans. J Mol Signal 2013; 8: 14

Christensen K, Johnson TE, Vaupel JW. The quest for genetic determinants of human longevity: challenges and insights. Nat Rev Genet 2006; 7: 436–448

Citri A, Malenka RC. Synaptic Plasticity: Multiple Forms, Functions, and Mechanisms. Neuropsychopharmacology 2008; 33: 18–41

Cohen AA, Ferrucci L, Fülöp T, Gravel D, Hao N, Kriete A, Levine ME, Lipsitz LA, Olde Rikkert MGM, Rutenberg A, Stroustrup N, Varadhan R. A complex systems approach to aging biology. Nat Aging 2022; 2: 580–591

Curtsinger JW, Fukui HH, Townsend DR, Vaupel JW. Demography of Genotypes: Failure of the Limited Life-Span Paradigm in *Drosophila melanogaster*. Science 1992; 258: 461–463

Curtsinger JW, Gavrilova NS, Gavrilov LA. Biochemigraphy of Aging and Age-Specific Mortality in Drosophila melanogaster. *In* Handbook of the Biology of Aging. pp. 267–294. Elsevier.

Dato S, Crocco P, Rambaldi Migliore N, Lescai F. Omics in a Digital World: The Role of Bioinformatics in Providing New Insights Into Human Aging. Front Genet 2021; 12: 689824

De Boer R, Smith RL, De Vos WH, Manders EMM, Van Der Spek H. In Vivo Visualization and Quantification of Mitochondrial Morphology in C. elegans. *In* Mitochondrial Medicine. V Weissig and M Edeas (eds.), pp. 397–407. Springer US, New York, NY.

De Lima Camillo LP, Asif MH, Horvath S, Larschan E, Singh R. Histone mark age of human tissues and cells. 2023;

De Magalhães JP, Curado J, Church GM. Meta-analysis of age-related gene expression profiles identifies common signatures of aging. Bioinformatics 2009; 25: 875–881

De Magalhães JP, Lagger C, Tacutu R. Integrative genomics of aging. *In* Handbook of the Biology of Aging. pp. 151–171. Elsevier.

Demetrius L. Mortality plateaus and directionality theory. Proc R Soc Lond B Biol Sci 2001; 268: 2029–2037

Demontis F, Piccirillo R, Goldberg AL, Perrimon N. Mechanisms of skeletal muscle aging: insights from *Drosophila* and mammalian models. Dis Model Mech 2013; : dmm.012559

Derisbourg MJ, Hartman MD, Denzel MS. Modulating the integrated stress response to slow aging and ameliorate age-related pathology. Nat Aging 2021; 1: 760–768

Dhondt I, Petyuk VA, Bauer S, Brewer HM, Smith RD, Depuydt G, Braeckman BP. Changes of Protein Turnover in Aging Caenorhabditis elegans. Mol Cell Proteomics 2017; 16: 1621–1633

Domon B, Aebersold R. Options and considerations when selecting a quantitative proteomics strategy. Nat Biotechnol 2010; 28: 710–721

Doty RL, Shaman P, Applebaum SL, Giberson R, Siksorski L, Rosenberg L. Smell Identification Ability: Changes with Age. Science 1984; 226: 1441–1443

Evans SA, Voan Teo Y, Hinthorn SJ, Clark K, Ito T, Sedivy JM, Neretti N. Single-Cell Transcriptomics Reveals Global Markers of Transcriptional Diversity across Different Forms of Cellular Senescence. Aging Biol 2023; 1: 20230008

Ewald CY, Landis JN, Abate JP, Murphy CT, Blackwell TK. Dauer-independent insulin/IGF-1-signalling implicates collagen remodelling in longevity. Nature 2015; 519: 97–101

Feil R, Fraga MF. Epigenetics and the environment: emerging patterns and implications. Nat Rev Genet 2012; 13: 97–109

Fontana L, Partridge L. Promoting Health and Longevity through Diet: From Model Organisms to Humans. Cell 2015; 161: 106–118

Franceschi C, Garagnani P, Parini P, Giuliani C, Santoro A. Inflammaging: a new immune–metabolic viewpoint for age-related diseases. Nat Rev Endocrinol 2018; 14: 576–590

Fries JF. Aging, Natural Death, and the Compression of Morbidity. N Engl J Med 1980; 303: 130–135

Gallagher SR. SDS-Polyacrylamide Gel Electrophoresis (SDS-PAGE). Curr Protoc Essent Lab Tech 2012; 6

Gems D, Riddle DL. Genetic, Behavioral and Environmental Determinants of Male Longevity in Caenorhabditis elegans. Genetics 2000; 154: 1597–1610

Hall DM, Sattler GL, Sattler CA, Zhang HJ, Oberley LW, Pitot HC, Kregel KC. Aging Lowers Steady-State Antioxidant Enzyme and Stress Protein Expression in Primary Hepatocytes. J Gerontol A Biol Sci Med Sci 2001; 56: B259–B267

Hanahan D, Weinberg RA. The hallmarks of cancer. Cell 2000; 100: 57–70

Hanahan D, Weinberg RA. Hallmarks of cancer: the next generation. Cell 2011; 144: 646–674

Harrington AJ, Hamamichi S, Caldwell GA, Caldwell KA. *C. elegans* as a model organism to investigate molecular pathways involved with Parkinson's disease. Dev Dyn 2010; 239: 1282–1295

Hayflick L. The limited in vitro lifetime of human diploid cell strains. Exp Cell Res 1965; 37: 614–636

Hertzog C, Kramer AF, Wilson RS, Lindenberger U. Enrichment Effects on Adult Cognitive Development: Can the Functional Capacity of Older Adults Be Preserved and Enhanced? Psychol Sci Public Interest 2008; 9: 1–65

Hood L, Flores M. A personal view on systems medicine and the emergence of proactive P4 medicine: predictive, preventive, personalized and participatory. New Biotechnol 2012; 29: 613–624

Hoogewijs D, Houthoofd K, Matthijssens F, Vandesompele J, Vanfleteren JR. Selection and validation of a set of reliable reference genes for quantitative sod gene expression analysis in C. elegans. BMC Mol Biol 2008; 9: 9

Hou Z, Jiang P, Swanson SA, Elwell AL, Nguyen BKS, Bolin JM, Stewart R, Thomson JA. A cost-effective RNA sequencing protocol for large-scale gene expression studies. Sci Rep 2015; 5: 9570

Houtkooper RH, Argmann C, Houten SM, Cantó C, Jeninga EH, Andreux PA, Thomas C, Doenlen R, Schoonjans K, Auwerx J. The metabolic footprint of aging in mice. Sci Rep 2011; 1: 134

Huang C, Xiong C, Kornfeld K. Measurements of age-related changes of physiological processes that predict lifespan of *Caenorhabditis elegans*. Proc Natl Acad Sci 2004; 101: 8084–8089

Hughes KA, Reynolds RM. Evolutionary and mechanistic theories of aging. Annu Rev Entomol 2005; 50: 421–445

Hughes KA, Alipaz JA, Drnevich JM, Reynolds RM. A test of evolutionary theories of aging. Proc Natl Acad Sci U S A 2002; 99: 14286–14291

Jänes J, Dong Y, Schoof M, Serizay J, Appert A, Cerrato C, Woodbury C, Chen R, Gemma C, Huang N, Kissiov D, Stempor P, Steward A, Zeiser E, Sauer S, Ahringer J. Chromatin accessibility dynamics across C. elegans development and ageing. eLife 2018; 7: e37344

Jeayeng S, Thongsroy J, Chuaijit S. Caenorhabditis elegans as a Model to Study Aging and Photoaging. Biomolecules 2024; 14: 1235

Jin L, Bi Y, Hu C, Qu J, Shen S, Wang X, Tian Y. A comparative study of evaluating missing value imputation methods in label-free proteomics. Sci Rep 2021; 11: 1760

Johnson AA, Shokhirev MN, Shoshitaishvili B. Revamping the evolutionary theories of aging. Ageing Res Rev 2019; 55: 100947

Johnson SC, Dong X, Vijg J, Suh Y. Genetic evidence for common pathways in human age-related diseases. Aging Cell 2015; 14: 809–817

Jones OR, Scheuerlein A, Salguero-Gómez R, Camarda CG, Schaible R, Casper BB, Dahlgren JP, Ehrlén J, García MB, Menges ES, Quintana-Ascencio PF, Caswell H, Baudisch A, Vaupel JW. Diversity of ageing across the tree of life. Nature 2014; 505: 169–173

Jowett B. The politics of Aristotle: introduction and translation. Clarendon Press 1885

Jung R, Lechler MC, Fernandez-Villegas A, Chung CW, Jones HC, Choi YH, Thompson MA, Rödelsperger C, Röseler W, Kaminski Schierle GS, Sommer RJ, David DC. A safety mechanism enables tissue-specific resistance to protein aggregation during aging in C. elegans. HA Tissenbaum (ed.). PLOS Biol 2023; 21: e3002284

Kaletsky R, Murphy CT. The role of insulin/IGF-like signaling in *C. elegans* longevity and aging. Dis Model Mech 2010; 3: 415–419

Kenyon C, Chang J, Gensch E, Rudner A, Tabtiang R. A C. elegans mutant that lives twice as long as wild type. Nature 1993; 366: 461–464

Kenyon CJ. The genetics of ageing. Nature 2010; 464: 504–512

Keshavarz M, Xie K, Bano D, Ehninger D. Aging – What it is and how to measure it. Mech Ageing Dev 2023a; 213: 111837

Keshavarz M, Xie K, Schaaf K, Bano D, Ehninger D. Targeting the “hallmarks of aging” to slow aging and treat age-related disease: fact or fiction? Mol Psychiatry 2023b; 28: 242–255

Kim S, Bi X, Czarny-Ratajczak M, Dai J, Welsh DA, Myers L, Welsch MA, Cherry KE, Arnold J, Poon LW, Jazwinski SM. Telomere maintenance genes SIRT1 and XRCC6 impact age-related decline in telomere length but only SIRT1 is associated with human longevity. Biogerontology 2012; 13: 119–131

Kim SK. Common aging pathways in worms, flies, mice and humans. J Exp Biol 2007; 210: 1607–1612

Kirkwood TBL. Understanding the odd science of aging. Cell 2005; 120: 437–447

Kirkwood TBL, Austad SN. Why do we age? Nature 2000; 408: 233–238

Kong W, Hui HWH, Peng H, Goh WWB. Dealing with missing values in proteomics data. PROTEOMICS 2022; 22: 2200092

Kriete A. Robustness and aging—A systems-level perspective. Biosystems 2013; 112: 37–48

Laemmli UK. Cleavage of Structural Proteins during the Assembly of the Head of Bacteriophage T4. Nature 1970; 227: 680–685

Lawrence M, Gentleman R, Carey V. rtracklayer: an R package for interfacing with genome browsers. Bioinformatics 2009; 25: 1841–1842

Lewis KN, Mele J, Hayes JD, Buffenstein R. Nrf2, a Guardian of Healthspan and Gatekeeper of Species Longevity. Integr Comp Biol 2010; 50: 829–843

Li C-L, Pu M, Wang W, Chaturbedi A, Emerson FJ, Lee SS. Region-specific H3K9me3 gain in aged somatic tissues in Caenorhabditis elegans. A Brunet (ed.). PLOS Genet 2021; 17: e1009432

Li Y, Ge X, Peng F, Li W, Li JJ. Exaggerated false positives by popular differential expression methods when analyzing human population samples. Genome Biol 2022; 23: 79

Liang V, Ullrich M, Lam H, Chew YL, Banister S, Song X, Zaw T, Kassiou M, Götz J, Nicholas HR. Altered proteostasis in aging and heat shock response in C. elegans revealed by analysis of the global and de novo synthesized proteome. Cell Mol Life Sci 2014; 71: 3339–3361

Linford NJ, Kuo T-H, Chan TP, Pletcher SD. Sensory Perception and Aging in Model Systems: From the Outside In. Annu Rev Cell Dev Biol 2011; 27: 759–785

Lipman R, Galecki A, Burke DT, Miller RA. Genetic loci that influence cause of death in a heterogeneous mouse stock. J Gerontol A Biol Sci Med Sci 2004; 59: 977–983

Lithgow GJ, White TM, Melov S, Johnson TE. Thermotolerance and extended life-span conferred by single-gene mutations and induced by thermal stress. Proc Natl Acad Sci U S A 1995; 92: 7540–7544

Liu Y, Beyer A, Aebersold R. On the Dependency of Cellular Protein Levels on mRNA Abundance. Cell 2016; 165: 535–550

López-Otín C, Blasco MA, Partridge L, Serrano M, Kroemer G. The hallmarks of aging. Cell 2013; 153: 1194–1217

Love MI, Huber W, Anders S. Moderated estimation of fold change and dispersion for RNA-seq data with DESeq2. Genome Biol 2014; 15: 550

Lund J, Tedesco P, Duke K, Wang J, Kim SK, Johnson TE. Transcriptional profile of aging in C. elegans. Curr Biol CB 2002; 12: 1566–1573

Ma R, Kutchy NA, Chen L, Meigs DD, Hu G. Primary cilia and ciliary signaling pathways in aging and age-related brain disorders. Neurobiol Dis 2022; 163: 105607

Manhas R, Rath PC. Ribosome, Protein Synthesis, and Aging. *In* Models, Molecules and Mechanisms in Biogerontology. PC Rath (ed.), pp. 67–87. Springer Singapore, Singapore.

Martin GM. The biology of aging: 1985-2010 and beyond. FASEB J Off Publ Fed Am Soc Exp Biol 2011; 25: 3756–3762

Mattson MP, Arumugam TV. Hallmarks of Brain Aging: Adaptive and Pathological Modification by Metabolic States. Cell Metab 2018; 27: 1176–1199

Mckay SJ, Johnsen R, Khattra J, Asano J, Baillie DL, Chan S, Dube N, Fang L, Goszczynski B, Ha E, Halfnight E, Hollebakken R, Huang P, Hung K, Jensen V, Jones

SJM, Kai H, Li D, Mah A, Marra M, Mcghee J, Newbury R, Pouzyrev A, Riddle DL, Sonnhammer E, Tian H, Tu D, Tyson JR, Vatcher G, Warner A, Wong K, Zhao Z, Moerman DG. Gene Expression Profiling of Cells, Tissues, and Developmental Stages of the Nematode C. elegans. Cold Spring Harb Symp Quant Biol 2003; 68: 159–170

Medawar PB. An Unsolved Problem of Biology: An Inaugural Lecture Delivered at University College, London, 6 December, 1951. H.K. Lewis and Company

Meng X, Yang S, Camp VJA. The Interplay Between the DNA Damage Response, RNA Processing and Extracellular Vesicles. Front Oncol 2020; 9: 1538

Metchnikoff E. The nature of man: studies in optimistic philosophy. Arno Press, New York

Miller B, Messias E, Miettunen J, Alaräisänen A, Järvelin M-R, Koponen H, Räsänen P, Isohanni M, Kirkpatrick B. Meta-analysis of Paternal Age and Schizophrenia Risk in Male Versus Female Offspring. Schizophr Bull 2011; 37: 1039–1047

Mohallem R, Schaser AJ, Aryal UK. Molecular Signatures of Neurodegenerative Diseases Identified by Proteomic and Phosphoproteomic Analyses in Aging Mouse Brain. Mol Cell Proteomics 2024; 23: 100819

Molina-Serrano D, Kyriakou D, Kirmizis A. Histone Modifications as an Intersection Between Diet and Longevity. Front Genet 2019; 10: 192

Moqri M, Herzog C, Poganik JR, Justice J, Belsky DW, Higgins-Chen A, Moskalev A, Fuellen G, Cohen AA, Bautmans I, Widschwendter M, Ding J, Fleming A, Mannick J, Han J-DJ, Zhavoronkov A, Barzilai N, Kaeberlein M, Cummings S, Kennedy BK, Ferrucci L, Horvath S, Verdin E, Maier AB, Snyder MP, Sebastiano V, Gladyshev VN. Biomarkers of aging for the identification and evaluation of longevity interventions. Cell 2023; 186: 3758–3775

Morrison JH, Baxter MG. The ageing cortical synapse: hallmarks and implications for cognitive decline. Nat Rev Neurosci 2012; 13: 240–250

Mueller LD, Rauser CL, Rose MR. Does aging stop? Oxford University Press, New York

Neff F, Flores-Dominguez D, Ryan DP, Horsch M, Schröder S, Adler T, Afonso LC, Aguilar-Pimentel JA, Becker L, Garrett L, Hans W, Hettich MM, Holtmeier R, Hölter SM, Moreth K, Prehn C, Puk O, Rácz I, Rathkolb B, Rozman J, Naton B, Ordemann R, Adamski J, Beckers J, Bekeredjian R, Busch DH, Ehninger G, Graw J, Höfler H, Klingenspor M, Klopstock T, Ollert M, Stypmann J, Wolf E, Wurst W, Zimmer A, Fuchs H, Gailus-Durner V, Hrabe De Angelis M, Ehninger D. Rapamycin extends murine lifespan but has limited effects on aging. J Clin Invest 2013; 123: 3272–3291

Nikhil KL, Ratna K, Sharma VK. Life-history traits of Drosophila melanogaster populations exhibiting early and late eclosion chronotypes. BMC Evol Biol 2016; 16: 46

Nordin S, Monsch AU, Murphy C. Unawareness of Smell Loss in Normal Aging and Alzheimer's Disease: Discrepancy between Self-Reported and Diagnosed Smell Sensitivity. J Gerontol B Psychol Sci Soc Sci 1995; 50B: P187–P192

Ogg S, Paradis S, Gottlieb S, Patterson GI, Lee L, Tissenbaum HA, Ruvkun G. The Fork head transcription factor DAF-16 transduces insulin-like metabolic and longevity signals in C. elegans. Nature 1997; 389: 994–999

On the nature of the function expressive of the law of human mortality, and on a new mode of determining the value of life contingencies. In a letter to Francis Baily, Esq. F. R. S. &c. By Benjamin Gompertz, Esq. F. R. S. Abstr Pap Print Philos Trans R Soc Lond 1833; 2: 252–253

Parrinello S, Coppe J-P, Krtolica A, Campisi J. Stromal-epithelial interactions in aging and cancer: senescent fibroblasts alter epithelial cell differentiation. J Cell Sci 2005; 118: 485–496

Pettan-Brewer C, Treuting PM. Practical pathology of aging mice. Pathobiol Aging Age Relat Dis 2011; 1

Rath PC. Models, Molecules and Mechanisms in Biogerontology: Cellular Processes, Metabolism and Diseases. Springer Singapore Pte. Limited, Singapore 2019

Rera M, Azizi MJ, Walker DW. Organ-specific mediation of lifespan extension: More than a gut feeling? Ageing Res Rev 2013; 12: 436–444

Ricklefs RE. Evolutionary Theories of Aging: Confirmation of a Fundamental Prediction, with Implications for the Genetic Basis and Evolution of Life Span. Am Nat 1998; 152: 24–44

Riera CE, Dillin A. Emerging Role of Sensory Perception in Aging and Metabolism. Trends Endocrinol Metab 2016; 27: 294–303

Rindfleisch A, Malter AJ, Ganesan S, Moorman C. Cross-Sectional versus Longitudinal Survey Research: Concepts, Findings, and Guidelines. J Mark Res 2008; 45: 261–279

Rose MR. Evolutionary Biology of Aging. Oxford University Press 1994

Rose MR, Drapeau MD, Yazdi PG, Shah KH, Moise DB, Thakar RR, Rauser CL, Mueller LD. Evolution of late-life mortality in Drosophila melanogaster. Evol Int J Org Evol 2002; 56: 1982–1991

Ruprecht NA, Singhal S, Schaefer K, Panda O, Sens D, Singhal SK. A Review: Multi-Omics Approach to Studying the Association between Ionizing Radiation Effects on Biological Aging. Biology 2024; 13: 98

Rye M, Sætrom P, Håndstad T, Drabløs F. Clustered ChIP-Seq-defined transcription factor binding sites and histone modifications map distinct classes of regulatory elements. BMC Biol 2011; 9: 80

Santra M, Dill KA, De Graff AMR. Proteostasis collapse is a driver of cell aging and death. Proc Natl Acad Sci 2019; 116: 22173–22178

Scifo E, Szwajda A, Soliymani R, Pezzini F, Bianchi M, Dapkunas A, Dębski J, Uusi-Rauva K, Dadlez M, Gingras A-C, Tyynelä J, Simonati A, Jalanko A, Baumann MH, Lalowski M. Proteomic analysis of the palmitoyl protein thioesterase 1 interactome in SH-SY5Y human neuroblastoma cells. J Proteomics 2015; 123: 42–53

Shavlakadze T, Morris M, Fang J, Wang SX, Zhu J, Zhou W, Tse HW, Mondragon-Gonzalez R, Roma G, Glass DJ. Age-Related Gene Expression Signature in Rats Demonstrate Early, Late, and Linear Transcriptional Changes from Multiple Tissues. Cell Rep 2019; 28: 3263-3273.e3

Sulston JE, Horvitz HR. Post-embryonic cell lineages of the nematode, Caenorhabditis elegans. Dev Biol 1977; 56: 110–156

Sun R, Sauter D. Sustained Stress Reduces the Age Advantages in Emotional Experience of Older Adults: Commentary on Carstensen et al. (2020). Psychol Sci 2021; 32: 2035–2041

Tan BL, Norhaizan ME, Liew W-P-P, Sulaiman Rahman H. Antioxidant and Oxidative Stress: A Mutual Interplay in Age-Related Diseases. Front Pharmacol 2018; 9: 1162

Tao J, Hao Y, Li X, Yin H, Nie X, Zhang J, Xu B, Chen Q, Li B. Systematic Identification of Housekeeping Genes Possibly Used as References in Caenorhabditis elegans by Large-Scale Data Integration. Cells 2020; 9: 786

Tarkhov AE, Alla R, Ayyadevara S, Pyatnitskiy M, Menshikov LI, Shmookler Reis RJ, Fedichev PO. A universal transcriptomic signature of age reveals the temporal scaling of Caenorhabditis elegans aging trajectories. Sci Rep 2019; 9: 7368

Taylor RC, Dillin A. Aging as an Event of Proteostasis Collapse. Cold Spring Harb Perspect Biol 2011; 3: a004440–a004440

Tissenbaum HA, Guarente L. Increased dosage of a sir-2 gene extends lifespan in Caenorhabditis elegans. Nature 2001; 410: 227–230

Toth ML, Melentijevic I, Shah L, Bhatia A, Lu K, Talwar A, Naji H, Ibanez-Ventoso C, Ghose P, Jevince A, Xue J, Herndon LA, Bhanot G, Rongo C, Hall DH, Driscoll M. Neurite Sprouting and Synapse Deterioration in the Aging Caenorhabditis elegans Nervous System. J Neurosci 2012; 32: 8778–8790

Troen BR. The biology of aging. Mt Sinai J Med N Y 2003; 70: 3–22

Turi Z, Lacey M, Mistrik M, Moudry P. Impaired ribosome biogenesis: mechanisms and relevance to cancer and aging. Aging 2019; 11: 2512–2540

Ullah Z, Tao Y, Huang J. Integrated Bioinformatics-Based Identification and Validation of Neuroinflammation-Related Hub Genes in Primary Open-Angle Glaucoma. Int J Mol Sci 2024; 25: 8193

Van Heemst D. Insulin, IGF-1 and longevity. Aging Dis 2010; 1: 147–157

Vaupel JW, Johnson TE, Lithgow GJ. Rates of Mortality in Populations of *Caenorhabditis elegans*. Science 1994; 266: 826–826

Vaupel JW, Carey JR, Christensen K, Johnson TE, Yashin AI, Holm NV, Iachine IA, Kannisto V, Khazaeli AA, Liedo P, Longo VD, Zeng Y, Manton KG, Curtsinger JW. Biodemographic trajectories of longevity. Science 1998; 280: 855–860

Vidović T, Ewald CY. Longevity-Promoting Pathways and Transcription Factors Respond to and Control Extracellular Matrix Dynamics During Aging and Disease. Front Aging 2022; 3: 935220

Vogel C, Marcotte EM. Insights into the regulation of protein abundance from proteomic and transcriptomic analyses. Nat Rev Genet 2012; 13: 227–232

Voutetakis K, Chatziioannou A, Gonos ES, Trougakos IP. Comparative Meta-Analysis of Transcriptomics Data during Cellular Senescence and *In Vivo* Tissue Ageing. Oxid Med Cell Longev 2015; 2015: 1–17

Wang L, Karpac J, Jasper H. Promoting longevity by maintaining metabolic and proliferative homeostasis. SA Davies, JAT Dow, and K Lukowiak (eds.). J Exp Biol 2014; 217: 109–118

Wang X, Fang H, Huang Z, Shang W, Hou T, Cheng A, Cheng H. Imaging ROS signaling in cells and animals. J Mol Med 2013; 91: 917–927

Wei Dai YY. Genomic Instability and Cancer. J Carcinog Mutagen 2014; 05

Wei Y-N, Hu H-Y, Xie G-C, Fu N, Ning Z-B, Zeng R, Khaitovich P. Transcript and protein expression decoupling reveals RNA binding proteins and miRNAs as potential modulators of human aging. Genome Biol 2015; 16: 41

Wieser D, Papatheodorou I, Ziehm M, Thornton JM. Computational biology for ageing. Philos Trans R Soc B Biol Sci 2011; 366: 51–63

Williams GC. PLEIOTROPY, NATURAL SELECTION, AND THE EVOLUTION OF SENESCENCE. Evolution 1957; 11: 398–411

Wong L, Chong YS, Lin W, Kisiswa L, Sim E, Ibáñez CF, Sajikumar S. Age-related changes in hippocampal-dependent synaptic plasticity and memory mediated by p75 neurotrophin receptor. Aging Cell 2021; 20: e13305

Wu L, Xie X, Liang T, Ma J, Yang L, Yang J, Li L, Xi Y, Li H, Zhang J, Chen X, Ding Y, Wu Q. Integrated Multi-Omics for Novel Aging Biomarkers and Antiaging Targets. Biomolecules 2021; 12: 39

Xie K, Neff F, Markert A, Rozman J, Aguilar-Pimentel JA, Amarie OV, Becker L, Brommage R, Garrett L, Henzel KS, Hölter SM, Janik D, Lehmann I, Moreth K, Pearson BL, Racz I, Rathkolb B, Ryan DP, Schröder S, Treise I, Bekeredjian R, Busch DH, Graw J, Ehninger G, Klingenspor M, Klopstock T, Ollert M, Sandholzer M, Schmidt-Weber C, Weiergräber M, Wolf E, Wurst W, Zimmer A, Gailus-Durner V, Fuchs H, Hrabě De Angelis M, Ehninger D. Every-other-day feeding extends lifespan but fails to delay many symptoms of aging in mice. Nat Commun 2017; 8: 155

Xie K, Fuchs H, Scifo E, Liu D, Aziz A, Aguilar-Pimentel JA, Amarie OV, Becker L, Da Silva-Buttkus P, Calzada-Wack J, Cho Y-L, Deng Y, Edwards AC, Garrett L, Georgopoulou C, Gerlini R, Hölter SM, Klein-Rodewald T, Kramer M, Leuchtenberger S, Lountzi D, Mayer-Kuckuk P, Nover LL, Oestereicher MA, Overkott C, Pearson BL, Rathkolb B, Rozman J, Russ J, Schaaf K, Spielmann N, Sanz-Moreno A, Stoeger C, Treise I, Bano D, Busch DH, Graw J, Klingenspor M, Klopstock T, Mock BA, Salomoni P, Schmidt-Weber C, Weiergräber M, Wolf E, Wurst W, Gailus-Durner V, Breteler MMB, Hrabě De Angelis M,

Ehninger D. Deep phenotyping and lifetime trajectories reveal limited effects of longevity regulators on the aging process in C57BL/6J mice. Nat Commun 2022; 13: 6830

Zhang S, Li F, Zhou T, Wang G, Li Z. Caenorhabditis elegans as a Useful Model for Studying Aging Mutations. Front Endocrinol 2020; 11: 554994

Zhao Y, Gilliat AF, Ziehm M, Turmaine M, Wang H, Ezcurra M, Yang C, Phillips G, McBay D, Zhang WB, Partridge L, Pincus Z, Gems D. Two forms of death in ageing Caenorhabditis elegans. Nat Commun 2017; 8: 15458

Živančević K, Baralić K, Jorgovanović D, Buha Djordjević A, Ćurčić M, Antonijević Miljaković E, Antonijević B, Bulat Z, Đukić-Ćosić D. Elucidating the influence of environmentally relevant toxic metal mixture on molecular mechanisms involved in the development of neurodegenerative diseases: In silico toxicogenomic data-mining. Environ Res 2021; 194: 110727

9 Acknowledgements

I would like to express my deepest gratitude to my supervisor, Prof. Dr. Dan Ehninger, for giving me the opportunity to work in his research group and complete my PhD at the German Center for Neurodegenerative Diseases. His unwavering support and invaluable advice have been instrumental throughout my PhD journey.

I am profoundly thankful to Prof. Dr. Andreas Mayr for serving as my second examiner, and to Prof. Dr. Ina Maja Vorberg and Prof. Dr. Bano Daniele for being part of my dissertation committee. Additionally, I extend my heartfelt thanks to all members of Prof. Dr. Bano Daniele's group. Their kindness, support, and the opportunity to work in the worm's lab facilities have been greatly appreciated.

I am also deeply grateful to the current and former members of the 'Translational Biogereontology' lab for their friendship, constant help, support, and advice. It has been a true pleasure working with all of you. I would like to express my special thanks to Dr. Kristina Schaaf, Dr. Melisande Richard, Dr. Maryam Keshavarz, Dr. Enzo Scifo, and Dr. Kan Xie. I will never forget Dr. Scifo's invaluable contributions to the transcriptomic and proteomic analysis in this thesis. Dr. Maryam Keshavarz provided essential guidance on the project process and writing. I am full of gratitude that Dr. Melisande Richard and Dr. Kristina Schaaf paid special attention to our students' physical and mental health during our PhD life.

Furthermore, I wish to express my gratitude to the other research groups at the DZNE, the animal caretakers, and the scientific and administrative support staff. Your assistance has been crucial to my research.

I extend my heartfelt thanks to the Precise team, the Statistics and Machine Learning team, and the Office assistance team, especially Debbie and Nancy, for their support and contributions throughout my research.

Finally, to my family and friends, your constant loving support has been my foundation. I could not have done this without you.